1-1-2010

Theoretical And Experimental Investigation Of Thermodiffusion (Soret Effect) In A Porous Medium

Tawfiq J. Jaber
Ryerson University

THEORETICAL AND EXPERIMENTAL INVESTIGATION OF THERMODIFFUSION (SORET EFFECT) IN A POROUS MEDIUM

By

TAWFIQ J. JABER

B.Sc., University of Technology, Baghdad, 1991
M.A.S.c., University of Technology, Baghdad, 1994
M.A.S.c., Ryerson University, Toronto, 2006

A dissertation presented to

Ryerson University

in partial fulfillment of the

requirements for the degree of

DOCTOR OF PHILOSOPHY

in the Program of

MECHANICAL ENGINEERING

Toronto, Ontario, Canada, 2010

Author's Declaration

I hereby declare that I am the sole author of this dissertation.

I authorize Ryerson University to lend this dissertation to other institutions or individuals for the purpose of scholarly research.

Tawfiq Jaber

I further authorize Ryerson University to reproduce this dissertation by photocopying or by other means, in total or in part, at the request of other institutions or individuals for the purpose of scholarly research.

Tawfiq Jaber

Abstract

Theoretical and Experimental Investigation of Thermodiffusion (Soret effect) in a Porous Medium

Doctor of Philosophy

TAWFIQ J. JABER

Mechanical Engineering

Ryerson University

2010

Thermodiffusion (the Soret effect) is important for the study of compositional variation in hydrocarbon reservoirs. The development of research history, theoretical modeling and applications to multicomponent hydrocarbon mixtures is included in this work. The Firoozabadi model appears to be an appropriate model for thermodiffusion estimation for hydrocarbon mixtures, and it is derived based on the equation of entropy generation rate and four postulates in non-equilibrium thermodynamics. Two equations of state, the Peng-Robinson Equation of State (PR-EoS) and the volume translated Peng Robinson Equation of State (vt-PR-EoS), have been used to estimate the thermodynamic properties of mixtures.

In this work, different cases are presented: first, a new thermodiffusion cell designed to perform high pressure measurements in a porous medium has been validated at atmospheric pressure. Two systems were investigated, (1) 1,2,3,4-tetrahydronaphtalene (THN) and n-dodecane (nC12), and (2) isobutylbenzene (IBB) and n-dodecane at 50% of mass fraction. Experimental results revealed an excellent agreement with benchmark values and a good agreement with theoretical data. Second, the thermal expansion and concentration expansion coefficients and the viscosity of mixtures are necessary properties for the determination of the thermodiffusion coefficient. The densities of binaries of nC12, IBB and THN for pressures from 0.1 to 20 MPa and a temperature centred on 25°C, were measured. By a derivative method, the thermal expansion and

concentration expansion coefficients were determined. Viscosities were directly measured using a high pressure high temperature viscometer.

Finally, the thermosolutal convections of two ternary mixtures, methane (C1), n-butane (nC4) and n-dodecane (nC12) at a pressure of 35.0 MPa and nC12, THN, and IBB at atmospheric pressure, in a porous medium, were investigated over a wide range of permeability. The effect of permeability in the homogeneous and heterogeneous porous media on fluid transport was studied with consideration of thermodiffusion and molecular diffusion. In the analysis of the homogeneous porous medium, it was found that, for permeability below 300 mD, the thermodiffusion for both mixtures was dominant; and above this level, buoyancy convection became the dominant mechanism. Also, the viscosity was found to influence the evaluation of the molecular and thermodiffusion coefficients. In the case of the heterogeneous porous medium, the impact of the permeability ratio on the composition of the mixture components, velocity in the porous medium and on the separation ratio was investigated. It was found that the heterogeneity of porous medium has a significant influence on the composition of the mixture components.

Acknowledgements

I would like to thank Professor Ziad Saghir, my supervisor, for his guidance during my PhD program; I am grateful to him for all precious advices.

I would also like to thank Dr. Henri Bataller, who helped me during my experimental part at Laboratoire des Fluides Complexes, Pau University, France. Also, I would like to thank my Supervisory Committee Members: Dr. Jacob Friedman and Dr. Marcello Papini for their valuable suggestions. Special thanks go to Prof. Greg Kawall, the Director of graduate studies.

I acknowledge the financial support of the Canadian Space Agency (CSA), the Natural Sciences and Engineering Research Council of Canada (NSERC) and Ryerson University.

I would like to express my deepest gratitude to my wife Rihab Jaralla. I thank her for her love, and patience. I would like to dedicate this thesis to my family members, my wife and my children, Mohamad, Ali and Hussain.

Table of Contents

List of Tables

List of Figures

Nomenclature

C_p — The heat capacity at constant pressure, [J. kg^{-1} K^{-1}]

D — The molecular or Fick's diffusion coefficient in a free fluid, [m^2·s^{-1}]

D^* — The molecular diffusion coefficient in a porous medium, [m^2·s^{-1}]

D_T — The thermodiffusion coefficient in a free fluid, [m^2·s^{-1} K^{-1}]

D_T^* — The thermodiffusion coefficient in a porous medium, [m^2·s^{-1} K^{-1}]

$\bar{D}_{ij}$ — The Maxwell-Stephan diffusion coefficient, [m^2.s^{-1}]

f_i — The fugacity of component i, [N.m^{-2}]

g — The gravitational acceleration [m/s^2]

$\bar{H}_i$ — The partial molar enthalpy of component i, [J/mol]

I — The light intensity

J_i — The molar diffusive flux of component i, [mole/m^2/s]

j_i — The mass diffusion flux of component i, [kg/m^2/s]

$\vec{J}_{mi}$ — The molar diffusion flux vector [mole.m^{-2}.s^{-1}]

k — The thermal conductivity [W.m^{-1}.K^{-1}]

$\Bbbk_i$ — The wave number of the beam with refractive index n_i

k_{ij} — The interaction parameter between the ith and jth components

L_{ij} — The Onsager coefficient or the phenomenological coefficient

M — The molecular weight of the mixture, [kg/kmol]

M_i — The molecular weight of component i, [kg/kmol]

mD — The milli-darcy (1 mD= 9.87x10^{-16} m^2) is a unit of permeability

Nu — The Nusselt number, [-]

n — The number of components in the mixture [-]

P — The pressure, [Pa]

P_c — The critical pressure, [Pa]

Q_i — The heat of transport [J/mol]

Q_i^* — The net heat of transport [J/mol]

q	The separation ratio [-]
R	The universal gas constant, 8.314 [J/mol/K]
S_T	The Soret coefficient, [K^{-1}],
s_{vi}	The shift parameter of component i in vtPR-EoS
T	The temperature [K]
T_c	The critical temperature, [K]
T_r	The reduced temperature, [-]
t	Time [s]
$\bar{U}_i$	The partial molar internal energy of component i, [J/mole]
u	The velocity component in x-direction [m.s^{-1}]
v	The velocity component in y-direction [m.s^{-1}]
$\vec{V}$	The fluid velocity vector (u, v, w) [m.s^{-1}]
w	The velocity component in z-direction [m.s^{-1}]
x	The spatial coordination in x-direction [m]
x_i	The molar fraction of component i, [-]
y	The spatial coordination in y-direction [m]
Z	The compressibility factor [-]
z	The spatial coordination in z-direction [m]

Greek Symbols

α_T	The thermal diffusion factor, (-)
β_c	The coefficient of concentration expansion [-]
β_T	The Coefficient of thermal expansion [1/K]
ΔU_i^{vap}	The cohesive energy (also called the vaporization energy), [J/mol]
ΔU_i^{visc}	The viscous energy, [J/mol]
φ	The porosity [-]
Φ	The phase difference between the two laser beams at the point of the interference field, [rad]
κ	The permeability [m^2]

k	The wave number of the beams in air
μ_k	The chemical potential of component k, [J/mol]
η	The dynamic viscosity of the fluid mixture [kg.m^{-1}.s^{-1}]
ρ	The fluid mixture density [kg/m^3]
ρ_m	The molar density of fluid mixture [kmole/m^3]
σ	The rate of entropy production, [J/mol/s]
ω	The mass fraction [-]
w	The pulsation of the two laser beams
ω	The acentric factor [-]
ζ	The mixture viscosity parameter
τ_r	The relaxation time, [s]
τ_i	The ratio of cohesive energy and viscous energy
ψ_i	The volume fraction of molecules moving into a hole left by a molecule of type i

Subscripts

e	Effective
fl	Fluid mixture
m	Molar quantities,
s	Porous media or matrix

Chapter 1

1.1 Introduction

In a fluid mixture, diffusion is the general term used to describe the motion of one species with respect to another. The thermodiffusion phenomenon, also known as the Soret effect (S_T), is a coupling between a temperature gradient and its resulting mass flux in a multicomponent system. The Soret effect was discovered by German physicist Carl Ludwig (Ludwig, 1856) and later more deeply analysed by Swiss physicist Charles Soret (Soret, 1879 and 1880). This phenomenon appears in a wide range of physical and chemical processes in nature, and researchers have contributed to its study over the years, including studies of oil reservoir analysis, tar sand extraction, fluid separation, distillation, material processing and biotechnological applications. Comprehensive diffusion theories and accurate diffusion experiments are of great importance to the optimization of diffusion-dominant industrial processes. It is interesting to note that the thermodiffusion and molecular diffusion (also called Fickian diffusion, Fick 1855) are coupled processes; molecular diffusion tends to decrease a composition gradient which was created due to the thermodiffusion.

This work concentrates on the study of hydrocarbon mixtures (binary and ternary) in porous media. A new thermodiffusion cell designed to measure the molecular diffusion coefficient and the Soret coefficient of hydrocarbon binary systems in a porous medium, which is based on optical digital interferometry, is presented. Also, the most recently developed non-equilibrium thermodynamics model by Firoozabadi has been applied. The three dimensional study of the thermodiffusion process in porous media is the most realistic study, which will lead to the most complete understanding of the natural laws applicable to the thermodiffusion process.

The thermodiffusion in multicomponent systems, like ternary mixtures, is much more complicated than in binary mixtures for both experimental and theoretical work. There have been extensive experimental and theoretical studies of the molecular diffusion

coefficient in binary mixtures in the literature. Experimental data on the binary thermodiffusion coefficient in porous media are much scarcer than for molecular diffusion.

On the multicomponent thermodiffusion in liquid, very few models have been published. The Shukla-Firoozabadi (2000) multicomponent model (also known as the Firoozabadi model), based on their binary mixture model, is adopted to carry out a comparison with some latest results by Platten *et al*. (2004) and Leahy-Dios *et al*. (2005) by using two equations of state: Peng-Robinson and volume translated Peng-Robinson, respectively.

1.2 Research Objectives

The main objectives in this research are as follows:

1) To study and derive the Firoozabadi model for multicomponent mixtures, and obtain full understanding of this model and its application.

2) To measure molecular diffusion and thermodiffusion coefficients of binary mixtures of n-dodecane, isobutylbenzene and 1,2,3,4-tetrahydronaphthalene using an optical digital interferometer, to compare the results with benchmark values and theoretical values as well, and to prove the reliability of the digital interferometry technique. The theoretical values are determined by a computer code that can be used to simulate a thermodiffusion process as a function of temperature, pressure, and composition in a fluid mixture to investigate the Soret effect, and a FORTRAN program (in-house code) applying Firoozabadi's model was developed.

3) To numerically simulate the thermodiffusion for a hydrocarbon ternary mixture in a porous medium by applying different parameters such as the viscosity effect and a different range of permeabilites.

4) To simulate the thermodiffusion in a heterogeneous porous medium by applying different fracture orientations and study the effect of multi-permeability and multi-porosity on the mixture behaviour.

2

1.3 Thesis Organization

This thesis consists of seven chapters and is organized as follows:

- Chapter 1 presents an introduction to the thermodiffusion, literature review and the basic concept and diffusion equations.

- In Chapter 2, the theoretical derivation of the Firoozabadi model, that has been used to estimate the Soret coefficient for a multicomponent mixture, is presented; the governing equations for porous media are explained; these equations are mass continuity, Darcy's law and thermal energy conservation.

- In Chapter 3, the experimental technique used to measure the molecular diffusion coefficient and Soret coefficient for binary hydrocarbon fluid mixtures in a porous medium is presented and experimental data are discussed and compared with the benchmark values and numerical results.

- In Chapter 4, the comparison between experimental and theoretical estimation of the thermal expansion coefficient, concentration expansion coefficient, density and viscosity for three binary hydrocarbon mixtures under pressure up to 20 MPa are described and discussed.

- In Chapter 5, the theoretical model of thermosolutal convections of two hydrocarbon ternary mixtures in a homogenous porous medium under different permeabilities is carried out and discussed.

- In Chapter 6, a three-dimensional study of the permeability effect on convection in a heterogeneous porous medium filled with a ternary hydrocarbon mixture is described and discussed.

- Finally, Chapter 7 presents the conclusions and recommendations.

1.4 Literature Review

1.4.1 Theoretical models for thermal diffusion factor

In the thermodynamics of an irreversible process, there are two energy quantities: the heat of transport, Q_i, which is the amount of energy transported across a given reference plane per mole of the ith component. The heat of transport is interpreted as the energy difference between the energy required when a molecule of component i moves out of its position in a temperature field and the energy given up when its left hole is filled by one of its neighbour molecules. Q_i^* is the net heat of transport, (de Groot 1945), which is defined by:

$$Q_i^* = Q_i - \bar{H}_i \tag{1.1}$$

where $\bar{H}_i$ is the partial molar enthalpy of the ith component in the solution. In terms of the heat of transport, the flux equation for the ith component in a multicomponent constant pressure system (Dougherty and Drickamer 1955) is given by:

$$J_i = -\sum_{k=1}^{n} L_{ik} \left[\left(Q_k - \bar{H}_k \right) \frac{\nabla T}{T} + \sum_{i=1}^{n-1} \frac{\partial \mu_k}{\partial x_i} \nabla x_i \right] \tag{1.2}$$

where J_i is the flux of the component i, μ_k is the chemical potential of component k, T is the absolute temperature, x_i is the mole fraction of component i, and L_{ik} are phenomenological coefficients. For a binary mixture, the composition gradient resulting from a temperature gradient in the steady state (J_i) for the first component is given by:

$$\frac{\nabla x_1}{x_1} = -\frac{Q_1 - \bar{H}_1}{x_1 \left(\partial \mu_1 / \partial x_1 \right)} \frac{\nabla T}{T} = -\frac{Q_1^*}{x_1 \left(\partial \mu_1 / \partial x_1 \right)} \frac{\nabla T}{T} \tag{1.3}$$

where Eq. 1.1 has been used. In the same manner, the second component is:

$$\frac{\nabla x_1}{x_2} = -\frac{Q_2^*}{x_2\left(\partial \mu_2 / \partial x_1\right)}\frac{\nabla T}{T} \tag{1.4}$$

using Eqs 1.3 and 1.4, with the Gibbs-Duhem relations in the form:

$$x_1\frac{\partial \mu_1}{\partial x_1} + x_2\frac{\partial \mu_2}{\partial x_1} = 0 \tag{1.5}$$

$$x_1 Q_1^* + x_2 Q_2^* = 0$$

A relation between the concentration gradient and the temperature gradient at steady state is obtained as follows:

$$\frac{\nabla x_1}{x_1 x_2} = \frac{Q_2^* - Q_1^*}{x_1\left(\partial \mu_1 / \partial x_1\right)}\frac{\nabla T}{T} \tag{1.6}$$

For a binary system, the conventional flux equation may be written as follows:

$$J_1 = -\rho_m D\left(\nabla x_1 - \alpha_T x_1 x_2 \frac{\nabla T}{T}\right) = -\rho_m D\left(\nabla x_1 - S_T x_1 x_2 \nabla T\right) \tag{1.7}$$

where ρ_m is the molar density (mole/m^3), D is the molecular diffusion coefficient, $\alpha_T = TS_T$ is the thermal factor, and S_T is the Soret coefficient. For steady state ($J_1 + J_2 = 0$), from Eq. 1.7, one can obtain another relation between the composition and temperature gradients:

$$\frac{\nabla x_1}{x_1 x_2} = \alpha_T \frac{\nabla T}{T} \tag{1.8}$$

When Eq. 1.8 is compared with Eq. 1.6, a new expression for the thermal diffusion factor in terms of the net heat of transport and chemical potential for a binary system is introduced as follows:

$$\alpha_T = \frac{Q_2^* - Q_1^*}{x_1 \left(\partial \mu_1 / \partial x_1 \right)} \tag{1.9}$$

Eq. 1.9 is a general expression for the thermal diffusion factor. The thermal diffusion factor can be calculated through two main theoretical models: the phenomenological approach (or thermostatic approach) and the kinetic approach, which have been the basis of modeling the thermal diffusion factor in binary mixtures. Both approaches are based on the postulates in phenomenological theory of non-equilibrium thermodynamics. The theory of non-equilibrium thermodynamics is extended from equilibrium thermodynamics by introducing the following four postulates (Curie's postulates), Bird *et al.* (2002):

1. The equilibrium thermodynamics relations apply to systems that are not in equilibrium, provided that the gradients are not too large (*Quasi-equilibrium postulate*).
2. All fluxes in the system may be written as linear relations involving all the forces (*Linear postulate*).
3. No coupling of fluxes and forces occurs if the difference in tensorial order of the flux and force is an odd number (*Curie's postulate*).
4. In the absence of magnetic fields, the matrix of the coefficients in the flux-force relations is symmetric (*Onsager's reciprocal relations*).

Both the Haase model and the Kempers model use the thermostatic approach. The Haase model (1950) is based on the phenomenological theory, and the net heat of transport is interpolated with the partial molar enthalpy. Based on this assumption the net heat of transport for a binary mixture is given by:

$$Q_2^* - Q_1^* = \frac{M_1 M_2}{M_1 x_1 + M_2 x_2} \left(\frac{\bar{H}_2}{M_2} - \frac{\bar{H}_1}{M_1} \right) \tag{1.10}$$

where $\bar{H}_i$ is the partial molar enthalpy of component i, and M_i is the molecular weight of component i. By substituting Eq. 1.10 into Eq. 1.9, the thermal diffusion factor is expressed as:

$$\alpha_T^H = \frac{M_1 \bar{H}_2 - M_2 \bar{H}_1}{\left(M_1 x_1 + M_2 x_2 \right) x_1 \left(\partial \mu_1 / \partial x_1 \right)} \tag{1.11}$$

The thermal diffusion factor for an ideal fluid at standard state is given as:

$$\alpha_T^o = \frac{M_1 \bar{H}_2^o - M_2 \bar{H}_1^o}{RT \left(M_1 x_1 + M_2 x_2 \right)} \tag{1.12}$$

For an ideal fluid, the following relation $x_i \left(\partial \mu_i / \partial x_1 \right) = RT$ pertains, where R is the gas constant. The Haase model can be re-written as:

$$\alpha_T^H = \frac{\alpha_T^o RT \left(M_1 x_1 + M_2 x_2 \right) + M_1 \left(\bar{H}_2 - \bar{H}_2^o \right) - M_2 \left(\bar{H}_1 - \bar{H}_1^o \right)}{\left(M_1 x_1 + M_2 x_2 \right) x_1 \left(\partial \mu_1 / \partial x_1 \right)} \tag{1.13}$$

In 1989, Kempers proposed a thermodynamics theory of the thermal diffusion factor. This model was based on a statistical description of a two-bulb system. He obtained an expression for α_T by maximizing the partition function in the canonical ensemble of an idealized dual subsystem in a steady state; the net heat of transport and the thermal diffusion factor (for binary mixture) in Kempers model are expressed as:

$$Q_2^* - Q_1^* = \frac{\bar{V}_1 \bar{V}_2}{\bar{V}_1 x_1 + \bar{V}_2 x_2} \left(\frac{\bar{H}_2}{\bar{V}_2} - \frac{\bar{H}_1}{\bar{V}_1} \right) \tag{1.14}$$

$$\alpha_T^K = \frac{\overline{V}_1\overline{H}_2 - \overline{V}_2\overline{H}_1}{x_1\left(\partial\mu/\partial x_1\right)\left(\overline{V}_1 x_1 + \overline{V}_2 x_2\right)} \qquad (1.15)$$

where $\overline{V}_i$ is the partial molar volume of component i.

Both models (Haase and Kempers) have been tested previously for a few hydrocarbon mixtures using the Soave-Redlich-Kwong Equation of State (SRK-EoS), Soave (1972), and Peng-Robinson Equation of State, (Peng and Robinson, 1976). It is found that the comparisons of theoretical results with experimental data were found to be qualitative.

In the kinetic approach, the heat of transport is interpolated with the activation energy of molecular motion, which can be obtained from the viscosity of the mixture. Several expressions for the thermal diffusion factor can be obtained. For example, Dougherty and Drickamer (1955) obtained α_T in terms of the activation energies for molecular movements, given as:

$$\alpha_T^{DD} = \frac{\left(M_1\overline{V}_2 + M_2\overline{V}_1\right)\left(\Delta U_2^*/\overline{V}_2 - \Delta U_1^*/\overline{V}_1\right)}{x_1\left(\partial\mu_1/\partial x_1\right)2\left(M_1 x_1 + M_2 x_2\right)} \qquad (1.16)$$

where ΔU_i^* is the activation energy for molecular movement of component i, and is a function of viscosity and thermodynamic properties of the pure component.

The comparison between the theoretical results for α_T^{DD} with the experimental data has been shown that the Dougherty-Drickamer model does not perform better than the other two models as shown above. And this model suffers from some shortcomings; for instance, thermodynamic properties of the components were obtained from the approximate Scatchard-Hildebrand theory (Hildebrand and Scott, 1950). It is known that Scatchard-Hildebrand theory is unreliable in dealing with non-ideal mixtures under different conditions.

A new model is based on the method of irreversible thermodynamics suggested by Shukla and Firoozabadi (1998) which is based on the Dougherty-Drickamer model. They use more accurate thermodynamic properties of mixtures obtained from the volume-translated Peng-Robinson Equation of State. By following the physical interpretation of Dougherty and Drickamer (1955), it is not possible to directly evaluate the net heat of transport. Shukla and Firoozabadi relate it to the energy of detaching a molecule from its neighbours in the region of the mixture (W_{H_i}), and to the energy given up in that region when one molecule fills a hole (W_L), as follows:

$$Q_1^* = W_{H1} - \psi_1 W_L \tag{1.17}$$

$$Q_2^* = W_{H2} - \psi_2 W_L \tag{1.18}$$

where ψ_i is the volume fraction of molecules moving into a hole left by a molecule of type i in the mixture. Note that molecules may have different sizes and shapes. And the distribution of molecules to occupy holes in the mixture is completely random. Therefore, the probable energy, W_L, supplied to fill a hole left by a detached molecule is given by:

$$W_L = x_1 W_{H1} + x_2 W_{H2} \tag{1.19}$$

with

$$W_{H1} = -\frac{\bar{U}_1}{\tau_1}$$
$$\tag{1.20}$$
$$W_{H2} = -\frac{\bar{U}_2}{\tau_2}$$

where $\bar{U}_i$ is the partial molar internal energy of component i, and τ_i is the ratio of the energy of vaporization, ΔU_i^{Vap}, to the energy of viscous flow (or defined as the energy of activation for viscous flow) , ΔU_i^{visc} (Glasstone *et al.*, 1941)

ψ_i can be evaluated in terms of the partial molar volume and mole fraction as follows:

$$\psi_1 = \bar{V}_1 / \left(x_1 \bar{V}_1 + x_2 \bar{V}_2 \right)$$

$$\psi_2 = \bar{V}_2 / \left(x_1 \bar{V}_1 + x_2 \bar{V}_2 \right)$$

(1.21)

with the relation (satisfying the Gibbs-Duhem relation):

$$x_1 \psi_1 + x_2 \psi_2 = 1$$

(1.22)

using Eqs. 1.17-1.23 along with Eq. 1.9 the thermal diffusion factor is defined as:

$$\alpha_T^F = \frac{\left(\bar{U}_1 / \tau_1 - \bar{U}_2 / \tau_2 \right)}{x_1 \left(\partial \mu / \partial x_1 \right)} + \frac{\left(\bar{V}_2 - \bar{V}_1 \right) \left(x_1 \bar{U}_1 / \tau_1 + x_2 \bar{U}_2 / \tau_2 \right)}{x_1 \left(\partial \mu / \partial x_1 \right) \left(\bar{V}_1 x_1 + \bar{V}_2 x_2 \right)}$$

(1.23)

Eq. 1.23 represents the thermal diffusion factor for a binary mixture in the Shukla-Firoozabadi model, and it is an explicit function of partial molar internal energies and volumes, energy of vaporization and viscous flow, and chemical potential. Shukla and Firoozabadi (1998) applied this model to hydrocarbon systems, i.e., [1]C1/C3, C1/C4, C7/nC12, and C7/C16; non-polar non-hydrocarbon systems, i.e., Ar/CO_2, N_2/CO_2, H_2/N_2, and H_2/CO_2; hydrocarbon and non-hydrocarbon systems, i.e., C1/N_2 and C1/CO_2. They found that comparisons of theoretical results with experimental data show a good agreement. In particular, the predicted sign of the thermal diffusion factor is consistent with experimental observations in the mixtures. In their work, the equilibrium properties of mixtures were obtained from the volume translated Peng-Robinson Equation of State (vtPR-EoS), and the values of τ_i of different components are assumed to be equal for all fluids presented. From the viscosities of pure components, the values τ_i appear to vary

---

[1] C1 is methane, C3 is propane, C4 is butane, C7 is heptane, nC12 is n-dodecane, and C16 is Hecdecane also called Hexadecane

from 3.5 to 5; Shukla and Firoozabadi adopted the universal values for τ_i ($\tau_1 = 4$, $\tau_2 = 4$) for all fluids presented.

Firoozabadi *et al.* (2000), and Ghorayeb and Firoozabadi (2000) has developed their model from binary to multicomponent mixtures. They proposed the following expression for the net heat of transport for the *i*th component in an n-component mixture:

$$Q_i^* = -\frac{\Delta \overline{U}_i}{\tau_i} + \left(\sum_{j=1}^{n} \frac{x_j \Delta \overline{U}_j}{\tau_j} \right) \frac{\overline{V}_i}{\sum_{j=1}^{n} x_j \overline{V}_j} \qquad i = 1,\ldots\ldots,n \qquad (1.24)$$

The Firoozabadi model is considered to be the first model dealing with thermodiffusion in multicomponent mixtures. Pan *et al.* (2007) compared different multicomponent thermodiffusion models and concluded that the Firoozabadi model was the best in general. This model will be explained in detail in Chapter 2.

As far as we know, few simulations dealing with thermodiffusion in multicomponent mixtures have been reported. For now, only two models are available, which have been developed by Kempers (1989 and 2001) and Firoozabadi *et al.*, (2000).

1.4.2 Experimental methods for thermal diffusion factor

The Soret effect can be measured by using different techniques which have been divided into groups (Platten, 2006). The first group of techniques are the convection free systems and the second group of techniques use convective coupling. In the first group, at steady state and in absence of convection, the thermodiffusion is balanced by molecular diffusion resulting in zero diffusion flux ($J_i = 0$) as shown in the following equations:

$$J_i = \rho_m \left(D \nabla x_i + D_T x_1 (1 - x_2) \nabla T \right) \qquad (1.25)$$

$$S_T = \frac{\alpha_T}{T} = \frac{D_T}{D} = \frac{\nabla x_i}{x_1 (1 - x_1) \nabla T} \tag{1.26}$$

The first group include three different techniques to measure the thermodiffusion or Soret effect:

    (i)   Thermal Diffusion Forced Rayleigh Scattering (TDFRS).

    (ii)   Standard Soret Cell (SSC).

    (iii)   Laser Beam Deflection Technique (LBD).

In the TDFRS technique, (Kohler and Muller, 2002; Wiegand and Kohler, 2002; Wiegand, 2004; Polyakov *et al*., 2006), two laser beams intersect within the sample, which is a fluid mixture in a glass container, and create a holographic interference grating. At the intersection of the two laser beams, interference fringes are created. And by putting some chemically inert dye in the mixture, energy is absorbed from the light field and the sample is heated with the spatial periodicity of the grating. Typically, the amplitude of the temperature grating is of the order of 10 to 100 μK. The temperature gradients within this thermal grating give rise via the Soret effect to a build-up of a concentration modulation with the same spatial periodicity. Both the temperature and the concentration grating are accompanied by a refractive index grating. The Soret coefficient can be measured from the resulting experimental data.

The SSC, also called a thermal diffusion cell (Costeseque *et al*., 2004), consists of two horizontal rigid plane plates (e.g., copper or stainless steel). Both plates are maintained at different temperatures in order to create a vertical temperature gradient. The system usually is heated from above in order to avoid free convection. Both the Soret coefficient and molecular diffusion coefficient can be obtained by measuring the concentration changes caused by the temperature gradient.

The LBD use the same type of cell as described in above. The main difference being that two opposite lateral walls are made of glass of good optical quality. Kolodner *et al*.

(1988) and Zhang *et al.* (1996) applied this technique to measure the Soret effect for a binary mixture of water-ethanol.

In the second group of techniques (Convection-coupled), the idea is to study the change of the velocity field under the effect of thermodiffusion. Therefore, the important parameter is the solutal contribution to the buoyancy force. A Thermogravitational Column (TGC) is an example of the second group method (Bou-Ali *et al.*, 1998, Dutrieux *et al.*, 2002, Leahy-Dios *et al.*, 2005 and Haugen and Firoozabadi, 2007). The TGC method usually consists of two vertical concentric cylinders at two different temperatures in such a way as to create a horizontal temperature gradient. The liquid mixture is placed in a small gap between two vertical walls. Since the temperature gradient is horizontal, under the action of the Soret effect one component is displaced to the cold side and the other to the hot side. Due to the convection, the one at the cold side is transported to the bottom and the one that goes to the hot side is transported to the top of the cell. Thus, the combined effect of thermodiffusion and convection finally creates a vertical mass fraction gradient. The Soret coefficient can be obtained by measuring the concentration difference between the bottom and the top. The separation rate in this method is defined as the concentration difference between the top and the bottom cell. Platten *et al.* (2003) showed that the molecular separation or the difference in mass fraction between the top and bottom in a thermogravitational column can be substantially increased by inclining the column by an angle. In addition, the TGC can be used for porous media (Costesque *et al.*, 1994 and Costeseque and Loubet, 2003) and ternary mixtures, (Leahy-Dios *et al.*, 2005).

Costeseque *et al.* (2004) conducted experiments in both a free fluid and a porous medium with a vertical temperature gradient. It was found that, when the thermal conductivities of the fluid and solid matrix are of the same magnitude, the Soret coefficients do not differ significantly with respect to the case of the free fluid. Several researchers have published values of the Soret coefficient for organic molecules, polymers, and even electrolyte solutions. In particular, in 1999, research groups from different universities, who met at Fontainebleau, France, started a ground-based measurement campaign. The goal was to establish a reliable database of the Soret coefficient for three binary mixtures (Fontainebleau mixtures) composed of n-dodecane (nC12), Isobutylbenzene (IBB), and

1,2,3,4-tetrahydrophtalene (THN). As well, there was a clear desire to establish benchmark values for the Soret, thermal diffusion, and molecular diffusion coefficients so that they could be used to compare earth based results with results obtained through other means such as experiments in microgravity or numerical simulation. The values obtained from independent researchers were in strong agreement with each other, (Platten *et al.*, 2003).

1.5 Basic Concept and Equations for Diffusion

1.5.1 Fundamental properties of porous media

A porous medium can be defined as a multiphase material, which is a solid containing void spaces (pores), either connected or unconnected. In petroleum engineering, a porous medium, also called reservoir rock, stores crude oil and natural gas.

Porosity

The porosity of a porous media, which is defined as the ratio of the volume of the pores (void spaces) to the total bulk volume of the media, is given by:

$$\varphi = \frac{V_p}{V_P + V_s} \tag{1.27}$$

where φ is the porosity, V_p is the void volume or pore volume, and V_s is the solid volume or matrix volume.

Permeability

The permeability of a porous media can be defined as a measure of the connectivity of pore spaces. Mathematically, it is defined as the constant of proportionality in Darcy's law. A micro scale measurement of grain size distribution shows that different grain sizes

and shapes affect permeability. A traditional unit for permeability is the Darcy (D), or more commonly the millidarcy (mD) (1 Darcy=9.86923x10^{-13}m^2).

Tortuosity

The tortuosity (τ) is a fundamental property of the porous media and is given as a ratio of effective average path (actual path), L_e, of a fluid particle and the corresponding straight and shortest external distance (length between two points, L):

$$\tau = \frac{L_e}{L} \tag{1.28}$$

Also the tortuosity refers to the link between diffusion coefficients in free layers and in the porous media, (Nield and Bejan, 2006; Bear, 1972; de Marsily, 1986), such as:

$$D^* = \varphi D \quad \text{or} \quad D^* = \frac{D}{\tau^2}$$
$$D_T^* = \varphi D_T \quad \text{or} \quad D_T^* = \frac{D_T}{\tau^2} \tag{1.29}$$

where D is the diffusion coefficient in a free liquid, D^* is the diffusion coefficient in a porous medium, D_T is the thermodiffusion in a free liquid, and D_T^* the thermodiffusion in a porous medium. The value of the thermodiffusion coefficient is also affected by the solid matrix. The Soret coefficient should have the same value in a porous medium and in a free liquid, based on the argument that since both coefficients D and D_T are of the same nature, the corrections should be the same and therefore their ratio should be unaffected by the porous medium, Platten and Costeseque (2004).

1.5.2 Diffusion flux

Before explaining thermodiffusion, one needs to define the diffusion flux and several basic concepts. Two types of diffusion fluxes are often used in thermodiffusion research. First is the molar diffusion flux with a mole average velocity given by:

$$J_i = \rho_{mi}\left(v_i - v_a^{mol}\right) \tag{1.30}$$

where J_i is the molar diffusion flux of component i, v_a^{mol} is an arbitrary reference velocity (mole average reference), ρ_{mi} is the molar density of component i, and v_i is the velocity of component i. v_a^{mol} is defined by:

$$v_a^{mol} = \sum_i^n x_i v_i \tag{1.31}$$

where x_i is the mole fraction of component i and n is number of components in the mixture. In a similar way, the mass diffusion flux with respect to the velocity v_a^{mass} is define by:

$$j_i = \rho_i\left(v_i - v_a^{mass}\right) \tag{1.32}$$

where j_i is the mass diffusion flux of component i, v_a^{mass} is an arbitrary reference velocity (mass average reference), and ρ_i is mass density of component i. v_a^{mass} is defined by:

$$v_a^{mass} = \sum_{i=1}^n \omega_i v_i \tag{1.33}$$

where ω_i is the mass fraction of component i.

In the absence of convection, when a steady-state condition is reached, the diffusion flux will vanish, and for n-components mixture, two relationships from the definitions of diffusion fluxes, J_i and j_i can be found:

$$\sum_{i=1}^{n} J_i = 0 \tag{1.34}$$

$$\sum_{i=1}^{n} j_i = 0 \tag{1.35}$$

From the Eqs. 1.34 and 1.35, it can be concluded that only n-1 of the n diffusion fluxes are independent. The conventional diffusion fluxes equation can be expressed as follows:

$$\vec{J}_i = -\rho_m \left(\sum_{j=1}^{n-1} D_{ij}^{mol} \nabla x_j + D_{Ti}^{mol} \nabla T \right) \tag{1.36}$$

$$\vec{j}_i = -\rho \left(\sum_{j=1}^{n-1} D_{ij}^{mass} \nabla \omega_j + D_{Ti}^{mass} \nabla T \right) \tag{1.37}$$

where ρ is the mass density of the mixture, ρ_m is the molar density of the mixture, D_{ij}^{mol} and D_{ij}^{mass} are the molecular diffusion coefficient matrices (Fick's diffusion coefficient) corresponding to $\vec{J}_i$ and $\vec{j}_i$, respectively, D_{Ti}^{mol} and D_{Ti}^{mass} are the thermal diffusion coefficient matrices corresponding to $\vec{J}_i$ and $\vec{j}_i$, respectively, T is the temperature, ∇x_j is the vector of mole fraction gradients, $\nabla \omega_j$ is vector of mass fraction gradients and ∇T is the temperature gradient. The pressure diffusion contribution is not considered in Eqs 1.36 and 1.37, because its magnitude is about three orders smaller than that of thermodiffusion. In Eq. 1.36, $\vec{J}_i, \nabla x_j, D_{ij}^{mol}$, and D_{Ti}^{mol} are vectors, given by:

$$
\vec{J}_i = \begin{bmatrix} J_1 \\ J_1 \\ \vdots \\ J_{n-1} \end{bmatrix}, \quad D_{ij}^{mol} = \begin{bmatrix} D_{11}^{mol} & D_{12}^{mol} & \cdots & D_{1\,n-1}^{mol} \\ D_{21}^{mol} & D_{22}^{mol} & \cdots & D_{2\,n-1}^{mol} \\ \vdots & \vdots & \ddots & \vdots \\ D_{n-1\,1}^{mol} & D_{n-1\,2}^{mol} & \cdots & D_{n-1\,n-1}^{mol} \end{bmatrix},
$$

$$\tag{1.38}$$

$$
\nabla x_j = \begin{bmatrix} \nabla x_1 \\ \nabla x_2 \\ \vdots \\ \nabla x_{n-1} \end{bmatrix} \quad \text{and} \quad D_{Ti} = \begin{bmatrix} D_{T1} \\ D_{T1} \\ \vdots \\ D_{Tn-1} \end{bmatrix}
$$

For a binary mixture, Eqs 1.36 and 1.37 are given by:

$$
\vec{J}_1 = -\rho_m \left(D_{11}^{mol} \nabla x_1 + D_{T1}^{mol} \nabla T \right)
$$

$$\tag{1.39}$$

$$
\vec{j}_1 = -\rho \left(D_{11}^{mass} \nabla \omega_1 + D_{T1}^{mass} \nabla T \right)
$$

$$\tag{1.40}$$

Two important quantities, the Soret coefficient (S_T) and thermal diffusion factor (α_T) have been defined as:

$$
S_T = \frac{D_T}{D x_1 x_2} = \frac{D_T}{D \omega_1 \omega_2}
$$

$$\tag{1.41}$$

$$
\alpha_T = T S_T = T \frac{D_T}{D}
$$

$$\tag{1.42}$$

where D is the molecular diffusion coefficient and D_T is the thermodiffusion coefficient. By assuming the following relationship between D^{mol} and D^{mass} or D_T^{mol} and D_T^{mass}

$$
D = D_{11}^{mol} = D_{11}^{mass}
$$

$$\tag{1.43}$$

$$D_T = \frac{D_{T1}^{mol}}{x_1 x_2} = \frac{D_{T1}^{mass}}{\omega_1 \omega_2} \tag{1.44}$$

Eqs. 1.39 and 1.40 can be expressed by:

$$\vec{J}_1 = -\rho_m \left(D \nabla x_1 + D_T x_1 x_2 \nabla T \right) \tag{1.45}$$

$$\vec{j}_1 = -\rho \left(D \nabla \omega_1 + D_T \omega_1 \omega_2 \nabla T \right) \tag{1.46}$$

Eqs. 1.45 and 1.46 have been more frequently adopted in the literature to express $\vec{J}_1$ and $\vec{j}_1$.

Chapter 2

Theoretical Derivation of Firoozabadi Model for Multicomponent Mixtures and Governing Equations in a Porous Medium

2.1 Introduction

In the non-equilibrium thermodynamics, (de Groot and Mazur, 1984), the rate of entropy production, σ, can be written as:

$$\sigma = -\frac{1}{T^2}\left(\vec{J}_q - \sum_{k=1}^{n}\frac{\bar{H}_k}{M_k}\vec{J}_k\right)\bullet\nabla T - \frac{1}{T}\sum_{k=1}^{n}\vec{J}_k\bullet\left(\frac{\nabla_T\mu_k}{M_k} - \vec{F}_k\right) - \frac{1}{T}\Pi:\nabla\vec{v} - \frac{1}{T}\sum_{j=1}^{r}R_jA_j \qquad (2.1)$$

where $\vec{J}_q$ is the total heat flux, $\vec{J}_k$ is diffusion flux of component k, T is the temperature, $\bar{H}_k$ is the partial molar enthalpy of component k, M_k is the molecular weight of component k, μ_k is the chemical potential of component k, Π is the fluid stress tensor or viscous pressure tensor, $\vec{F}_k$ is the external force of component k, $\vec{v}$ is the average velocity ($\vec{v}=\sum_{i=1}^{n}x_i\vec{v}_i$), R_j is the chemical reaction rate, A_j is the chemical affinity of the reactions, and r is the total number of chemical reactions.

In Eq. 2.1, there are four thermodynamic driving forces: the gradient of temperature, the gradient of chemical potential and external force, the gradient of velocity, and the chemical reaction rate. A new heat flux expression, $\vec{J}_q^*$, can be introduced, which is the linear combination of the heat flux and internal diffusion mass fluxes:

$$\vec{J}_q^* = \vec{J}_q - \sum_{k=1}^{n}\frac{\bar{H}_k}{M_k}\vec{J}_k \qquad (2.2)$$

In a mixture consisting of n components, where the only external force is the gravity, and by assuming that there is no heat generation, viscous dissipation, and chemical reaction, the term F_K is eliminated because the total summation of J_k is zero, $(\sum_{k=1}^{n} \vec{J}_k = 0)$; the entropy production rate is simplified as:

$$\sigma = -\frac{1}{T^2}\vec{J}_q^* \cdot \nabla T - \frac{1}{T}\sum_{k=1}^{n-1}\vec{J}_k \cdot \nabla_T \left(\frac{\mu_k}{M_k} - \frac{\mu_n}{M_n} \right) \tag{2.3}$$

The phenomenological equation for heat flux and diffusion flux can be given as:

$$\vec{J}_q^* = L_{qq}\frac{1}{T^2}\nabla T - \frac{1}{T}\sum_{k=1}^{n-1}L_{qk}\left(\frac{\nabla_T \mu_k}{M_k} - \frac{\nabla_T \mu_n}{M_n} \right) \tag{2.4}$$

$$\vec{J}_i = -L_{iq}\frac{1}{T^2}\nabla T - \frac{1}{T}\sum_{k=1}^{n-1}L_{ik}\left(\frac{\nabla_T \mu_k}{M_k} - \frac{\nabla_T \mu_n}{M_n} \right), \quad i = 1,2,........n\text{-}1 \tag{2.5}$$

where L_{qq}, L_{qk}, L_{iq}, and L_{ik} are the phenomenological coefficients, (Onsager, 1931). From the fourth postulate, Onsager's reciprocal relation, the following relations exist:

$$L_{qi} = L_{iq}, \qquad i = 1,2,..........,n-1 \tag{2.6}$$

$$L_{ik} = L_{ki}, \qquad i,k = 1,2,..........,n-1 \tag{2.7}$$

The focus here is on diffusion flux, $\vec{J}_i$, because it is the aim of this work. By applying the following relations, the Gibbs-Duhem expression and the relations among chemical potential, the fugacity and the partial molar volume are:

$$\nabla_T \mu_n = \frac{1}{x_n}\left(\frac{1}{\rho_m}\nabla P - \sum_{j=1}^{n-1}x_j\nabla_T \mu_j \right) \tag{2.8}$$

$$\left.\frac{\partial \mu_i}{\partial x_j}\right|_{x_j,T,P} = RT \left.\frac{\partial \ln f_i}{\partial x_j}\right|_{x_j,T,P} \qquad i=1,2,.......,n, \quad j=1,2,.......,n-1 \tag{2.9}$$

$$\left.\frac{\partial \mu_i}{\partial P}\right|_{x_j,T} = \left.\frac{\partial V}{\partial n_i}\right|_{n_i,T,P} = \bar{V}_i \qquad i=1,2,..........,n \tag{2.10}$$

where x_j is the mole fraction of component j, and ρ_m is the molar density of the mixture; R, V, f_i and $\bar{V}_i$ are the universal gas constant, the total volume, the fugacity of component i, and the partial molar volume of component i, respectively. By using an equation of state, $\bar{V}_i$ and f_i can be obtained. The diffusion flux, Eq. 2.5, can be written in a new form:

$$\vec{J}_i = -\frac{RL_{ii}}{M_i x_i M_n x_n} \left\{ \frac{M_i x_i M_n x_n L_{iq}}{RL_{ii}} \frac{\nabla T}{T^2} + \frac{M_i x_i}{L_{ii}} \sum_{k=1}^{n-1} L_{ik} \sum_{j=1}^{n-1} \frac{M_j x_j + M_n x_n \delta_{jk}}{M_j} \sum_{l=1}^{n-1} \left.\frac{\partial \ln f_j}{\partial x_l}\right|_{x_l,T,P} \nabla x_l \right.$$

$$\left. + \frac{M_i x_i}{RTL_{ii}} \sum_{k=1}^{n-1} L_{ik} \left(\sum_{j=1}^{n-1} x_j \bar{V}_j + \frac{M_n x_n}{M_k} \bar{V}_k - \frac{1}{\rho_m} \right) \nabla P \right\}, \qquad i=1,........,n-1 \tag{2.11}$$

The diffusion flux vector, $J = (\vec{J}_1,....\vec{J}_{n-1})$ is written in short form:

$$J = -\rho_m (D\nabla x + D_T \nabla T + D_P \nabla P) \tag{2.12}$$

where $D = \left[D_{ij} \right]$, $D_T = (D_{T1},.....,D_{Tn-1})$, $D_P = (D_{P1},.....,D_{pn-1})$ and $\nabla x = (\nabla x_1,.......\nabla x_{n-1})$, the molecular or Fick's diffusion coefficients, D_{ij} (m²/s), the thermodiffusion coefficients, D_{Ti} (m²/s/K), and the pressure diffusion coefficients, D_{Pi} (m²/s/Pa) can be given based on Eq. 2.11 as:

$$D_{ij} = a_{in} d_{in} \frac{M_i x_i}{L_{ii}} \sum_{k=1}^{n-1} L_{ik} \sum_{l=1}^{n-1} \frac{M_l x_l + M_n x_n \delta_{lk}}{M_l} \left.\frac{\partial \ln f_l}{\partial x_j}\right|_{x_j,T,P}, \quad i,j=1,.....n-1 \tag{2.13}$$

22

$$D_{T_i} = a_{in}d_{in}M\frac{k_{Ti}}{T}, \qquad i = 1,.....,n-1 \tag{2.14}$$

$$D_{pi} = a_{in}d_{in}\frac{M_i x_i}{RTL_{ii}}\sum_{k=1}^{n-1}L_{ik}\left(\sum_{j=1}^{n-1}x_j\bar{V}_j + \frac{M_n x_n}{M_k}\bar{V}_k - \frac{1}{\rho_m}\right), \qquad i = 1,.....,n-1 \tag{2.15}$$

δ_{lk} is the Kronecker delta function, $\delta_{lk} = 1$ for $l=k$ and $\delta_{lk} = 0$ for $l \neq k$, M_i is the molecular weight of component i, M_n is the molecular weight of the reference component n, and M is the average molecular weight of the mixture ($M = \sum_{i=1}^{n}M_i x_i$), the coefficients a_{in}, d_{in}, and k_{Ti} are given by:

$$a_{in} = \frac{M_i M_n}{M^2} \tag{2.16}$$

$$d_{in} = \frac{RL_{ii}M^2}{\rho_m x_i x_n M_i^2 M_n^2} \tag{2.17}$$

$$k_{Ti} = \frac{L_{iq}x_i x_n M_i M_n}{RTML_{ii}} = \alpha_{Ti}x_i x_n \tag{2.18}$$

Comparing Eq. 2.18 and Eq. 2.14, one can get the following formulation

$$\alpha_{Ti} = \frac{\rho_m D_{Ti}TM_i M_n}{L_{ii}RM}, \quad i = 1,2,...........,n-1 \tag{2.19}$$

where k_{Ti} is the thermal diffusion ratio of component i, and α_{Ti} is the thermal diffusion factor of component i. The pressure diffusion is usually ignored in experimental approaches; because the magnitude of the pressure diffusion is about three orders smaller

than that of thermodiffusion. Therefore, the pressure in the mixture is assumed constant. Thus, the diffusion expression (Eq. 2.11) can be re-written as:

$$\vec{J}_i = -\frac{RL_{ii}}{M_i x_i M_n x_n}\left(\begin{array}{l}\dfrac{M_i x_i M_n x_n L_{iq}}{RL_{ii}}\dfrac{\nabla T}{T^2} + \\ \dfrac{M_i x_i}{L_{ii}}\displaystyle\sum_{k=1}^{n-1}L_{ik}\sum_{j=1}^{n-1}\dfrac{M_j x_j + M_n x_n \delta_{jk}}{M_j}\sum_{l=1}^{n-1}\dfrac{\partial f_j}{\partial x_l}\bigg|_{x_{l,T,P}} \nabla x_l,\end{array}\right) \tag{2.18}$$

Another method of expressing the heat flux in Eq. 2.2, $\vec{J}_q$, is based on combining the concept of irreversible thermodynamics and molecular kinetic theory involving the heat of transport (Tichacek $et\ al.$, 1956, and Denbigh, 1951):

$$\vec{J}_q = \sum_{k=1}^{n}\frac{Q_k}{M_k}\vec{J}_k \tag{2.19}$$

where Q_k is the heat of transport of component k. Therefore, the expression for $\vec{J}_q^*$ becomes:

$$\vec{J}_q^* = \sum_{k=1}^{n}\frac{Q_k - \bar{H}_k}{M_k}\vec{J}_k = \sum_{k=1}^{n}\frac{Q_k^*}{M_k}\vec{J}_k \tag{2.20}$$

where Q_k^* is the net heat of transport of component k. Consequently, Eq. 2.3 can be re-written in terms of the net heat of transport:

$$\sigma = -\frac{1}{T}\sum_{k=1}^{n-1}\left[\left(\frac{Q_k^*}{M_k} - \frac{Q_n^*}{M_n}\right)\frac{\nabla T}{T} + \nabla_T\left(\frac{\mu_k}{M_k} - \frac{\mu_n}{M_n}\right)\right]\cdot\vec{J}_k \tag{2.21}$$

Using Eq. 2.21, one can write the phenomenological equation for diffusion flux (Eq. 2.5) in the following form:

$$\vec{J}_i = -\frac{1}{T} \sum_{k=1}^{n-1} L_{ik} \left[\left(\frac{Q_k^*}{M_k} - \frac{Q_n^*}{M_n} \right) \frac{\nabla T}{T} + \nabla_T \left(\frac{\mu_k}{M_k} - \frac{\mu_n}{M_n} \right) \right], \quad i = 1, ..., n-1 \tag{2.22}$$

Comparing Eq. 2.22 with Eq. 2.5, the following formulation can be derived:

$$L_{iq} = \sum_{k=1}^{n-1} L_{ik} \left(\frac{Q_k^*}{M_k} - \frac{Q_n^*}{M_n} \right), \qquad i = 1, ..., n-1 \tag{2.23}$$

As introduced in Section 1.4.1, the net heat of transport of component i can be expressed by:

$$Q_i^* = -\frac{\Delta \bar{U}_i}{\tau_i} + \left(\sum_{j=1}^{n} \frac{x_j \Delta \bar{U}_j}{\tau_j} \right) \frac{\bar{V}_i}{\sum_{j=1}^{n} x_j \bar{V}_j}, \qquad i = 1, ..., n \tag{2.24}$$

2.2 Equation of State

It is a prerequisite to know reliable thermodynamic properties for the theoretical research on thermodiffusion. The thermodynamic properties are difficult to obtain fully from the literature and some of the properties are very difficult to measure accurately. It should be kept in mind that in all of the models mentioned in Chapter 1 some thermodynamic properties, including $\left(\frac{\partial \mu_1}{\partial x_1} \right)$, U_i, H_i and V_i, are required. These values, together with another important thermodynamic property density, need to be derived from the equation of state (EOS). Therefore, for a certain mixture of interest the accuracy of the model not only relies on the model, but also on the EOS of choice as well as the numerical method utilized in the calculation.

Two equations of state have been used in this research; the first is Peng-Robinson Equation of State (PR-EoS), (Peng and Robinson, 1976). It is one of the most popular cubic equations of state, and it is commonly used in the petroleum industry for hydrocarbon mixtures due to its simplicity and accuracy. The other equation of state is the volume translated Peng-Robinson Equation of State (vt-PR-EoS). In this equation of state, the molar volume in PR-EoS has been replaced by a corrected volume term. More details of these two equations of state will be introduced in the next sections.

2.2.1 Peng-Robinson Equation of State (PR-EoS)

Peng and Robinson (1976) suggested an equation of the form:

$$P = \frac{RT}{\bar{V} - b_p} - \frac{a_p(T)}{\bar{V}(\bar{V} + b_p) + b_p(\bar{V} - b_p)}$$

(2.25)

Where P is the pressure, $\bar{V}$ is the molar volume, a_p is the attraction parameter (temperature dependent), R is the universal gas constant, and b_p is the co-volume parameter which refers to the volume occupied by molecules under an infinitely high pressure.

The compressibility factor Z can be expressed as:

$$Z = \frac{P\bar{V}}{RT}$$

(2.26)

Based on the PR-EoS, Eq. 2.24 can be re-written:

$$Z = \frac{\bar{V}}{\bar{V} - b_p} - \frac{a_p(T)\bar{V}}{RT(\bar{V}(\bar{V} + b_p) + b_p(\bar{V} - b_p))}$$

(2.27)

where a_p and b_p are component-dependent parameters; b_p is independent of temperature and a_p is temperature and acentric factor dependent (ω). Both parameters can be calculated from critical pressure (P_c) and critical temperature (T_c) by:

$$a_p = 0.45724 \frac{R^2 T_c^2}{P_c} \left(1 + \lambda \left(1 - T_r^{1/2}\right)\right)^2 \tag{2.28}$$

$$b_p = 0.0778 \frac{R T_c}{P_c} \tag{2.29}$$

where T_r is the reduced temperature $(T_r = T/T_c)$, λ is a function of the acentric factor given by:

$$\lambda = 0.37464 + 1.5422\omega - 0.26992\omega^2 \qquad 0 < \omega < 0.5 \tag{2.30}$$

$$\lambda = 0.3796 + 1.485\omega - 0.1644\omega^2 + 0.01667\omega^3 \qquad 0.5 < \omega < 2 \tag{2.31}$$

For mixtures, the parameters a_p and b_p can be obtained according to certain mixing rules. The following mixing rule has been established for hydrocarbon mixtures:

$$a_p = \sum_{i=1}^{n} \sum_{j=1}^{n} x_i x_j a_{ij}^{0.5} \tag{2.32}$$

$$a_{ij} = (1 - k_{ij}) a_{pi}^{0.5} a_{pj}^{0.5} \tag{2.33}$$

$$b_p = \sum_{i=1}^{n} x_i b_{pi} \tag{2.34}$$

where a_{pi} and b_{pi} are the pure component parameters, x_i is the mole fraction, and k_{ij} is the interaction parameter between the ith and jth components. In this work, it should be noted that for simplicity, the binary interaction parameters for hydrocarbon mixtures are assumed to be zero in all the Equation of State.

2.2.2 The volume translated Peng-Robinson Equation of State (vtPR-EoS)

The volume translation method has been proposed to modify the original PR-EoS by Peneloux *et al.* (1982) and Jhaverl and Youngren (1988). In this method, the predicated molar volume from the original PR-EoS is corrected by introducing a shift parameter, s_{vi}, to obtain a new molar volume (corrected molar volume), which is expressed by this relation:

$$\bar{V}_{corrected} = \bar{V}_{PR-EoS} - x_i s_{vi} b_{pi} \tag{2.35}$$

The shift parameters will be calculated by matching the pure molar liquid volume from PR-EoS to experimental data when a reduced temperature is equal to 0.7 ($T_r = 0.7$).

2.3 Governing equations in porous medium

The purpose of this section is to introduce the governing partial differential equations that describe the mixture fluid flow in a reservoir where the porous matrix, thermo-solutal and gravitational driving force control the flow behaviour. To represent flow behaviour in porous media, suitable boundary and initial conditions must be considered and selected, and appropriate governing equations derived. Therefore, mass continuity, momentum conservation and energy conservation equations are introduced.

2.3.1 The mass continuity equation

The mass continuity equation is given by:

$$\frac{\partial \rho_m}{\partial t} + \nabla \bullet \left(\rho_m \vec{V} \right) = 0 \qquad (2.36)$$

where ρ_m is the molar density of the mixture. $\vec{V} = u\vec{i} + v\vec{j} + w\vec{k}$ is the average of the fluid mixture velocity vector, u, v and w are the velocity components of x, y and z directions, respectively. $\vec{v}$ has been given various names, by different authors, such as seepage velocity, superficial velocity, and Darcy velocity. The term Darcy velocity is selected for this work; taking an average of the fluid velocity over a volume element consisting of fluid only yields the intrinsic average velocity $\vec{V}$, which is related to the Darcy velocity, by the Dupuit-Forchheimer relationship, (Nield and Bejan, 2006), as:

$$\vec{v} = \varphi \vec{V} \qquad (2.37)$$

For multicomponent mixture, the continuity equation of component i is given as:

$$\frac{\partial (\rho_m x_i)}{\partial t} + \nabla \bullet \left(\rho_m x_i \vec{V} \right) = -\nabla \bullet \vec{J}_{mi}, \quad i = 1, 2, \ldots\ldots n\text{-}1 \qquad (2.38)$$

where $\vec{J}_{mi}$ is the molar diffusion flux of the ith component; x_i is the mole fraction of the component i; $\rho_{mi} = \rho_m x_i$ is the molar density of the ith component. The molar diffusion flux is subjected to a linear relationship of the driving forces of temperature and concentration gradients and it can be expressed by:

$$\left\{ \vec{J}_{mi} \right\} = -\rho_m \left(\sum_{j=1}^{n-1} \left[D_{ij}^* \right] \nabla X + \left\{ D_{Ti}^* \right\} \nabla T \right) \qquad (2.39)$$

For binary mixtures, $\nabla X = \nabla x_1$ and $\vec{J}_{mi} = \vec{J}_{m1}$, and for ternary mixtures, $\nabla X = \begin{pmatrix} \nabla x_1 \\ \nabla x_2 \end{pmatrix}$

and $\vec{J}_{mi} = \begin{pmatrix} \vec{J}_{m1} \\ \vec{J}_{m2} \end{pmatrix}$. D^*, and D_T^* are the molecular diffusion and thermodiffusion coefficients

of the fluid mixture in a porous medium, respectively.

2.3.2 Darcy's law

The porous matrix is assumed homogeneous and isotropic. Therefore, the Darcy's law is applied. This is an empirical law formulated by the French engineer H. Darcy, (Darcy, 1856), and it is applicable to creeping flow, which generally describes the dynamics of most flows through porous media; it is written as:

$$\vec{v} = -\frac{\kappa}{\eta}(\nabla P - \rho \vec{g}) \tag{2.40}$$

where κ is the permeability of a porous medium; η is the dynamic viscosity of the fluid mixture, ρ is the mass density of the fluid mixture, and $\vec{g}$ is the gravitational acceleration vector. By substituting the Darcy relation (Eq. 2.40) into the mass conservation equation (Eq. 2.36) the pressure can be derived from the obtained differential equation, which leads to the following equation for pressure:

$$\frac{\partial \rho_m}{\partial t} - \frac{\kappa}{\eta}\frac{\partial}{\partial x}\left(\rho_m\left(\frac{\partial P}{\partial x} + \rho g_x\right)\right)$$
$$-\frac{\kappa}{\eta}\frac{\partial}{\partial y}\left(\rho_m\left(\frac{\partial P}{\partial y} + \rho g_y\right)\right) - \frac{\kappa}{\eta}\frac{\partial}{\partial z}\left(\rho_m\left(\frac{\partial P}{\partial z} + \rho g_z\right)\right) = 0 \tag{2.41}$$

2.3.3 The thermal energy conservation equation

The thermal energy conservation equation for the matrix or solid phase can be expressed as follows, (Nield and Bejan, 2006):

$$(1-\varphi)(\rho C_p)_s \frac{\partial T_s}{\partial t} = (1-\varphi)k_s \nabla^2 T_s \tag{2.42}$$

where T_s is the temperature of the matrix or solid, For the fluid mixture inside the porous medium, it can be expressed as:

$$\varphi(\rho C_p)_{fl} \frac{\partial T_{fl}}{\partial t} + \varphi \vec{V} \bullet \nabla\left((\rho C_p)_{fl} T_{fl}\right) = \varphi k_{fl} \nabla^2 T_{fl} \tag{2.43}$$

where T_{fl} is the temperature of the fluid mixture. Since the velocity of the matrix is zero, and there is no viscous dissipation and heat generation in either porous medium or the fluid mixture. And since in addition, thermal equilibrium was assumed between the solid and the liquid phases and occurs very quickly. The temperature of the matrix is assumed to be equal to the temperature of the fluid mixture $(T_s = T_{fl} = T)$. By adding, Eqs. 2.42 and 2.43, the energy conservation equation can be written as follows:

$$(\rho C_p)_e \frac{\partial T}{\partial t} + \vec{v} \bullet \nabla\left((\rho C_p)_{fl} T\right) = k_e \nabla^2 T \tag{2.44}$$

where $(\rho C_p)_e$ is the effective volumetric heat capacity and k_e is the effective thermal conductivity of the system. These effective physical parameters are related to the fluid properties and the solid matrix properties as follows:

$$(\rho C_p)_e = \varphi(\rho C_p)_{fl} + (1-\varphi)(\rho C_p)_s \tag{2.45}$$

31

$$k_e = \varphi k_{\mathrm{fl}} + (1 - \varphi)k_s \qquad\qquad\qquad (2.46)$$

where $(\rho C_p)_{\mathrm{fl}}$ is the fluid volumetric heat capacity, $(\rho C_p)_s$ is the matrix volumetric heat capacity, k_{fl} the fluid thermal conductivity, and k_s is the matrix or porous medium thermal conductivity.

Chapter 3

Measurement of Soret Coefficient in Porous Medium: Comparison with Numerical Model

In this chapter, the validation of a new thermodiffusion cell designed to measure the molecular diffusion coefficient and the Soret coefficient of hydrocarbon binary systems under high pressure in a porous medium is presented. The experimental apparatus and the procedures are explained in this chapter. The results of the experiment are compared with the benchmark values and the theoretical model, which is developed in this chapter.

3.1 Introduction

Several experimental methods were developed on the ground and in microgravity to measure both molecular diffusion and the Soret coefficients of binary mixtures at atmospheric pressure (Bou-Ali *et al.*, 2003, Wittko and Kohler, 2003, Van Vaerenbergh and Legros, 1998), in order to provide a good understanding of separation processes and molecular interaction.

Recently, the oil industry has shown a great interest in studying transport properties. Since conditions under which crude oil is found underground imply high pressure (HP) and diffusion in a porous medium, it is considered important to analyze the influence of the pressure and the interaction with a porous medium on the transport properties of liquid mixtures. This is done in order to achieve a better reliability of the algorithms used for the simulation of crude oil flow in the oil fields. Nevertheless, thermodiffusion data under reservoir conditions, i.e. at high pressures, are very scarce and not very recent [Rutherford and Drickamer (1954), Rutherford and Roof (1959)]. More recently, one may cite the high pressure measurements of the thermodiffusion coefficients made with a thermogravitational column (Urteaga *et al.* 2006, and Urteaga *et al.* 2008). This lack of HP measurements has led to the development of the Soret Coefficient for Crude Oil

(SCCO) project (Van Vaerenbergh *et al.*, 2009). The main objective of this project is to perform microgravity measurements of thermodiffusion of various mixtures under HP conditions. Additionally, in the frame of this project, a ground HP experimental device, to measure thermodiffusion and molecular diffusion in binary mixtures, was designed.

3.2 Experimental Setup

3.2.1 Experimental description of the apparatus

Figure 3.1 shows the experimental set up. The thermodiffusion cell is a cylinder, which is closed by two caps and connected to two thermoregulator baths that impose a thermal gradient along the axial direction of the cylinder. To avoid convection, a monolithic porous medium, which is silica (for silica porous medium, $\varphi = 0.45$ and $\kappa = 20$ mD), nearly fills the cell. Figure 3.3 shows the porous medium cylinder. At each extremity of the porous medium, a dead-volume allows the passage of a laser beam through sapphire windows. The cell, connected to the circuit of the filling and placed under the desired pressure, is installed in a Mach-Zehnder interferometer, as shown in Figure 3.1.

The inner diameter of the cell is $d = 10$ mm. The thickness of each dead-volume is 6.4 mm and the length of the porous medium in the middle of the cell is 32.2 mm, (Figure 3.2). The thermodiffusion cell is designed to test a liquid mixture for a range of pressure between 1 and 1000 bar, and for a range of temperature between 5 ^{o}C and 40 ^{o}C. Two thermocouples (type K) are located in the middle of the dead-volumes in order to measure the temperature. A constant frequency red He-Ne laser, (with wavelength $\lambda_0 = 632.8$ nm, linearly polarized and output 5.0 mW) is used as a light source. The cell is covered by an insulator, in order to prevent any heat transfer from the cell wall, and the capillary tube between the cell and the manometer is insulated with foam.

The following steps explain the procedure for filling the cell; the cell can be set in horizontal or vertical positions, while the cell filling is always made in a vertical position from the bottom:

1. The valve (V_1) between fluid reservoir and volumetric pump is closed. Valves V_3 and V_4 are opened;

2. A vacuum is made in the cell and in the volumetric pump; then valve V_4 is closed;

3. The vacuum valve (V_2, which is a three-way valve) between the vacuum pump and the cell is closed; then the vacuum pump is disconnected;

4. The valve (V_1) between the fluid reservoir and volumetric pump is opened. Due to the difference of pressure, the cell and the volumetric pump are filled;

5. The valves V_2 and V_4 are opened. A total of 100 cc of mixture to be studied circulates through the cell (under visual observation through the sapphire windows in the dead volumes, to make sure that there are no bubbles inside the cell);

6. Upon determining that the cell is totally filled, valve V4 is closed;

7. Finally, the desired pressure is achieved with a volumetric pump by pushing liquid into the cell; then valve V3 is closed and the volumetric pump is disconnected from the circuit.

The cell is positioned in a Mach-Zehnder interferometer in order to detect the variation of the refractive index between the hot and cold dead-volumes. A monochrome CCD camera (1004x1004 pixels) collects the interferograms generated by the interference of the two beams passing through the dead-volumes of the cell. A rotation of the beam-splitter BS_2 is necessary to obtain delocalised fringes in front of the monochrome CCD camera. Figure 3.4 shows the fringe direction, which depends on the cell position. When the cell is in the horizontal position, fringes are in the vertical direction, and vice versa. The interferograms grabbed by the CCD camera are recorded on a computer with the aid of custom-made software. For more details see Appendix A.
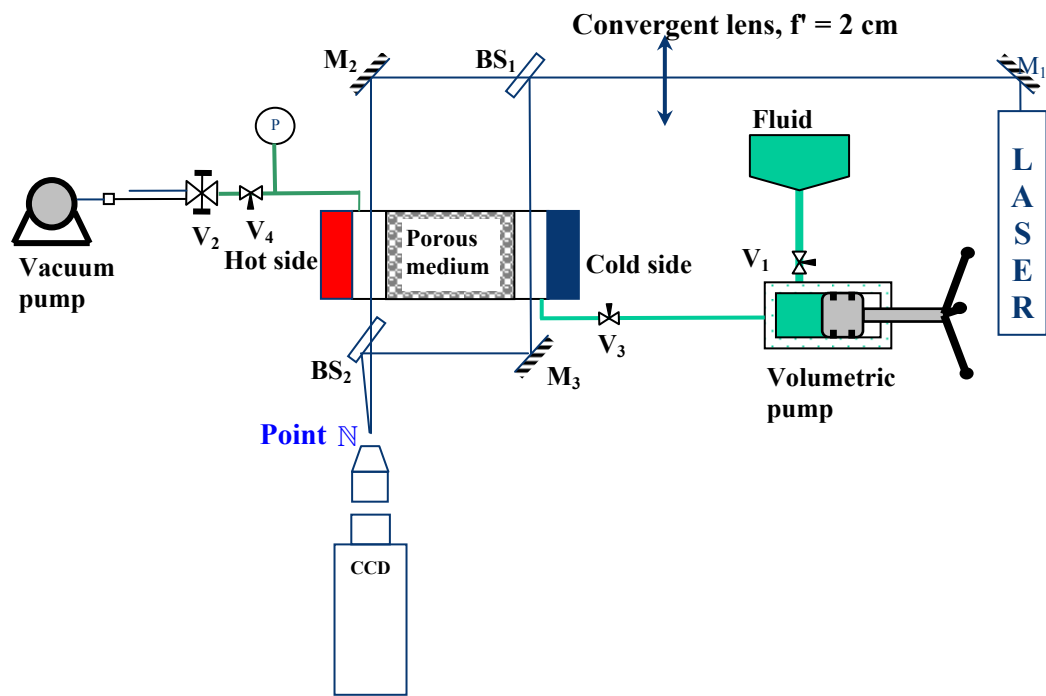
Figure 3.1: Experimental setup. M_1, M_2 and M_3 are mirrors; BS_1 and BS_2 are beam-splitters; V_1, V_2, V3 and V_4 are valves used for the filling of the cell.

Cell with insulator

Cell with out insulator
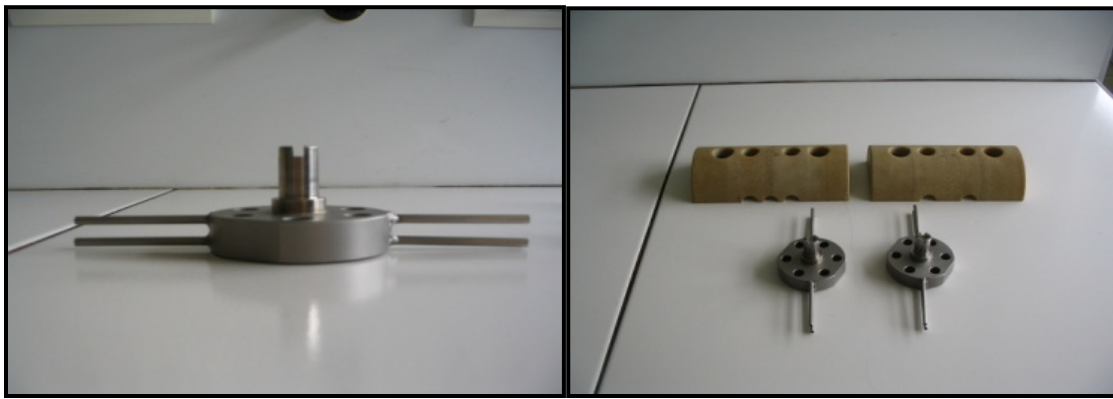
Cap

Cap and the insulator
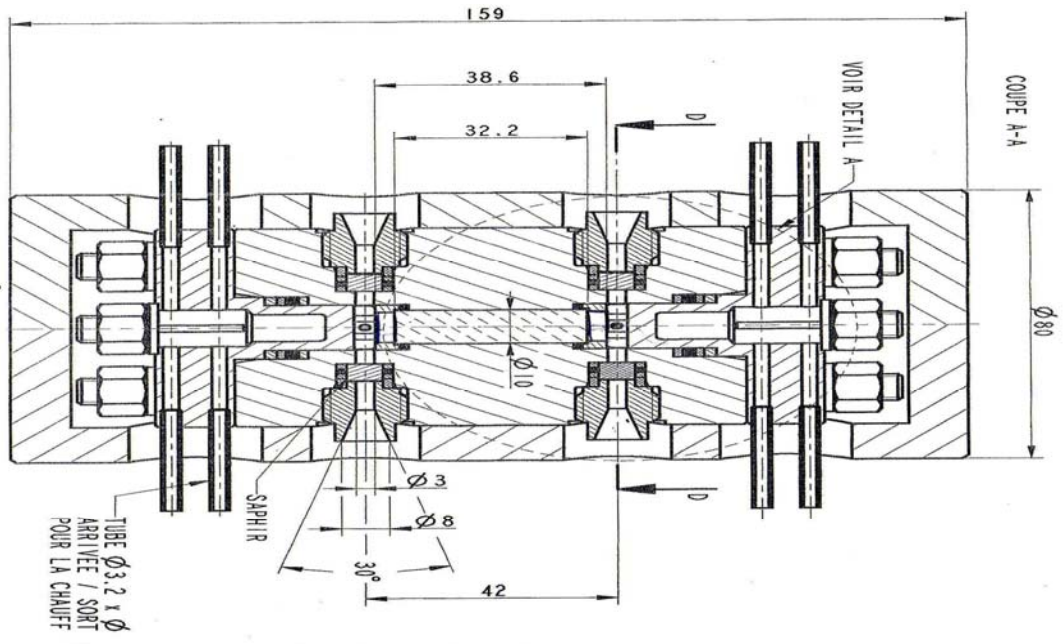
Figure 3.2: Cell design and geometrical configuration.

Figure 3.3: Photo of the porous medium used.

| (a) | (b) |
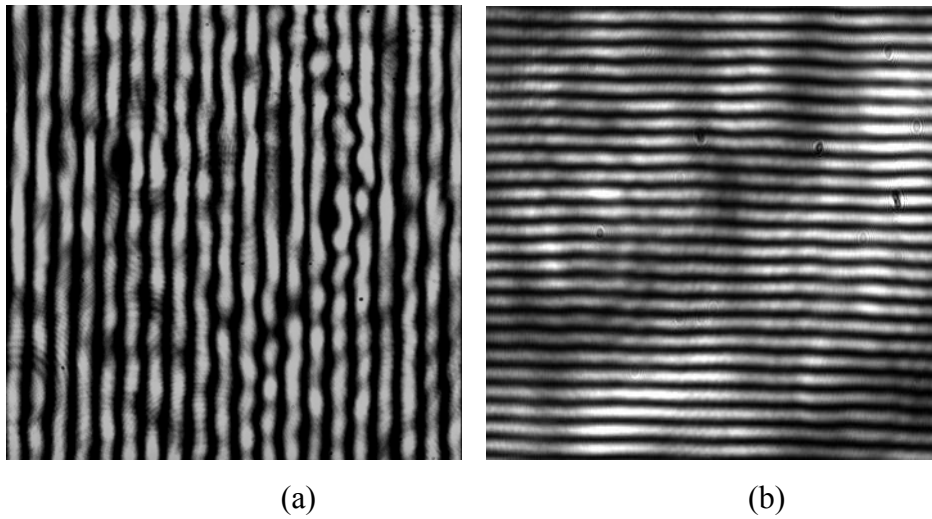
Figure 3.4: Interferogram recorded with a) the cell in horizontal position and b) the cell in vertical position.

The phase difference (Φ) between the two laser beams at the point of the interference field is represented by the difference between the phase of the beam that the crosses dead-volume at the hot side and the one that crosses the dead-volume at its cold side. The phase difference can be given as:

$$\Phi = \left(wt - k_2 d - kr \right) - \left(wt - k_1 d - kr - k\Delta \right) \tag{3.1}$$

where w is the pulsation of the two beams; k_2 is the wave number of the beam with refractive index n_2 at the hot side of the cell with thickness d; k_1 is the wave number of the beam with refractive index n_1 at the cold side (same thickness); k is the wave number of the beams in air; r corresponds to the distance covered in the air by the two beams when the interferometer is adjusted at the optical contact, and Δ is the supplementary path difference covered by the beam that crosses the cold dead-volume considering the rotation of the beam splitter BS$_2$. The phase difference at point $\mathbb{N}$ is simplified as follows:

$$\Phi = -\left(k_2 - k_1 \right) d + k\Delta \tag{3.2}$$

k_1 and k_2 are given in terms of the wave length (λ_0) in the vacuum as follows:

$$k_1 = \frac{2\pi n_1}{\lambda_0}, \quad \text{and} \quad k_2 = \frac{2\pi n_2}{\lambda_0} \tag{3.3}$$

Relation (3.2) becomes:

$$\Phi = -\frac{2\pi}{\lambda_0}\left(n_2 - n_1 \right) d + k\Delta \tag{3.4}$$

Initially, the two baths of the thermoregulators are set at the same temperature (low temperature). The refractive index is the same in the two dead-volumes. Then, from Eq. 3.4, the phase difference depends only on the rotation of BS$_2$. The right side of the cell is

heated (T_2) and the other side is kept at a low temperature (T_1) (assuming that the cell is in a horizontal position). And the top side of the cell is heated (if the cell is in a vertical position); therefore, $T_2 > T_1$. $\Delta T = T_2 - T_1$ is the temperature difference between the hot side and the cold side of the cell. The phase difference for each orientation of BS$_2$, is constant; Eq. 3.4 can be re-written as:

$$\Delta\Phi = -\frac{2\pi d}{\lambda_0}(\Delta n_2 - \Delta n_1) \tag{3.5}$$

where $\Delta\Phi$ is the total variation of the phase difference between the laser beams having crossed the hot side and clod side, and $\Delta n = \Delta n_2 - \Delta n_1$ represents the total variation of the refractive index between the hot side and the cold side. Eq. 3.5 can be re-written as:

$$\Delta\Phi = -\frac{2\pi d}{\lambda_0}\Delta n \tag{3.6}$$

For binary systems, the variation of refractive index is:

$$\Delta n = \frac{\partial n}{\partial T}\Delta T + \frac{\partial n}{\partial c}\Delta c \tag{3.7}$$

where Δc is the concentration difference of the densest component between the hot and the cold sides. Coefficients $\partial n/\partial T$ and $\partial n/\partial c$ are the so-called contrast factors (Wittko and Köhler, 2003). At this initial stage, the thermal kinetics provides a significant change in the magnitude of phase difference [Zhang *et al.* (1996), Urteaga *et al.* (2006)]. Hence, their effects are completely decoupled. At the beginning of the experiment, the thermal gradient is dominant, so Eq. 3.7 can be simplified:

$$\Delta n \approx \frac{\partial n}{\partial T}\Delta T \tag{3.8}$$

when $\partial n / \partial T < 0$, the phase difference at point $\mathbb{N}$ (Figure 3.1) is going to be increased (Eq. 3.6), and produces a scrolling of fringes. Once the thermal gradient is established, the second term in Eq. 3.7 becomes dominant due to the variation of the concentration promoted by the Soret effect. If $\partial n / \partial c > 0$, and the system presents a positive Soret coefficient (the densest component goes toward the cold side; therefore $\Delta c < 0$), the phase difference at point $\mathbb{N}$ will be increased with time. Therefore, for systems with a positive Soret coefficient, the mass diffusion must produce a scrolling of fringes in the same direction as the effect of the temperature.

3.2.2 Theoretical relations

During the second stage, when the concentration variation becomes dominant, the concentration difference of the densest component as a function of time is given by Mialdun and Shevtsova (2008), as follows:

$$\Delta c = S_T c_0 \left(1 - c_0\right) \Delta T \left[1 - \frac{8}{\pi^2} \sum_{n,odd} \frac{1}{n^2} \exp\left(-n^2 \frac{t}{\tau_r}\right)\right] \tag{3.9}$$

The two unknown parameters in the above equation are the Soret coefficient S_T and relaxation time τ_r; c_0 is the initial concentration of the densest component; t *is* the time. The relaxation time, where the diffusion takes place in the porous medium, is given by Mialdun and Shevtsova (2008), as follows:

$$\tau_r = \frac{L^2}{\pi^2 D^*} \tag{3.10}$$

where L is the length of diffusion inside the porous medium (L=32.2 mm), and D^* is the molecular diffusion coefficient in the porous medium, which is related to the molecular diffusion coefficient in the free liquid as:

$$D^* = \frac{D}{\tau^2} \tag{3.11}$$

where D is the molecular diffusion coefficient in the free liquid, which is a function of the temperature, and composition of the binary mixture. τ is the tortuosity of the molecular diffusion of the porous medium.

3.2.3 Analysis approach

The phase difference is deduced from the analysis of the interferogram on a single line converted in terms of intensity (gray levels, see Figure 3.5). Light intensity is fitted by:

$$I(x) = a\cos^2(bx - c') \tag{3.12}$$
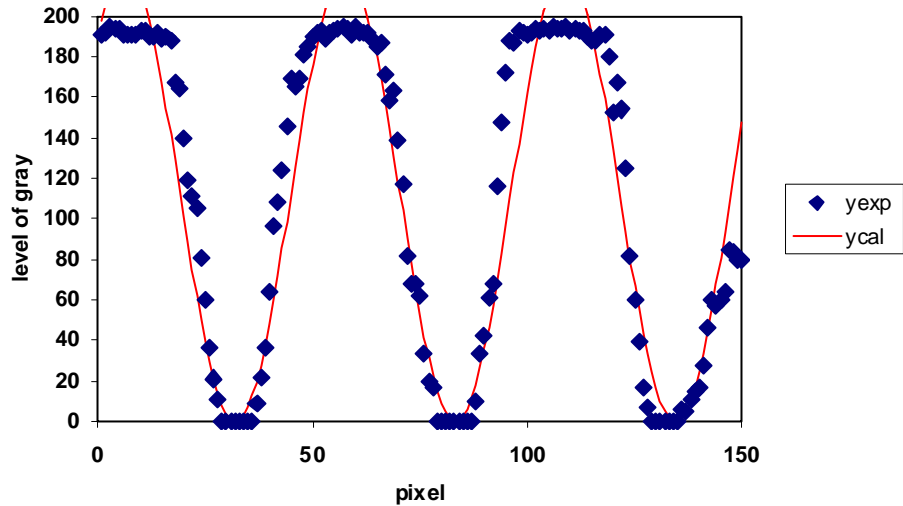
Figure 3.5: Gray level and adjustment of the first 150 pixels of the line 500 of an interferogram (THN/nC12 mixture 50 wt%; $T_{mean} = 25\ °C; \Delta T = 3\ °C$; time $= 512$ s).

The chosen line of pixels is positively oriented from the cold side to the hot side. a, b and c' are computed by the method of least squares. $c' = \Phi / 2$ at $x = 0$. As an adjustment constraint, the condition is imposed that the values of c' must be bounded between $-2/\pi$ and $+2/\pi$. For a continuous and uniform scrolling of fringes, the parameter c', therefore, presents discontinuities. By counting the number of discontinuities, the number

of scrolled fringes can be evaluated. For each scrolling of one fringe, the phase difference between the two laser beams varies by 2π. Then, the phase difference evolution of the second kinetic is fitted by:

$$\Delta\Phi(t) = A \times \left\{ 1 - \frac{8}{\pi^2} \sum_{n,odd} \frac{1}{n^2} \exp\left(-n^2 Bt\right) \right\} + C \qquad (3.13)$$

A, B and C are computed by using the method of least squares. In Eq. 3.13, three terms are retained in the sum leading to a sufficient accuracy (in the sum, n ranges 1 to3). From Eqs 3.6 and 3.7, the concentration difference can be given as:

$$\Delta c = -\frac{\lambda_0 \Delta\Phi}{2\pi d \dfrac{\partial n}{\partial c}} \qquad (3.14)$$

Comparing Eqs 3.9, 3.10, 3.11, 3.13 and 3.14, the following formulations can be derived:

$$S_T = \frac{A \times \lambda_0}{2\pi d \dfrac{\partial n}{\partial c} c_0 \left(1 - c_0\right) \Delta T} \qquad (3.15)$$

$$D = \frac{B \times L^2 \times \tau^2}{\pi^2} \qquad (3.16)$$

3.3 Results and Discussion

3.3.1 Strategy for the validation of the cell

The systems of the benchmark of Fontainebleau are the three binary mixtures of n-dodecane (nC12), isobutylbenzene (IBB) and 1,2,3,4-tetrahydronaphtalene (THN) for a concentration of 50 wt% at a temperature of 25 °C and at atmospheric pressure. The benchmark of the thermodiffusion coefficient D_T, molecular diffusion coefficient D and

Soret coefficient S_T and the values of the contrast factor $(\partial n / \partial c)_{P,T}$ measured for the three different mixtures are shown in Table 3.1, (Platten *et al*., 2003).

Table 3.1: Benchmark values for thermodiffusion coefficient D_T, molecular diffusion coefficient D and Soret coefficient S_T and contrast factors $(\partial n / \partial c)_{P,T}$ at 1 atm and $T = 25\ °C$.

Mixture (50-50 wt%)	D_T ($10^{-12}\ m^2s^{-1}K^{-1}$)	D ($10^{-10}\ m^2s^{-1}$)	S_T ($10^{-3}\ K^{-1}$)	$(\partial n / \partial c)_{P,T}$
IBB-nC12	3.7 ± 0.2	9.5 ± 0.4	3.9 ± 0.1	0.0628 ± 0.0004
THN-nC12	5.9 ± 0.3	6.21 ± 0.06	9.5 ± 0.5	0.1170 ± 0.0004
THN-IBB	2.8 ± 0.1	8.5 ± 0.6	3.3 ± 0.3	0.0544 ± 0.0004

From Eqs. 3.13, 3.14 and 3.15, it is possible to predict which system would present the strongest values of the Soret coefficient and contrast factor, and which would give the strongest amplitude variation for the phase difference between the two laser beams for the second kinetic due to the mass diffusion. For this reason, the interferogram analysis method was tested and the validation of the cell was made on the THN-nC12 system. The two other mixtures presented weaker values for Soret coefficient and contrast factor. Then, the sensitivity of the analysis method was tested on the IBB-nC12 system.

Since the benchmark was measured at atmospheric pressure, the pressure in the cell was kept at the atmospheric value for all experiments in this work. A recent numerical simulation done on the geometry of the cell has shown that in the horizontal position the characteristic times to reach the steady states are different in dead-volumes and in the porous medium, (Melnikov *et al*., 2009). An interaction at interfaces between the dead-volumes and the porous medium, which would affect the diffusion in the cell, was suspected. For this reason, it was decided to validate the cell in the vertical position with top heating in order to avoid convection.

3.3.2 Set-up in vertical position

3.3.2.1 IBB-nC12 system

The thermodiffusion cell is filled with the binary mixture of IBB (50 wt%) and nC12 (50 wt%) at the mean temperature of 25 ^oC and atmospheric pressure. The cell is heated from the top, and the difference of the temperature between the two thermoregulator baths is equal to $\Delta T' = 5$ ^oC (this difference is between the temperatures inside the two caps). Figure 3.6 shows the temperature distribution versus time in the dead-volumes that was measured with thermocouples in one of the experiments. It can be seen from this figure that the temperature difference is less that 5 ^oC, because the measurement of the temperature difference is taken at the centre the dead volumes. The program simultaneously acquires the relevant parameters of the cell, namely, pressure and temperature of the hot and cold dead- volumes via the NI-USB-9162 data acquisition card.
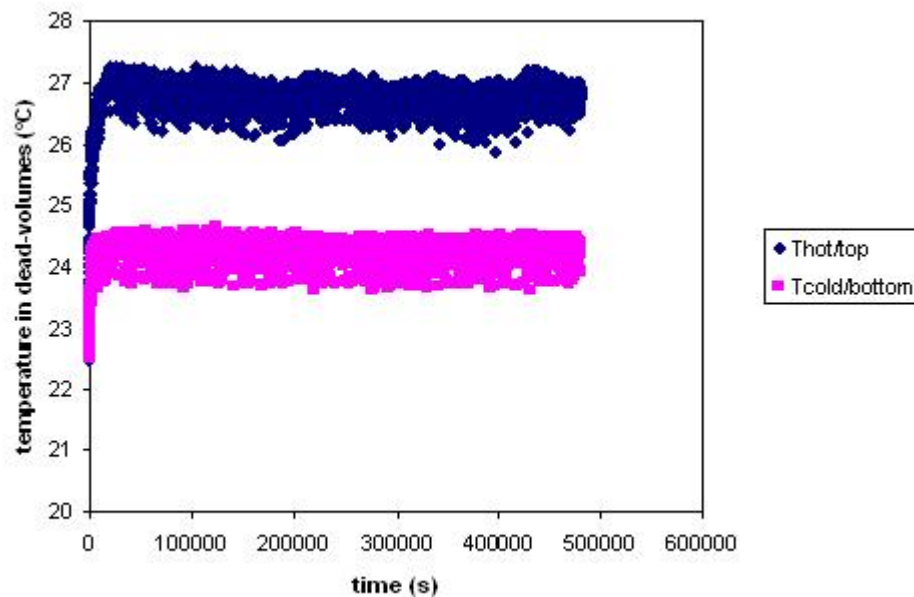
Figure 3.6: Temperature versus time in dead-volumes for the system IBB-nC12 (50 wt%, $T_{mean}=$ 25 °C, $\Delta T' = 5$ ^oC, 1atm, vertical position).

In Figure 3.7, the phase difference between the beam that crossed the hot dead-volume and the beam that crossed the cold dead-volume is plotted. It can be seen that a fast variation is obtained due to the thermal effect (first kinetic); after that a weak variation is observed due to the concentration effect (second kinetic). For both kinetics, the variation of the phase difference has the same sign, which indicates a positive sign for the Soret coefficient. Figure 3.8 shows the details only of the second kinetic of the phase difference for two experiments in the same configuration but with different durations of experiment, i.e. 5-day and 7-day. The initial value of the phase difference in the second experiment is less than in the first one, because the measured difference of temperature in the cell is lower in this experiment ($\Delta T = 3$ ^{o}C for the 7 days experiment and $\Delta T = 2$ ^{o}C for the 5 days experiment, in which are measured between the two dead-volumes). Error bars in Figures 3.7 and 3.8 are not represented the error in the measurement, but they show that the phase difference is measured in a period of time.
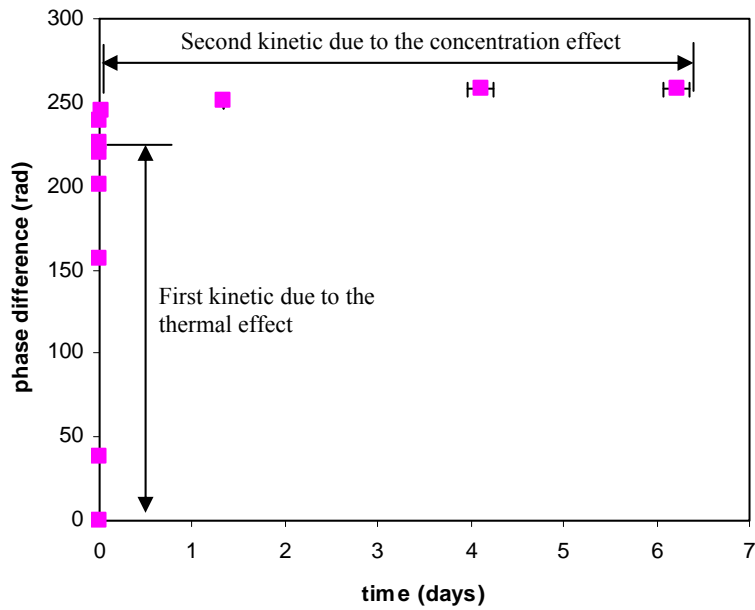
Figure 3.7: Phase difference versus time (nC12-IBB, 50 wt%., $T_{mean} = 25$ °C, $\Delta T' = 5$ °C, 1 atm, vertical position),
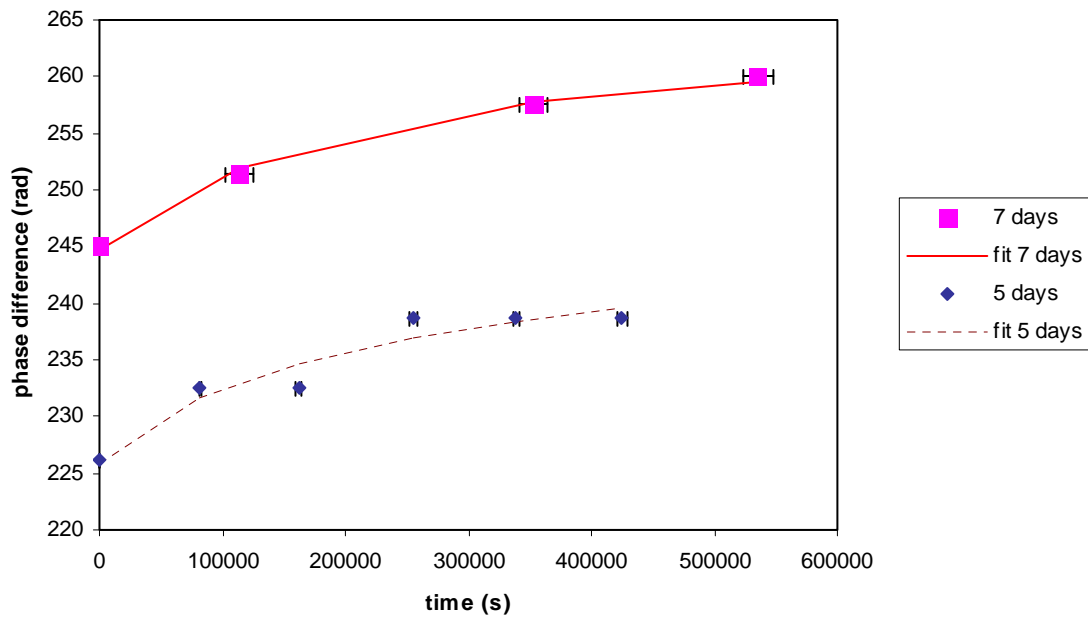
Figure 3.8: Second kinetic of the phase difference evolution for different durations of experiments (IBB-nC12, 50 wt%, $\Delta T' = 5$ °C, 1 atm, vertical position).

In Table 3.2, the results of the adjustment of the two kinetics from Eq. 3.13 are reported. Parameters *A*, *B* and *C* are adjusted by using the method of least squares. Once these values are estimated, the value of tortuosity τ for the porous medium is determined. For both experiments, the same value of τ was found and it is near 1.4. Furthermore, this value is in good agreement with values that have been proposed by previous researchers, Platten *et al.* (2003). The difference between this work value of *D* and the value of the Benchmark of Fontainebleau is less than 1% for both experiments (7 days and 5 days). The same value of parameter B has been found for both experiments (as shown in Table 3.2); the same value of *D* was found, based on Eq. 3.16. A positive sign was found for the Soret coefficient, which is consistent with the literature data. For the experiment of 7 day's duration, a very good agreement was found with the benchmark values and it is much better than that of the 5 day's experiment. The measurement of S_T was based on Eq. 3.15, where the contrast factor ($\partial n / \partial c$) for the IBB-nC12 mixture has been taken from Wittko and Kohler (2003). To reduce the difference, an increase in the experiment duration (more than 7 days) is here recommended.

Table 3.2: Measured difference of temperature *ΔT*, adjustment parameters A, B and C, molecular diffusion coefficient in free liquid *D*, Soret coefficient S_T and (IBB-nC12 50 wt%, T_{mean} = 25 °C, $\Delta T' = 5$ °C, 1 atm).

Duration of the experiment	ΔT (°C)	A	B (10^{-6} s^{-1})	C	D (10^{-10} m^2.s^{-1})	Difference with benchmark	S_T (10^{-3} K^{-1})	Difference with benchmark
7 days	3	18.05	3.80	243.47	9.47	-0.316%	3.95	1.28%
5 days	2	17.91	3.80	224.53	9.47	-0.34%	5.7	31.57%

A new experiment was performed, with a temperature difference of $\Delta T' = 10$ °C between the and the mean temperature T_{mean} = 25 °C was kept the same as in the previous experiments. Figure 3.9 displays temperature distribution of the dead-volumes versus time that was measured with the thermocouples. In Figure 3.10, the phase difference between the laser beam that crosses the hot dead-volume and the laser beam that crosses the cold dead-volume is plotted. In Figure 3.11, the details of the second kinetic are presented.

Table 3.3 shows the results of the adjustment of the second kinetics with Eq. 3.13. An excellent agreement is found between measured D and S_T values and the benchmark values as shown in Table 3.3. The value of the tortuosity is almost the same as in the previous experiments ($\tau \approx 1.4$). The average difference of temperature between dead-volumes was measured ($\Delta T = 4.2$ $^{\circ}$C).
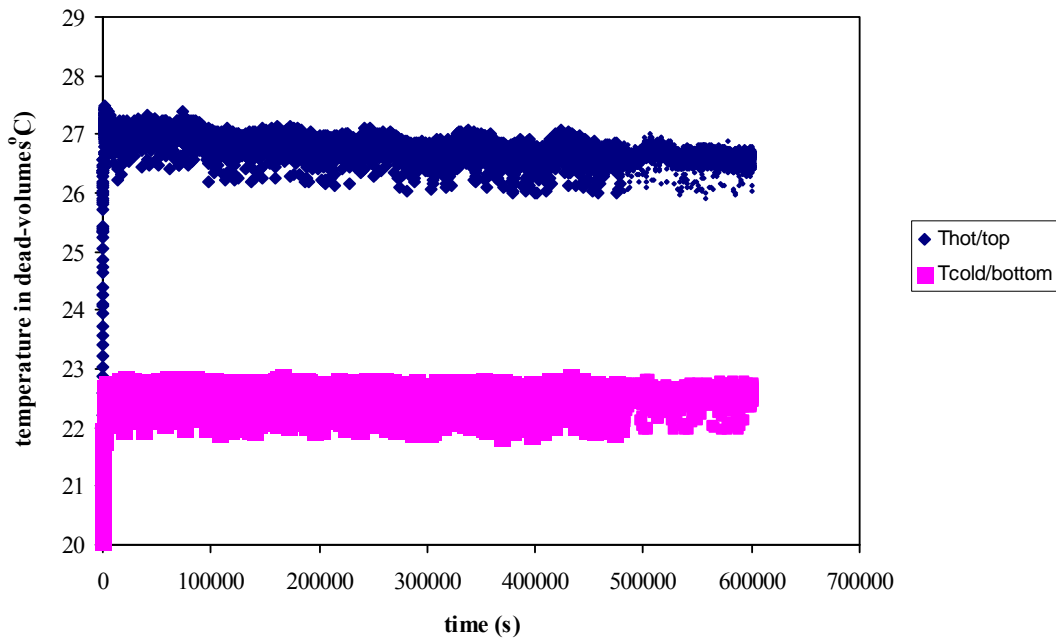
Figure 3.9: Temperature versus time in dead-volumes for the system IBB-nC12 (50 wt%, $T_{mean}=$ 25 °C, $\Delta T' = 10$ $^{\circ}$C, 1atm, vertical position).
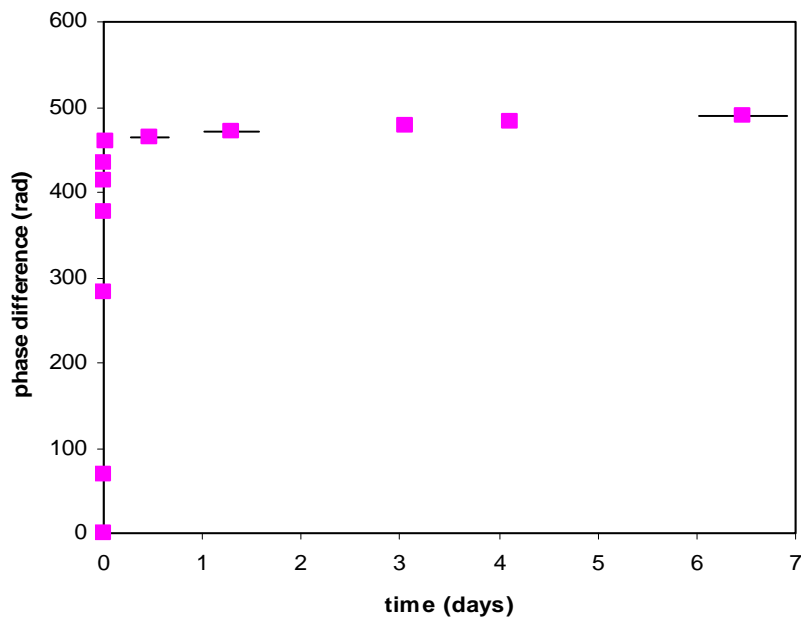
Figure 3.10: Phase difference versus time (nC12-IBB, 50 wt%, T_{mean} = 25 °C, $\Delta T'$ = 5 $^{\circ}$C, 1 atm, vertical position).
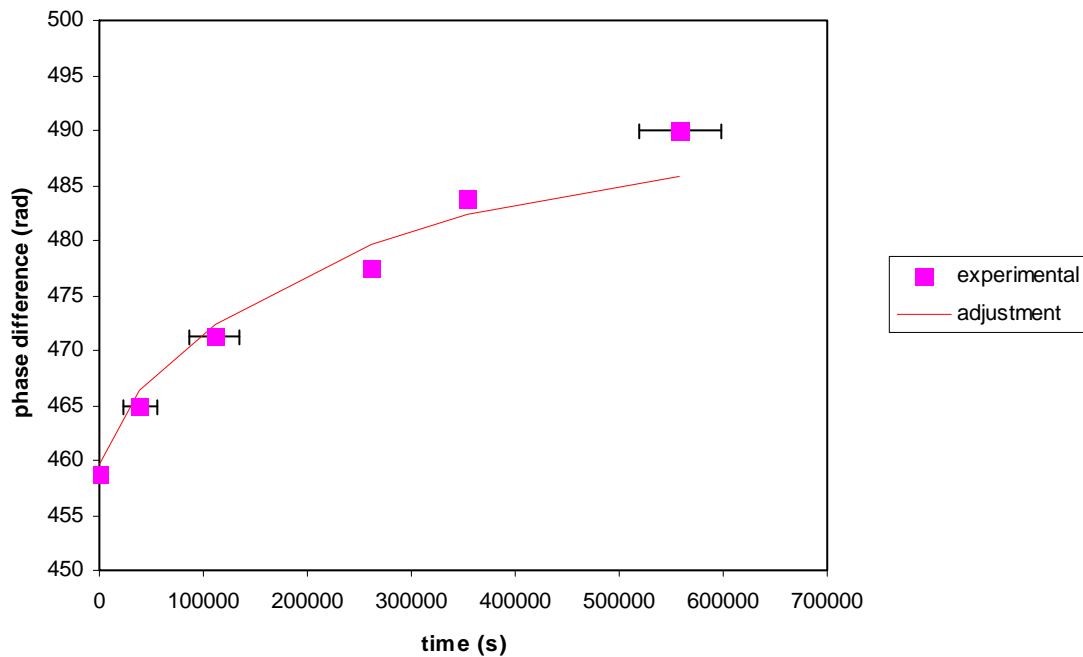
Figure 3.11: Second kinetic of the phase difference evolution for different durations of experiments (IBB-nC12, 50 wt%, $\Delta T' = 10$ $^{\circ}$C, 1 atm, vertical position).

Table 3.3: Adjustment parameters A, B and C, molecular diffusion coefficient in free liquid D, Soret coefficient S_T (IBB-nC12 50 wt%, $T_{mean} = 25$ °C, $\Delta T' = 10$ °C, 1 atm).

Duration of the experiment	A	B $(10^{-6}$ s$^{-1})$	C	D $(10^{-10}$ m^2.s$^{-1})$	Difference with benchmark	S_T $(10^{-3}$ K$^{-1})$	Difference with benchmark
7 days	30.90	3.96	257.63	9.49	-0.105%	4.1	4.878%

3.3.2.2 THN-nC12 system

The cell was filled with a new system of THN (50 wt%) and nC12 (50 wt%) at the mean temperatures T_{mean} = 25 °C and atmospheric pressure. The cell was heated from the top, and the temperature difference between the two baths was set to $\Delta T' = 5$°C. Figure 3.12 shows the details of the second kinetic of the phase difference between the beams that cross the dead-volumes.
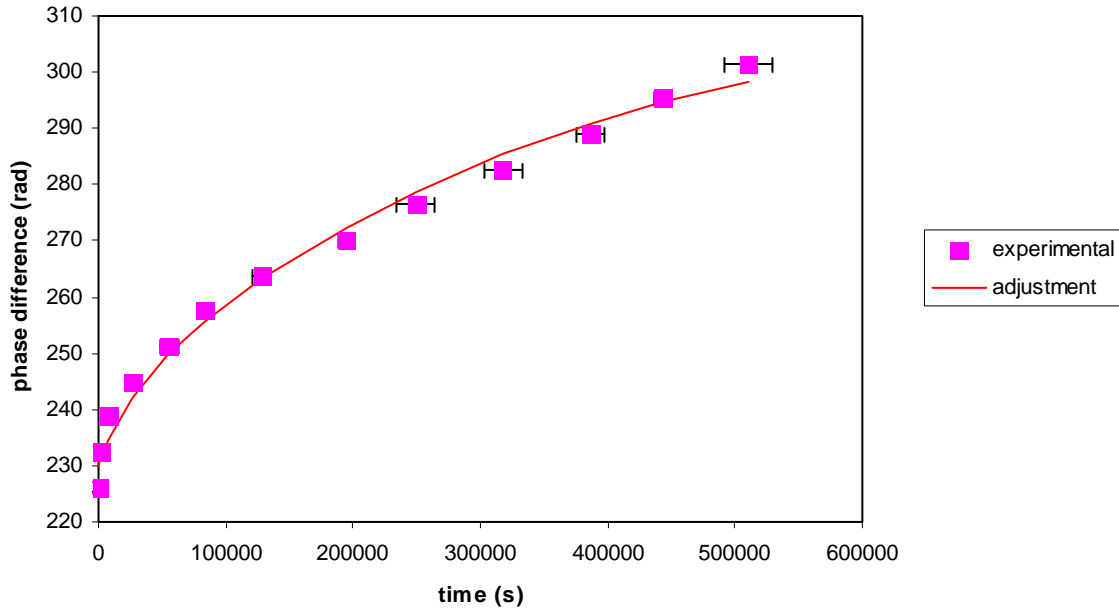
Figure 3.12: Second kinetic of the phase difference evolution for different durations of experiments (THN-nC12, 50 wt%, $\Delta T' = 5$ °C, 1 atm, vertical position).

51

The same procedure was applied for the second kinetic and the results of the adjustment of the second kinetic from Eq. 3.13 are shown in Table 3.4. Once again, a very good agreement is found between these experimental data and the benchmark values. The relative difference between the molecular diffusion coefficient and the value given in literature remains smaller than 1%. The value of the tortuosity is close to the previous one ($\tau \approx 1.4$).

Table 3.4: Adjustment parameters A, B and C, molecular diffusion coefficient in free liquid D, Soret coefficient S_T (THN-nC12 50 wt%., T_{mean} = 25 °C, $\Delta T' = 5$ °C, 1 atm).

Duration of the experiment	A	B (10^{-6} s^{-1})	C	D (10^{-10} $m^2.s^{-1}$)	Difference with benchmark	S_T (10^{-3} K^{-1})	Difference with benchmark
6 days	94.09	2.70	223.59	6.20	-0.162	11.0	13.63%

3.3.3 Experimental cell set-up in the horizontal position

A set of experiments was performed for the cell at the horizontal position. The IBB-nC12 (50-50 wt%) was tested at the mean temperature T_{mean} = 25 °C and atmospheric pressure. The cell was heated from the left side. When the difference of the temperature between the two thermoregulator baths was equal to $\Delta T' = 5$ °C, a transient diffraction pattern grew up, causing the interference fringes to move quickly at the beginning of the experiment, (see Figure 3.13). The phenomenon of diffraction pattern is not perceptible when the set-up is in vertical position. The reason behind this phenomenon is that the convection is established quickly in the dead-volumes when the cell is in horizontal position; thus, the procedure of analysis of interferograms becomes difficult.

(a)   (b)   (c)
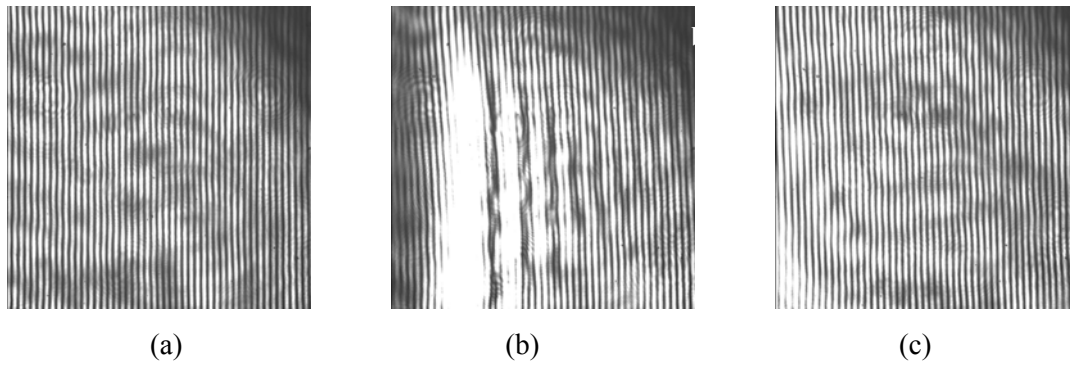
Figure 3.13: Interferogram (IBB-nC12, 50 wt%, $T_{mean} = 25$ °C, $\Delta T' = 5$ ^{o}C, 1 atm, horizontal position) images time recorded for the cell: a) 0 s, b) 1 min and c) 10 min.

Figure 3.14 shows the details of the second kinetic of the phase difference between the beams that cross dead-volumes. The results of the adjustment of the second kinetic from Eq. 3.13 are shown in Table 3.5.
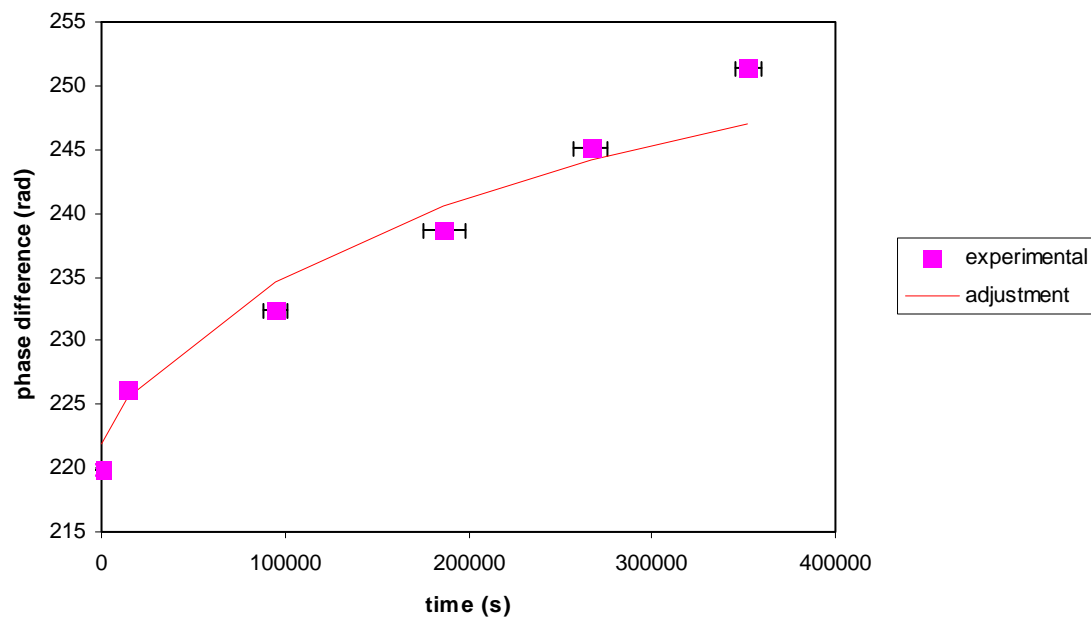
Figure 3.14: Second kinetic of the phase difference evolution for different durations of experiments (IBB-nC12, 50 wt%, $\Delta T' = 5$ ^{o}C, 1 atm, horizontal position).

Table 3.5: Adjustment parameters A, B and C, molecular diffusion coefficient in free liquid D, Soret coefficient S_T (IBB-nC12, 50 wt%., T_{mean} = 25 °C, $\Delta T'$ = 5 °C, 1 atm, horizontal position).

Duration of the experiment	ΔT (°C)	A	B (10^{-6} s^{-1})	C	D (10^{-10} m^{2}s^{-1})	Difference with benchmark	S_T (10^{-3} K^{-1})	Difference with benchmark
4 days	3	34.25	3.98	219.55	9.54	0.42%	7.34	46.86%

A good agreement for the molecular diffusion coefficient with the benchmark values was found, while there was a significant discrepancy between the Soret coefficient of this experiment and the benchmark value (error is equal to 46.86%). We recommend performing all the experiments in the future at vertical position by applying a vertical temperature gradient.

3.4 Numerical Model

3.4.1 Model description

A two-dimensional vertical porous medium, with a horizontal length (W) of 10 mm and height (*H*) of 32.2 mm is used. Two layers are added to the porous medium to represent the dead-volumes: one at the top of the porous medium and the second at the bottom, (see Figure 3.15). The porous medium is heated from the top at 27.5 °C and the bottom wall maintained at 22.5 °C, while lateral walls are assumed to be adiabatic. Silica is used as a porous material, and it is saturated with the fluid mixture. The properties of the porous medium and of the fluid mixtures are given in Table 3.6. The binary mixtures filling the vertical porous medium consist of nC12-THN, nC12-IBB and THN-IBB for a concentration of 50 wt%. In this work, all simulations are conducted at atmospheric pressure.
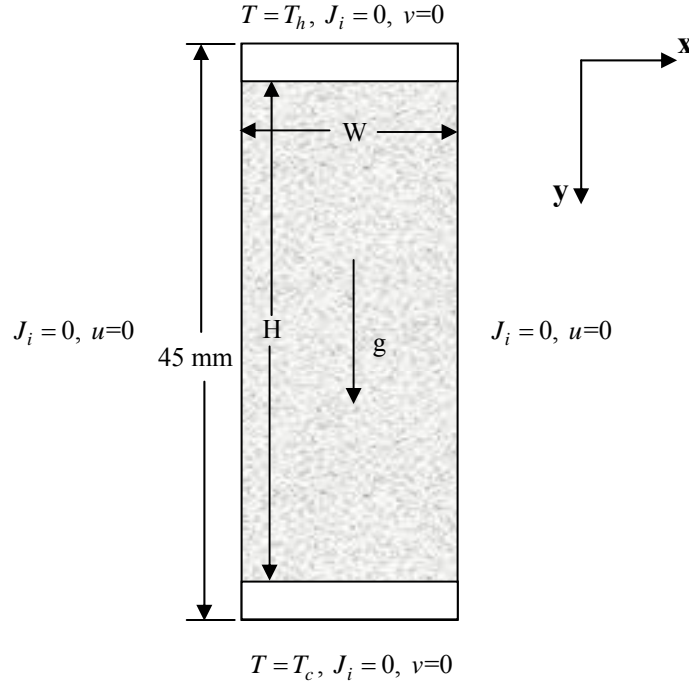
Figure 3.15: Schematic diagram of the porous medium and the boundary conditions.

Table 3.6: Physical properties of the porous material and fluid mixture, T_{mean}=25 °C and 1 atm.

Name	Value	Unit
Porous medium height H	32.2	mm
Porous medium horizontal length W	10.0	mm
Top wall temperature T_h	27.5	°C
bottom wall temperature T_c	22.5	°C
Pressure at the centre of the cavity	0.1013	MPa
Silica density	2220	kg.m^{-3}
Silica heat capacity	745	J.kg^{-1}.K^{-1}
Silica thermal conductivity	1.38	W.m^{-1}.K^{-1}
Silica porosity	0.45	
Silica porous medium permeability	20	mD
Silica porous medium tortuosity	≈ 1.4	-
THN-nC12 mixture compositions	50-50	(% mass fr.)
THN-nC12 mixture heat capacity	1890.55	J.kg^{-1}.K^{-1}
THN-nC12 mixture thermal conductivity	0.132	W.m^{-1}.K^{-1}
THN-IBB mixture compositions	50-50	(% mass fr.)
THN-IBB mixture heat capacity	1722.90	J.kg^{-1}.K^{-1}
THN-IBB mixture thermal conductivity	0.1260	W.m^{-1}.K^{-1}
IBB-nC12 mixture compositions	50-50	(% mass fr.)
IBB-nC12 mixture heat capacity	1979.98	J.kg^{-1}.K^{-1}
IBB-nC12 mixture thermal conductivity	0.128	W.m^{-1}.K^{-1}

3.4.2 Mathematical model

As introduced in section 1.3.2, the mass diffusion flux in an n-component fluid can be expressed as follows:

$$\vec{j}_i = -\rho \left(\sum_{j=1}^{n-1} D_{ij} \nabla \omega_j + D_{T,i} \nabla T \right) \tag{3.17}$$

where $\vec{j}_i$ is the mass diffusion flux of the ith component, ρ is the density, ω_j is the mass fraction of component j, T is the temperature. D_{ij} and $D_{T,i}$ are the molecular diffusion and thermodiffusion coefficients of the fluid mixture, respectively. Both thermodiffusion and molecular diffusion coefficients, as introduced in Chapter 2, are described through the theory of non-equilibrium thermodynamics. In an n-component fluid, the molecular diffusion and thermodiffusion coefficients can be expressed by:

$$\left. \begin{array}{l} D_{ij} = \dfrac{R}{\rho x_n M_n} \sum_{k=1}^{n-1} L_{ik} \sum_{l=1}^{n-1} \dfrac{x_l M_l + x_n M_n \delta_{lk}}{M_j} \left. \dfrac{\partial \ln f_l}{\partial x_j} \right|_{x_j T} \\ \\ D_{T,i} = \dfrac{L_{iq}}{\rho T^2} \end{array} \right\} \tag{3.18}$$

The thermodynamic properties of the fluid mixtures at equilibrium have been calculated using the volume-translated Peng-Robinson Equation of State (vt-PR-EoS). After the diffusion coefficient values (D_{ij}, and D_T) are calculated, these values were implemented in a porous medium model, applying the two-dimensional governing equation of the porous medium as introduced in section 2.3.

The porous medium governing equations are solved numerically subject to the boundary conditions of zero mass flux at the rigid wall, zero velocity (only the normal components)

at the rigid wall, fixed temperatures at the top and bottom walls but isothermal at lateral walls. The boundary conditions are shown in Figure 3.15 and the numerical solution procedure will be explained in detail in Chapter 5.

3.4.4 Comparison of experimental data with numerical model

In this section, numerical results of three binary mixtures of THN, IBB and nC12 are presented. In addition, a comparison between the experimental data and the theoretical values is given in Table 3.8. Figure 3.16 shows the temperature contours along the vertical direction; the temperature gradient is only in the vertical direction.

The numerical results of the THN-nC12 mixture are presented in details; the THN-IBB and IBB-nC12 mixture results are only given through the coefficient values (D, D_T, and S_T) in Table 3.7.

Temp.

	300.29
	299.98
	299.67
	299.36
	299.05
	298.74
	298.43
	298.12
	297.81
	297.50
	297.19
	296.88
	296.57
	296.26
	295.95
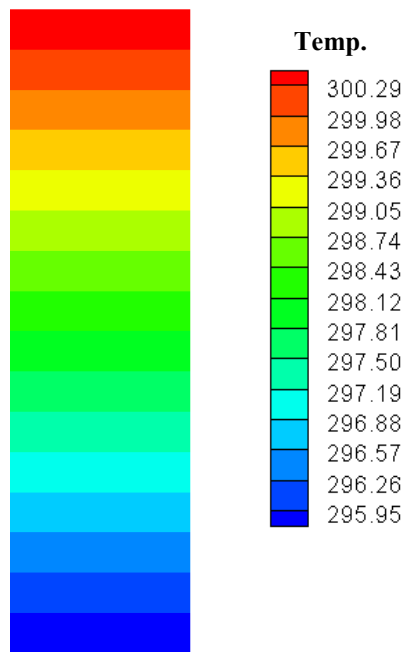
Figure 3.16: Temperature distribution along the vertical position.

Figures 3.18 and 3.19 display the composition variation along the vertical position in the centre of the cavity for THN and nC12 components in the THN-nC12 mixture. It can be seen that due to the Soret effect, the THN concentration (heavier component) migrates to the cold side, while the lighter component (nC12) moves towards the hot side. Also, two dead-volumes are included: one at the top side and another at the bottom side (the permeability and the porosity are assumed to be high value in order to mimic the dead-volumes). The concentration of THN and nC12 deviates somewhat from linearity in the dead-volume regions, because the convection effect is significant in these regions. The same behaviour was found for the other mixture components (THN-IBB and IBB-nC12 mixtures).

Figure 3.19 represents density variation in the centre of the cavity along the vertical position for three mixtures: THN-nC12, THN-IBB, and IBB-nC12. The data in this figure are at $\Delta T = 5^o C$ and at 50 wt%. The density variation along the vertical position is linear, as expected, since the temperature variation is linear and the pressure is assumed constant inside the cavity.
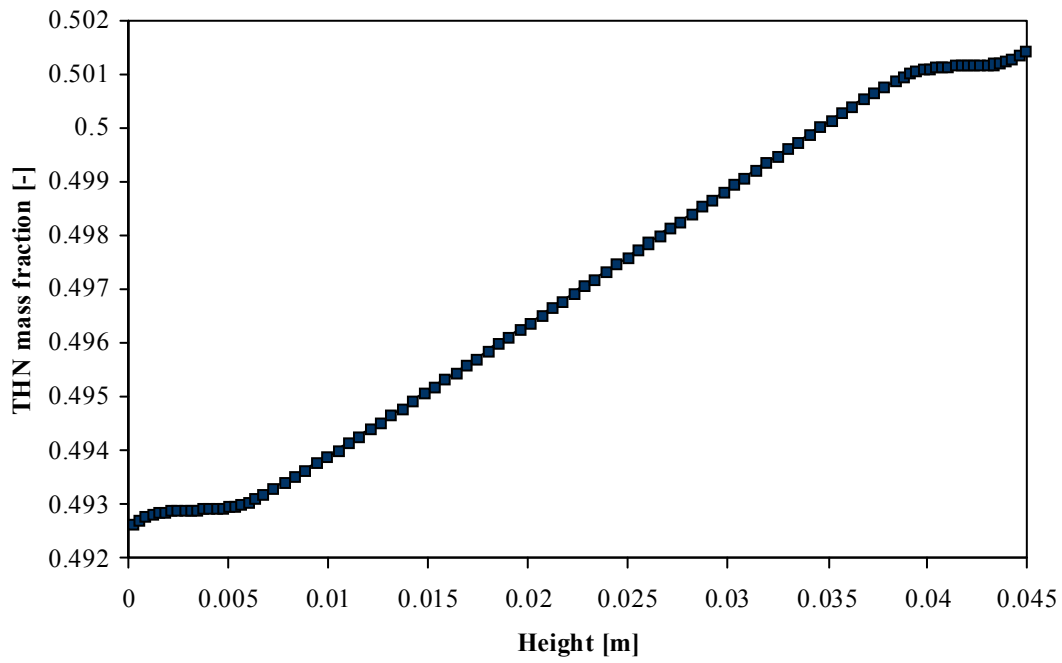
Figure 3.17: THN mass fraction distributions in the centre of the cavity along the vertical position, THN-nC12 mixture.
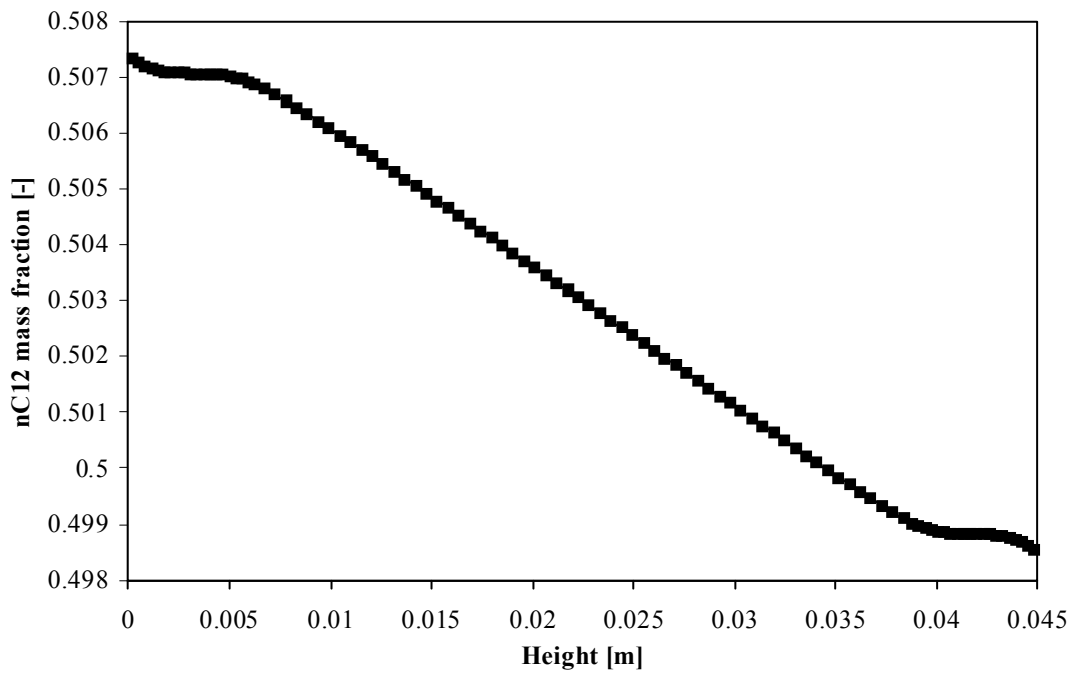
Figure 3.18: nC12 mass fraction distributions in the centre of the cavity along the vertical position, THN-nC12 mixture.
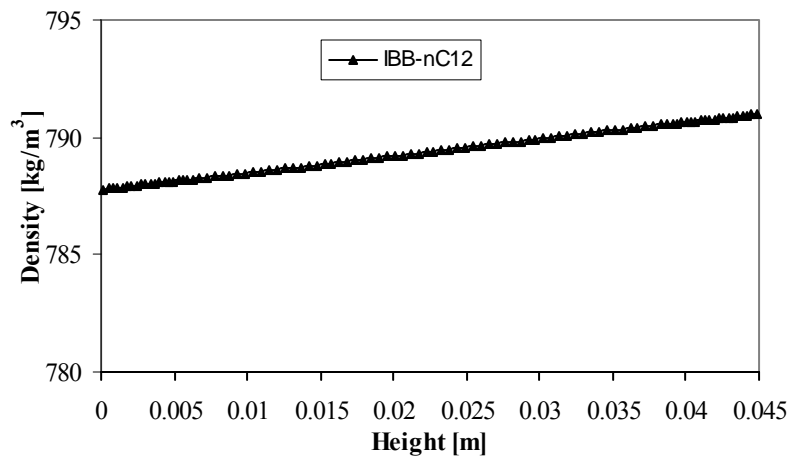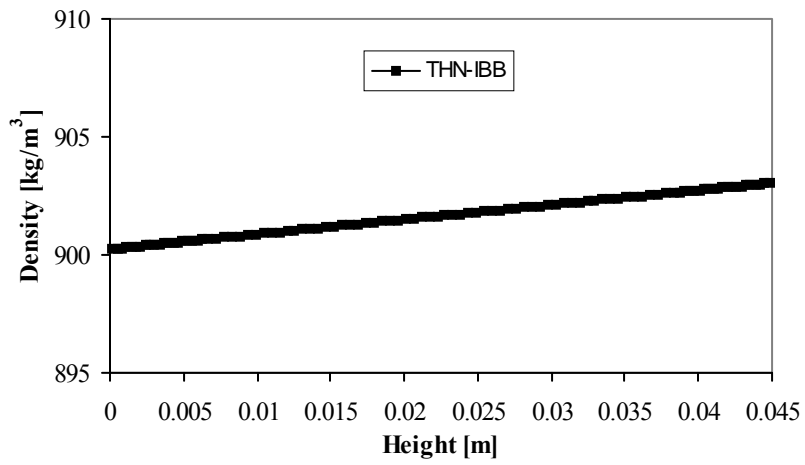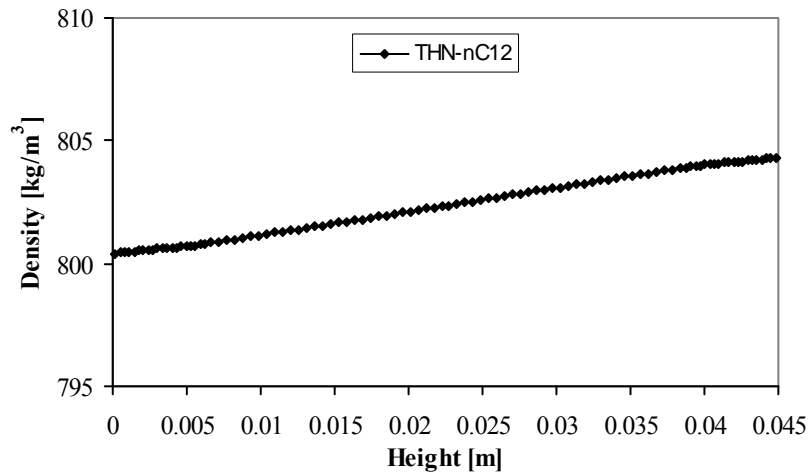
Figure 3.19: Density distribution for three binary mixtures in the centre cavity along the vertical direction.

In Table 3.7, the molecular diffusion coefficient, Thermodiffusion coefficient, and Soret coefficient in a porous medium are calculated. Table 3.8 shows a comparison between this work results (which consists of two parts; experimental and numerical) and benchmark values. It can be see that a good agreement was found between the theoretical approach, which is based on the Shukla and Firoozabadi model, and the experimental approach. For instance, the percentage error for the THN-nC12 mixture between the experimental data and the theoretical values for D and S_T are equal to 2.09% and 18%, respectively. It is also found that the IBB-nC12 mixture presents a weaker value of the Soret coefficient ($S_T = 4.95 \times 10^{-3}$ K^{-1}) with regard to the THN-nC12 mixture ($S_T = 9.025 \times 10^{-3}$ K^{-1}), and this observation has been noticed in the experimental data and benchmark value.

Table 3.7: Model in vertical position, the coefficient values for porous medium, T$_{mean}$= 25 $^{\circ}$C and 1 atm.

Mixture (50-50 wt%)	$D^*(10^{-10} \text{m}^2.\text{s}^{-1})$ (Theo.)	$D_T^*(10^{-12} \text{m}^2.\text{s}^{-1}\text{K})$ (Theo.)	$S_T(10^{-3}\text{K}^{-1})$ (Theo.)
THN-nC12	3.10	2.20	9.02
THN-IBB	5.55	1.56	2.85
IBB-nC12	4.48	1.62	4.95

Table 3.8: Theoretical and experimental molecular diffusion and Soret coefficients for three binary mixtures, T_{mean}= 25 $^{\circ}$C and 1 atm (for 1.4 tortuosity 1.4).

Mixture	THN-nC12 (50-50 wt%)		THN-IBB (50-50 wt%)		IBB-nC12 (50-50 wt%)	
	$D/10^{-10}$ m^2.s^{-1}	$S_T/10^{-3}$ K^{-1}	$D/10^{-10}$ m^2.s^{-1}	$S_T/10^{-3}$ K^{-1}	$D/10^{-10}$ m^2.s^{-1}	$S_T/10^{-3}$ K^{-1}
Theoretical	6.076	9.020	10.87	2.85	8.780	4.95
Experimental	6.20	11.0	--------	-------	9.47±0.02	3.95±0.15
Benchmark	6.21±0.06	9.5±0.5	8.5±0.6	3.3±0.3	9.5±0.4	3.9±0.1
Error Theo. -Exp.	2.09%	18.0%	------	-------	7.28%	-25.31%
Error Theo.-Bench	2.12%	5.05%	-19.45%	13.63%	7.57%	-26.92%
Error Exp.-Bench.	-0.162%	13.63%	--------	--------	-0.316%	1.28%

3.5 Summary

In this work, a new thermodiffusion cell designed for high pressure was validated at atmospheric pressure. The cell was installed in a Mach-Zehnder interferometer, with each beam crossing one of the dead-volumes. Two mixtures of the Benchmark of Fontainebleau have been tested in the vertical position (THN-nC12 and IBB-nC12 at 50 wt% and T_{mean} =25 °C). From the analysis of the second kinetic of the evolution of the phase difference between the laser beam that passes through the hot dead-volume and the laser beam that passes through the cold dead-volume, the diffusion coefficient in free liquid, D, and Soret coefficient, S_T, of the two mixtures and the tortuosity τ for the porous medium were determined. For both mixtures, an excellent agreement was found between the molecular diffusion coefficient of this work and the benchmark values, and the percentage error was less than 1%. In addition, it was found that the difference between the Soret coefficients for this work and the benchmark data is acceptable for the experiments of duration up to seven days. To improve the determination of S_T with the cell in a vertical position, it is suggested to increase the value of the imposed temperature gradient and increasing the time of the experiment (about two weeks in order to reach the steady state condition). The value of the tortuosity of the porous medium is close to 1.4, which is consistent with the literature data. Also it was found that the theoretical results are in good agreement with the experimental data.

When the cell was set in the horizontal position, convection in dead-volumes became possible. For a difference of the temperature applied between thermoregulator baths ($\Delta T' = 5 \ ^{\circ}C$) a diffraction pattern came up and at the beginning of the experiment, and the procedure of analysis of interferograms became difficult.

Chapter 4

Experimental and Theoretical Estimation of the Thermal Expansion Coefficient, Concentration Expansion Coefficient and Viscosity for Binary Mixtures under Pressure up to 20 MPa

In this chapter, the densities of three binary mixtures of n-dodecane (nC12), isobutylbenzene (IBB) and 1,2,3,4-tetrahydronaphtalene (THN) for pressures varying from 0.1 to 20 MPa at an average temperature of 25 °C were measured. By a derivative method, the thermal expansion and concentration expansion coefficients for binary mixtures of equal mass fraction have been determined. In addition viscosities have been measured and compared with theoretical estimates. In order to accurately predict the thermal expansion and concentration expansion coefficients, the densities of the binary mixtures were calculated using Peng-Robinson and volume translated Peng-Robinson Equations of State.

4.1 Introduction

In recent years, due to limited energy resources, the characterization of petroleum reservoirs has gained a lot of interest. In this context especially knowledge of transport properties of hydrocarbon mixtures such as linear alkanes and organic ring compounds is very important (Montel, 1998 and Van Vaerenbergh *et al.*, 2005). Different techniques exist to determine the thermal diffusive properties of liquid mixtures (Platten, 2006). The thermogravitational columns have been validated in a benchmark test for three binary hydrocarbon mixtures (Platten *et al.*, 2003). With this technique, the value of the thermodiffusion coefficient of a binary at the steady-state is given by Blanco *et al.*, (2006):

$$D_T = -\frac{ga^4}{504} \frac{\beta_T}{\omega_0(1-\omega_0)\beta_c\eta_m} \frac{\partial\rho}{\partial z} \tag{4.1}$$

where g is the acceleration of gravity, β_T the thermal expansion coefficient of the mixture, β_c the concentration expansion coefficient of the mixture, η_m the dynamic viscosity of the mixture, a the "gap" (distance between the inner cylinder and the exterior cylinder of the column where the fluid of study is), ω_0 the initial mass fraction of the densest component in the binary mixture and $\partial\rho/\partial z$ the vertical gradient of density ρ in the column at the steady-state. The parameters β_T, β_T, and η_m are therefore thermophysical properties needed for the determination of the thermodiffusion coefficient.

The systems of the benchmark of Fontainebleau, (Platten *et al.*, 2003), are composed of binaries THN and nC12, THN and IBB and IBB and nC12 (mass fraction of 50% and mean temperature of 25 °C). Measurements of thermodiffusion coefficient under high pressure are in progress (Urteaga *et al.*, 2008), but thermophysical properties and molecular and thermodiffusion coefficients are known for these systems only at atmospheric pressure.

The aim of this work is to provide these properties at high pressure. In this work, the measurements for the thermal expansion and concentration expansion coefficients and for the viscosity of the binaries of the benchmark of Fontainebleau for pressures varying from 0.1 to 20 MPa at 25 °C are presented. The predicted coefficients from the Peng-Robinson, and volume translated Peng-Robinson Equations of State are compared with the measured values. The Lohrenz-Bray-Clark model was used for the prediction of the viscosities.

4.2 Experimental Setup

The THN (99%), nC12 (99%) and IBB (99%) were purchased from Sigma-Aldrich. The properties of the three components are given in Table 4.1, where ω_i is the acentric factor and s_{vi} is a shift parameters as they are introduced in sections 2.2.1 and 2.2.2.

Table 4.1: Pure component parameters for PR-EoS and vt-PR-EoS.

Component	PR & vt-PR			
	T_C (K)	P_C (MPa)	ω_i	s_{vi}
IBB	650.15	3.0398	0.3811	-0.0805
THN	720.15	3.6200	0.3278	0.0146
nC12	658.20	1.8239	0.5734	0.0985

4.2.1 Apparatus

Densities of the binary mixtures were measured with a high pressure-high temperature vibrating tube densimeter *DMA HPM* (Anton-Paar). An *mPDS-2000V3* evaluation unit was connected to DAM HPM in order to read out the measurement data. The complete experimental assembly has been described in detail by Lagourette *et al.* (1992), (see Figure B.1 Appendix B). The measurement principle is based on the determination of the oscillation period of the vibrating U-tube densimeter which contains the sample (fluid mixture); the oscillation period, Λ in seconds, can be defined by:

$$\Lambda(T,p) = 2\pi\sqrt{\frac{m_o + \rho(T,p)V(T,p)}{C}} \tag{4.2}$$

where m_o is the mass of the U-tube empty, V is the internal volume of the tube, ρ is the sample density, and C is the spring constant ($N.m^{-1}$). Re-arrangement Eq. 4.2 leads to a simple relation, where density is linearly related to the square of the measured period of oscillation:

$$\rho(T,p) = A(T,p)\Lambda^2 + B(T,p) \tag{4.3}$$

where

$$A(T,p) = \frac{C}{4\pi^2 V(T,p)}$$

(4.4)

$$B(T,p) = -\frac{m_o}{V(T,p)}$$

The parameters $A(T,p)$ and $B(T,p)$ are determined theoretically from measuring the period of oscillation for two reference substances of known density (e.g. distilled water and ethanol) as calibration samples over the whole range of pressure and temperature. Taking into account the accuracy of measurements of the temperature, the pressure, and the period of oscillation measurement for two reference substance and the studied systems, the overall experimental uncertainty in the reported density values is estimated to be $\pm$ 5.0x10^{-4} g/cm^3. This uncertainty is similar to those that are reported in previous studies by Comunas *et al.* (2008), and Miyake *et al.* (2008).

A falling body high pressure high temperature viscometer (HPHTV-100 semi-automatic Stony Brook Scientific) was used to measure the viscosity of the compressed liquids. In this apparatus, a stainless steel cylinder falls vertically through a fluid of unknown viscosity at given conditions of temperature and pressure. A measurement of the falling body terminal velocity allows a determination of the fluid viscosity. The viscosity is a function of the falling body time, the density difference between the cylinder and the fluid. A toluene has been used as calibrating fluid, (Vieira *et al.*, 1997). Decane has been used to verify the calibration (Oliveira *et al.*, 1992 and Kashiwagi and Makita 1995). Each measurement of the falling time was repeated three times at thermal and mechanical equilibrium, and it is reproducible to better than 1%. The final value is an average of these measurements. The total uncertainty of the obtained viscosity values was estimated to be within 2%, which is comparable to the values estimated by other authors for similar devices, as has been discussed in previous papers (Et-Tahir *et al.*, 1995 and Leahy-Dios and Firoozabadi 2007). Viscosity values at 0.1, 4, and 10 MPa are given in Table 4.5. The

viscosity at 20 MPa was not measured experimentally, because of the 14 MPa limitation of the viscosimeter.

4.2.2 Methods

The thermal expansion coefficient is given by:

$$\beta_T = -\frac{1}{\rho_0}\left(\frac{\partial \rho}{\partial T}\right)_{P,\omega} \tag{4.5}$$

where ρ_0 is the density of the mixture at the temperature T_0 and $(\partial \rho/\partial T)$ is the derivative of the density with temperature at T_0 and at a mass fraction of 50%. Figure 4.1 shows the experimental data of densities for five temperatures centred on 25 °C and for pressures varying from 0.1 MPa to 20 MPa for the mixture of IBB and nC12.

The results were fitted by a linear function using the method of least squares. Considering the uncertainty of the measurements and the sensitivity of the method of least squares adjustment, the uncertainty of β_T is estimated to be $\pm\ 0.3 \times 10^{-4}$ K^{-1} for the three systems at all pressures (0.1-20 MPa). It is found that the results for 0.1 MPa are in an agreement with those published by Leahy-Dios and Firoozabadi (2007) for the same systems at atmospheric pressure.

The concentration expansion coefficient is given by:

$$\beta_c = \frac{1}{\rho_0}\left(\frac{\partial \rho}{\partial \omega}\right)_{P,T} \tag{4.6}$$

where ω is the mass fraction of the densest component. The temperature is now fixed and the density on a small interval of concentrations centred at $\omega_0 = 0.5$ is measured. The approach for the determination of β_c is the same as the one used for the measurement of

the β_T. Figure 4.2 shows the densities for five mass fractions of the densest component for the mixture of IBB-nC12 and are presented at different pressures.
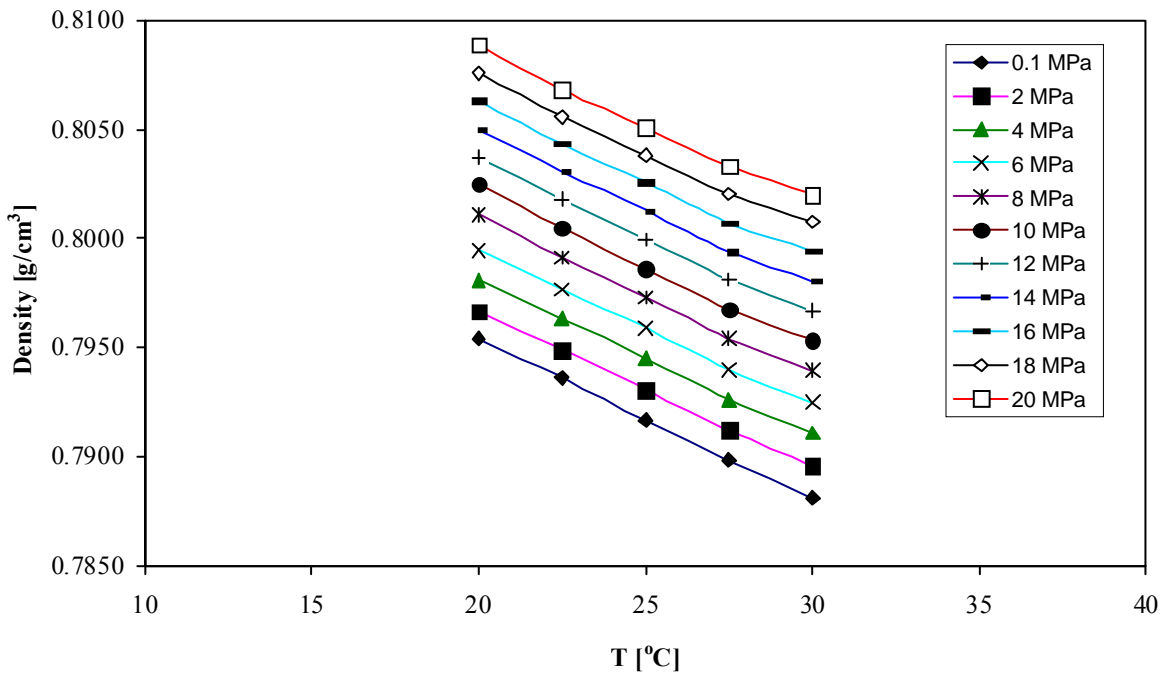
Figure 4.1: Density of IBB-nC12 mixture as a function of the temperature and for different pressures (0.1-20 MPa).

The uncertainty of β_c is estimated to be ± 0.009 for IBB-nC12 mixture, ± 0.01 for THN-nC12 mixture and ±0.008 for THN-IBB mixture. The results of 0.1 MPa are in agreement with those published in the literature for the same systems at atmospheric pressure, Leahy-Dios and Firoozabadi (2007). Figure 4.3 and Figure 4.4 show the densities of THN-nC12 mixture with temperature and mass fraction at different pressures, respectively. Figure 4.5 and Figure 4.6 show the densities of THN-IBB mixture with temperature and mass fraction at different pressures, respectively. A similar observation for mixture IBB-nC12 is found for the other two mixtures.
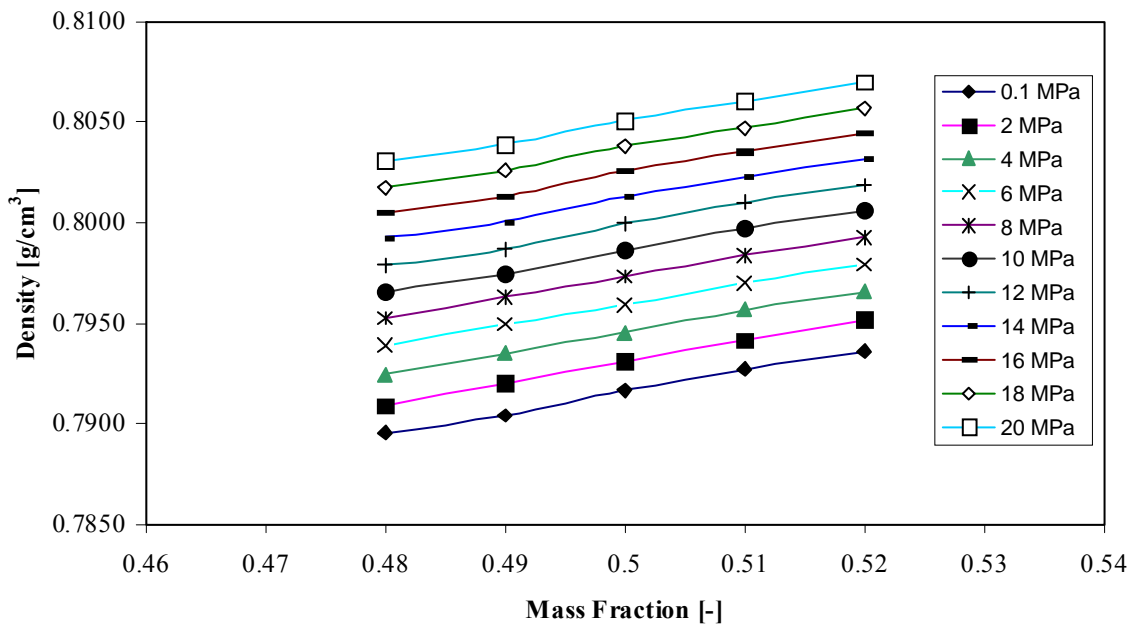
Figure 4.2: Density of IBB-nC12 mixture at 25 °C as function of the mass fraction of the densest component and for different pressures (0.1-20 MPa).
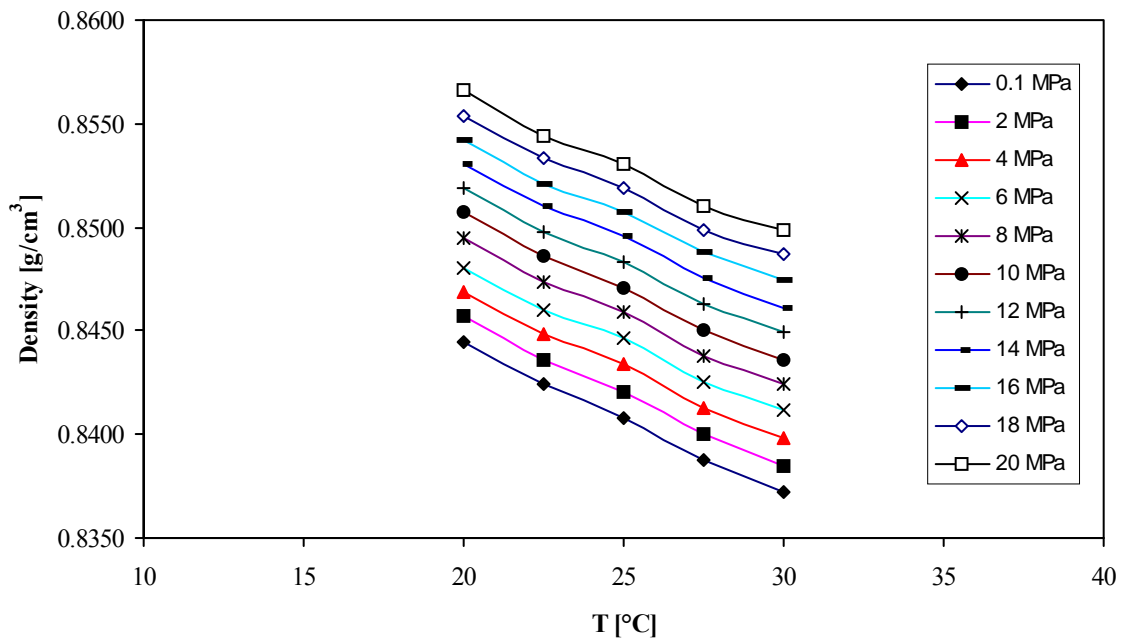
Figure 4.3: Density of THN-nC12 mixture at 25 °C as a function of the temperature and for different pressures (0.1-20 MPa).
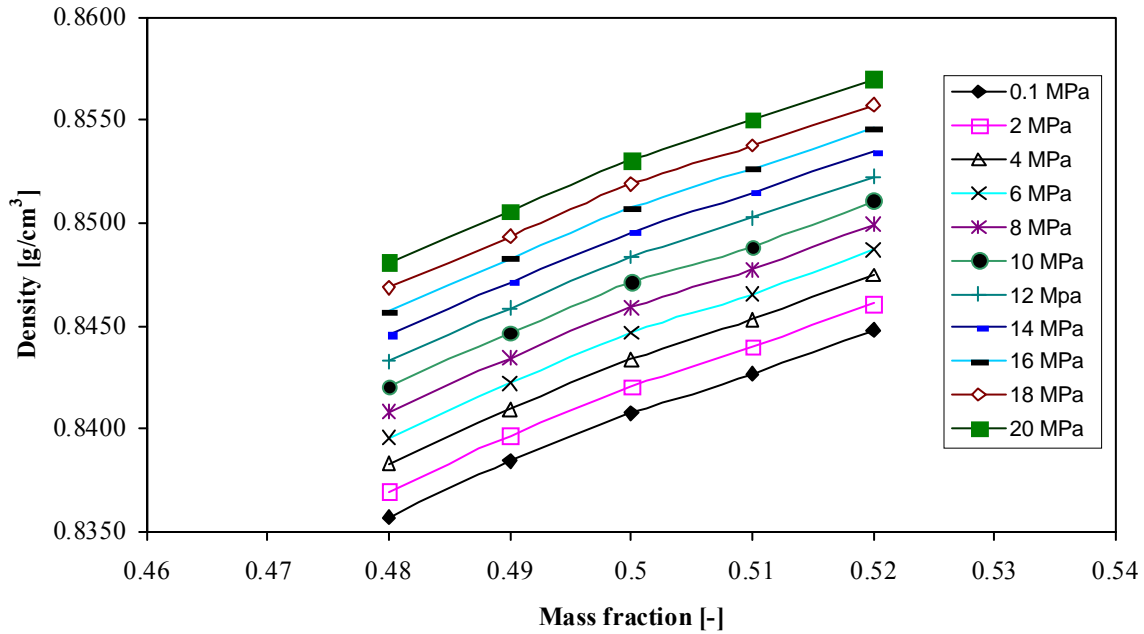
Figure 4.4: Density of the THN-nC12 mixture at 25 °C as function of the mass fraction of the densest component and for different pressures (0.1-20 MPa).
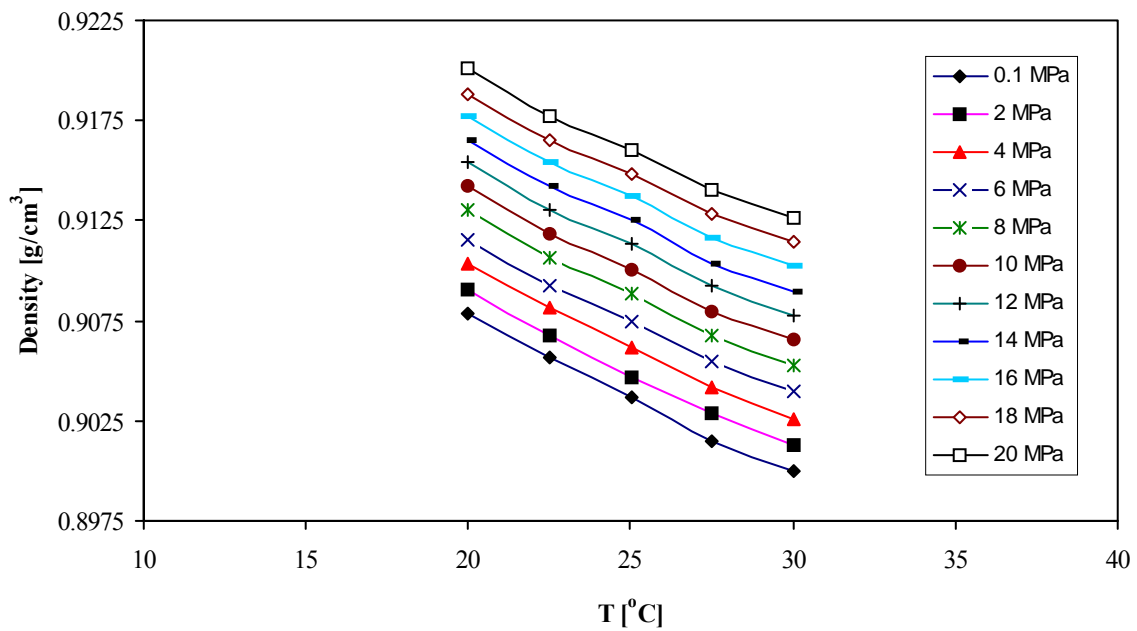
Figure 4.5: Density of the THN-IBB mixture at 25 °C as a function of the temperature and for different pressures (0.1-20 MPa).
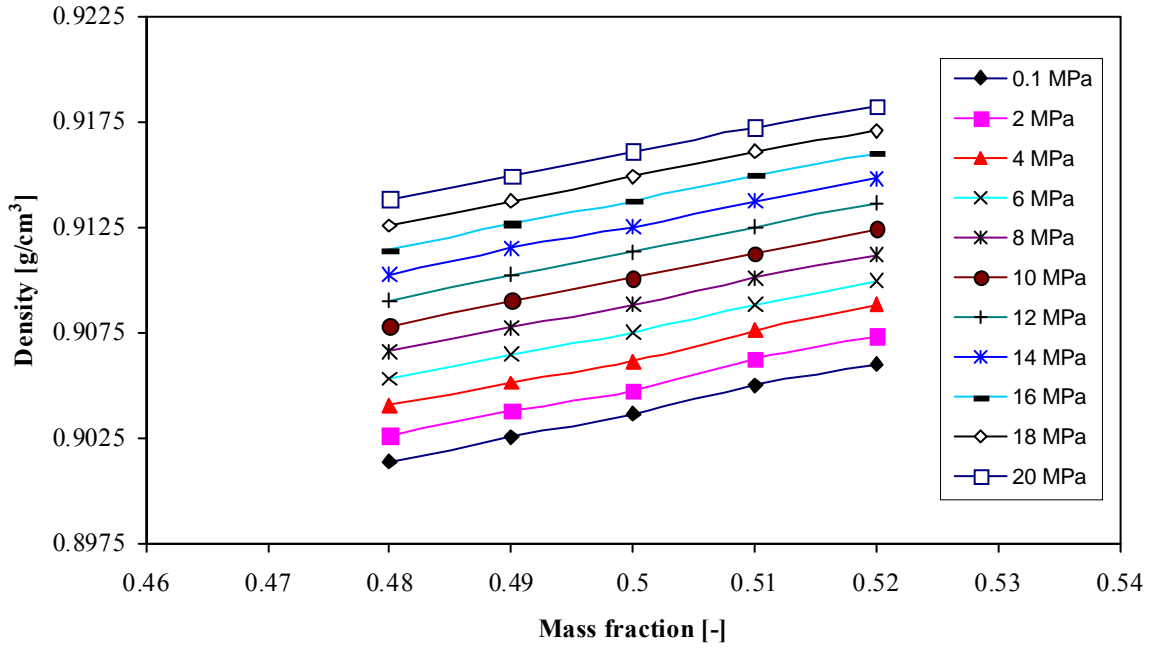
Figure 4.6: Density of THN-IBB mixture at 25 °C as function of the mass fraction of the densest component and for different pressures (0.1-20 MPa).

4.3 Theoretical Approach

For the evaluation of the density, the compressibility factor of the mixtures has been calculated with different equations of state. The compressibility factor Z in Peng-Robinson Equation of State (PR-EoS), as introduced in section 2.2, can be written as follows:

$$Z = \frac{\bar{V}}{\bar{V} - b_p} - \frac{a_p(T)\bar{V}}{RT\left(\bar{V}\left(\bar{V} + b_p\right) + b_p\left(\bar{V} - b_p\right)\right)} \tag{4.7}$$

The pure component parameters a_p (attraction parameter) and b_p (co-volume) can be calculated from critical properties and also depend on the temperature and acentric factor, as shown in Eqs. 2.27 and 2.28.

It has been found that the density prediction appears to be more accurate when the volume translated Peng-Robinson Equation of State (vt-PR-EoS) is used. The vt-PR-EoS is proposed by Péneloux *et al.* (1982). The shift parameters s_{vi} (Table 4.1) were calculated by Jhaverl and Youngren (1988).

The viscosity of the fluid mixtures (η) in cP is obtained with a method proposed by Lohrenz *et al.* (1964), which was based on predicting the viscosity of reservoir fluids from their compositions, as follows:

$$\eta = \eta^* + \frac{\left(\xi^4 - 10^{-4}\right)}{\zeta} \tag{4.8}$$

where η^* and ζ are given by:

$$\eta^* = \frac{\sum_{i=1}^{n} x_i \eta_i \sqrt{M_i}}{\sum_{i=1}^{n} x_i \sqrt{M_i}} \tag{4.9}$$

$$\zeta = \frac{\left(\sum_{i=1}^{n} x_i T_{ci}\right)^{1/6}}{\left(\sum_{i=1}^{n} x_i M_i\right)^{1/2} \left(\sum_{i=1}^{n} x_i P_{ci}\right)^{2/3}} \tag{4.10}$$

and

$$\xi = 0.1023 + 0.023364 \rho_r + 0.05833 \rho_r^2 - 0.40758 \rho_r^3 + 0.0093324 \rho_r^4 \tag{4.11}$$

where η_i is the viscosity, T_{ci} is the critical temperature, P_{ci} is the critical pressure, and M_i is the molecular weight of the *i*th component. ξ is a variable related to the reduced

density with a fourth order polynomials. $\rho_r = \rho / \rho_c{}'$ is the reduced density of the mixture. ρ is the density of the liquid mixture calculated using the P-R-EoS and ρ_c' is the pseudocritical density of the mixture.

4.4 Results and Discussion

The measured mixture densities have been compared with densities which were calculated using PR-EoS and vt-PR-EoS for pressures varying from 0.1 MPa to 20 MPa. Comparison is given in Table 4.2; the full results of the experimental measurement of the densities for the three binary mixtures are shown in Appendix B. As one may notice, the vt-PR-EoS proves to be more efficient for predicting the densities than the PR-EoS. For the vt-PR-EoS the disagreement with the experimental densities is the same for the three binaries. PR-EoS gives good results only for the THN-IBB system (mixture of aromatics), which is logical, given that cubic equations are not suitable for long alkanes. It is noticed that the performances of the equations of state are independent of the pressure, presumably because the temperature is not very high.

The thermal expansion and concentration expansion coefficients have been calculated (using PR-EoS and vt-PR-EoS) from the densities calculated for temperatures centred on 25 °C and for mass fractions centred on 50%, and with the same methodology used for experimental data. The comparison between the measured and the calculated thermal expansion coefficients and the concentration expansion coefficients for different pressures (from 0.1 to 20 MPa) are given in Table 4.3 and Table 4.4, respectively. From these tables, the comparisons with measured values show that vt-PR-EoS has better agreement with experiments than the PR-EoS.

73

Table 4.2: Theoretical and experimental densities for binary mixtures (50 wt% and 25 °C).

P (MPa)	Exp. ρ (g.cm^{-3})	PR-EoS ρ (g.cm^{-3})	difference	vt-PR-EoS ρ (g.cm^{-3})	difference
IBB-nC12					
0.1	0.7917	0.7518	5.04%	0.7669	3.13%
4	0.7945	0.7543	5.06%	0.7695	3.15%
10	0.7986	0.7579	5.10%	0.7733	3.17%
20	0.8051	0.7632	5.20%	0.7787	3.28%
THN-nC12					
0.1	0.8407	0.7745	7.87%	0.8221	2.21%
4	0.8434	0.7767	7.91%	0.8246	2.23%
10	0.8471	0.78	7.92%	0.8282	2.23%
20	0.8530	0.7847	8.01%	0.8336	2.27%
THN-IBB					
0.1	0.9036	0.9016	0.22%	0.8745	3.22%
4	0.9061	0.9039	0.24%	0.8767	3.24%
10	0.9101	0.9073	0.31%	0.8799	3.32%
20	0.9161	0.9122	0.43%	0.8846	3.44%

Table 4.3: Theoretical and experimental thermal expansion coefficient for binary mixtures (50 wt% and 25 °C).

P (MPa)	Exp. $B_T.10^4$ (K^{-1})	PR-Eos $B_T.10^4$ (K^{-1})	difference	vt-PR-EoS $B_T.10^4$ (K^{-1})	difference
IBB-nC12					
0.1	9.3	6.06	34.8%	6.18	33.5%
4	8.9	5.73	35.7%	5.94	33.3%
10	9.0	5.29	41.2%	5.64	37.3%
20	8.6	4.70	45.4%	5.24	39.1%
THN-nC12					
0.1	8.6	5.56	35.4%	5.90	31.4%
4	8.3	5.28	36.3%	5.60	32.5%
10	8.4	4.92	41.5%	5.19	38.2%
20	8.0	4.42	44.7%	4.62	42.3%
THN-IBB					
0.1	8.8	5.76	34.6%	5.59	36.5%
4	8.5	5.53	35.0%	5.34	37.2%
10	8.5	5.21	38.7%	5.01	41.1%
20	8.1	4.76	41.3%	4.54	44.0%

Table 4.4: Theoretical and experimental concentration expansion coefficient for binary mixtures (50 wt% and 25 °C).

P (MPa)	Exp. β_c		PR-EoS β_c	difference		vt-PR-EoS β_c	difference
IBB-nC12							
0.1	0.13		0.266	-104.6%		0.104	20.0%
4	0.13		0.265	-103.8%		0.103	20.8%
10	0.13		0.265	-103.8%		0.101	22.3%
20	0.12		0.264	-120.0%		0.010	91.7%
THN-nC12							
0.1	0.27		0.335	-24.1%		0.256	5.2%
4	0.27		0.334	-23.7%		0.254	5.9%
10	0.26		0.332	-27.7%		0.252	3.1%
20	0.26		0.329	-26.5%		0.249	4.2%
THN-IBB							
0.1	0.13		0.070	46.2%		0.153	-17.7%
4	0.13		0.070	46.2%		0.153	-17.7%
10	0.13		0.068	47.7%		0.152	-16.9%
20	0.12		0.067	44.2%		0.151	-25.8%

Using the Lohrenz-Bray-Clark model for estimating the viscosity of the mixtures (Eq. 4.8) and the calculated densities (PR-EoS and vt-PR-EoS), it was possible to evaluate viscosities for each binary mixture and from each equation of state. The comparison between the measured and the calculated viscosities for pressures varying from 0.1 to 20 MPa is given in Table 4.5. The viscosity values at 0.1, 4 and 10 MPa are given, but the viscosity at 20 MPa was not measured experimentally, because of the 14 MPa limitation of the viscosimeter. The results reveal that the Lohrenz-Bray-Clark model, combined with the vt-PR-EoS, gives better agreement with measured data than the PR-EoS for the prediction of the viscosity of the three binaries. The percentage error was found to range from 11% to 18% when the vt-PR-EoS was used and from 14% to 37.5% for PR-EoS.

Table 4.5: Theoretical and experimental viscosities for binary mixtures (50 wt% and 25 °C).

P (MPa)	Exp. η (cP)		PR-EoS η (cP)	difference		vt-PR-EoS η (cP)	difference
IBB-nC12							
0.1	1.09		0.764	29.9%		0.902	17.2%
4	1.14		0.786	31.1%		0.930	18.4%
10	1.22		0.818	33.0%		0.970	20.5%
20	--		0.866	--		1.033	--
THN-nC12							
0.1	1.46		0.965	33.9%		1.691	-15.8%
4	1.53		0.989	35.4%		1.746	-14.1%
10	1.64		1.026	37.4%		1.827	-11.4%
20	--		1.082	--		1.954	--
THN-IBB							
0.1	1.33		1.540	-15.8%		1.156	13.1%
4	1.37		1.580	-15.3%		1.182	13.7%
10	1.43		1.638	-14.5%		1.221	14.6%
20	--		1.731	--		1.282	--

4.5 Summary

The thermal expansion and concentration expansion coefficients and the viscosity of mixtures are necessary properties for the determination of the thermodiffusion coefficient. The densities of binaries of nC12, IBB and THN for pressures going from 0.1 to 20 MPa for temperatures centred on 25 °C and for concentrations centred on 50% have been measured. By a derivative method, the thermal expansion and concentration expansion coefficients at 25 °C and 50% mass fraction were determined. Viscosities were directly measured using high pressure high temperature viscometer (HPHTV-100). In order to accurately predict the thermal and concentration expansion coefficients, an attempt was made first to calculate the densities of the binaries using PR-EoS and vt-PR-EoS. The comparisons with measured densities show that vt-PR-EoS has better agreement with experiments than the PR-EoS. From calculated densities, the thermal expansion and concentration expansion coefficients were evaluated. The combination of the model of Lohrenz-Bray-Clark for the viscosity of liquid mixtures, and the densities calculated with the two equations of state proved to be inefficient for the prediction of the viscosities of the binaries.

Chapter 5

Soret Effect for a Ternary Mixture in a Porous Cavity: Modeling with Variable Diffusion Coefficients and Viscosity

In this chapter, a three-dimensional porous cavity is filled with two ternary mixtures. The first mixture consists of methane (C1), n-butane (nC4) and n-dodecane (nC12) at a pressure of 35.0 MPa and the second ternary mixture is nC12, THN, and IBB at 1 atmospheric pressure. Theses are used to investigate numerically the flow interaction due to the presence of thermodiffusion and buoyancy forces. A lateral heating condition is applied. The molecular diffusion and thermodiffusion coefficients are functions of temperature, concentration and viscosity of mixture components.

5.1 Introduction

The thermodiffusion process can occur in both liquid and gaseous mixtures. Studies based on the thermodynamics of irreversible processes have shown that thermodiffusion in liquids, along with the effect of natural convection, can in fact greatly influence the composition distribution in hydrocarbon reservoirs.

The Ludwig-Soret effect is commonly represented by the thermodiffusion coefficient, especially for multicomponent mixtures. The theoretical study of this effect is usually carried out based on non-equilibrium thermodynamics, de Groot and Mazur (1984). Recently, a large amount of research has been done on thermodiffusion in porous media by Haugen and Firoozabadi (2005), and Platten (2005). It is known that convection has a significant influence on the accuracy of Soret coefficient measurements. Utilization of porous media may help in reducing the convection-induced distortion. Costeseque *et al*. (2004) conducted diffusion experiments in both free and porous media in a Soret cell. They reported that the molecular diffusion and thermodiffusion coefficients in porous media were related to those in clear fluid via the tortuosity. However the Soret coefficient

(the ratio of molecular diffusion coefficient to thermodiffusion coefficient for binary mixtures) is identical for both configurations.

Riley and Firoozabadi (1998) presented a model to investigate the effects of natural convection and diffusion (thermal, pressure and fickian) on a single-phase binary mixture of methane and n-butane in a horizontal cross-sectional reservoir in the presence of a prescribed linear temperature field. The compositional distribution in the reservoir under both horizontal and lateral heating conditions was carefully examined. It was found that increasing the permeability increased the horizontal compositional variation. A local maximum and/or minimum value exists in the compositional gradient as a function of the permeability. Delware *et al.* (2004) studied these phenomena for a binary system in a square cavity. The energy equation is solved simultaneously allowing the observing of temperature variation in the model. Various thermal boundary conditions are examined. Their results revealed that in the lateral heating case the Soret effect is found to be weak, whereas in the bottom heating case the Soret effect is more pronounced.

Firoozabadi *et al*. (2000) developed a model for thermal diffusion factors in multicomponent non-ideal mixtures. This model was based on the thermodynamics of irreversible processes where the effects of both equilibrium and non-equilibrium properties are incorporated. The equilibrium properties, such as partial internal energies and fugacities, were estimated using the volume-translated Peng-Robinson equation of state. On the other hand, the non-equilibrium properties, such as viscosity, were accounted for by incorporating the energy of viscous flow. This model has been used by Jiang *et al*. (2008) to examine the thermodiffusion convection of a water-ethanol mixture in porous medium under high pressure.

To the best of our knowledge, the only thermodiffusion measurement for hydrocarbon ternary mixtures is reported by Leahy-Dios *et al*., (2005). In this work, an experiment was done by using the thermogravitational column method, and they measured the thermodiffusion coefficient for two different ternary mixtures: one of the mixtures consisted of normal alkane (nC12) and two aromatics (IBB and THN), and the second

mixture consisted of two normal alkanes (octane and decane) and one aromatic (1-methylnaphthalene). Their results revealed that in the ternary mixture of octane-decane-1-methylnaphthalene, a sign of the thermodiffusion coefficient for decane is changed as the composition changes, despite the fact that the two normal alkanes are similar.

In this work, attempts are made in simulating the thermosolutal convection of two ternary mixtures. In addition, a comparison is made between the experimental data of the ternary mixture (Leahy-Dios *et al.*, 2005) and the theoretical results using the Firoozabadi model with two equations of state (PR-EoS and vt-PR-EoS).

5. 3 Model Description

The porous cavity has a horizontal length of 32 mm, a width of 10 mm, and a vertical height of 10 mm, as shown in Figure 5.1. The porous material is Al_2O_3 powder; and the cavity is saturated with the ternary fluid mixture. Physical properties of the liquid mixtures and the porous medium are given in Table 5.1. The left wall of the cavity is kept at a temperature of T_c=10 ^{o}C and the right wall at T_h=50 ^{o}C. Due to the Soret effect, component separation will happen in the porous cavity even under the gravity condition; and the system will gradually reach the steady state. The pressure in the cavity is maintained at 35.0 MPa for C1-nC4-nC12 mixture and 1 atm for nC12-IBB-THN mixture.
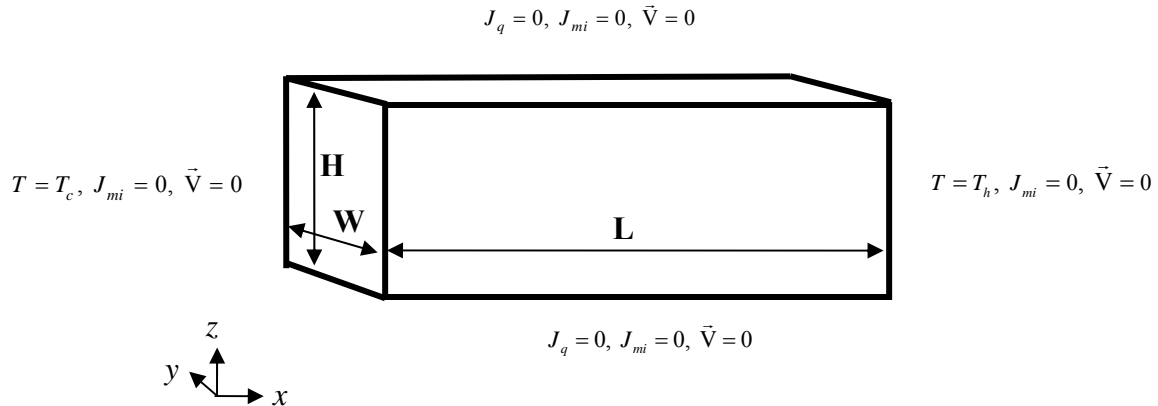
Figure 5.1: Schematic diagram of the horizontal porous cavity and boundary conditions.

79

Table 5.1: Physical properties of the mixture and porous material, T_{ave} =303 K.

Name	Value	Unit
Porous cavity length L	32	mm
Porous cavity width W	10.0	mm
Porous cavity height H	10.0	mm
Left wall temperature T_1	10	℃
Right wall temperature T_2	50	℃
Pressure at the centre of the cavity	35.0, 0.1013	MPa
Al_2O_3 density	3983.6	kg/m³
Al_2O_3 heat capacity	786.2745	J/kg/K
Al_2O_3 thermal conductivity	43	W/m/K
Al_2O_3 porosity	0.4	
Al_2O_3 porous medium permeability	$10^0 \sim 10^7$	mD
Al_2O_3 porous medium tortuosity	1.3	
C1-nC4-nC12 mixture compositions	50-20-30	(% mole fr.)
C1-nC4-nC12 mixture heat capacity	2355.4	J/kg/K
C1-nC4-nC12 mixture thermal conductivity	0.1158	W/m/K
nC12-THN-IBB mixture compositions	33.3-33.3-33.4	(% mass fr.)
nC12-THN-IBB mixture heat capacity	1885.9	J/kg/K
nC12-THN-IBB mixture thermal conductivity	0.123	W/m/K

5.4 Governing Equations and Boundary Conditions

The mass continuity equation is shown as:

$$\frac{\partial \rho_m}{\partial t} + \nabla \bullet \left(\rho_m \vec{V} \right) = 0 \tag{5.1}$$

For a multicomponent mixture, the continuity equation of component i is given as:

$$\frac{\partial (\rho_{mi})}{\partial t} + \nabla \bullet \left(\rho_{mi} \vec{V} \right) = -\nabla \bullet \vec{J}_{mi}, \quad i = 1, 2, ...n\text{-}1 \tag{5.2}$$

where $\vec{J}_{mi}$ is the molar diffusion flux of the ith component. The mole flux is subjected to a linear relationship to the driving forces of temperature and concentration gradient, and it can be expressed by:

$$\{\vec{J}_{mi}\} = -\rho_m \left(\sum_{j=1}^{n-1} \left[D_{ij}^* \right] \nabla X + \left\{ D_{Ti}^* \right\} \nabla T \right) \tag{5.3}$$

where T is the temperature. For binary mixtures, $\nabla X = \nabla x_1$ and $\vec{J}_{mi} = \vec{J}_{m1}$, and for ternary mixtures, $\nabla X = \begin{pmatrix} \nabla x_1 \\ \nabla x_2 \end{pmatrix}$ and $\vec{J}_{mi} = \begin{pmatrix} \vec{J}_{m1} \\ \vec{J}_{m2} \end{pmatrix}$. D^* and D_T^* are the molecular diffusion and thermodiffusion coefficients of the fluid mixture in the porous medium, respectively, which are related to the molecular diffusion coefficient and thermodiffusion coefficient in free liquid as:

$$\left[D_{ij}^* \right] = \frac{1}{\tau_M^2} \left[D_{ij} \right], \quad \left\{ D_{Ti}^* \right\} = \frac{1}{\tau_T^2} \left\{ D_{Ti} \right\} \tag{5.4}$$

where D and D_T are the molecular and thermodiffusion coefficients, which are functions of the temperature and composition of the fluid mixture. τ_M, and τ_T are tortuosities for the molecular diffusion and thermodiffusion coefficients in the porous cavity, respectively. Based on Costeseque's findings (2004), the molecular diffusion and thermodiffusion tortuosities were set equal to the tortuosity of the porous medium. The porous matrix is assumed homogeneous and isotropic. Therefore the Darcy equation is applied:

$$\vec{V} = -\frac{\kappa}{\varphi\eta} (\nabla P - \rho \vec{g}) \tag{5.5}$$

where κ and φ are the permeability and the porosity of the porous medium, respectively. By substituting the Darcy relation, Eq. 5.5, into the mass conservation equation, Eq. 5.1,

the pressure can be solved from the obtained differential equation, which leads to the following equation for pressure:

$$\frac{\partial\left(\rho_m\right)}{\partial t} - \frac{\kappa}{\varphi\eta}\frac{\partial}{\partial x}\left(\rho_m\left(\frac{\partial P}{\partial x}+\rho g_x\right)\right)$$
$$-\frac{\kappa}{\varphi\eta}\frac{\partial}{\partial y}\left(\rho_m\left(\frac{\partial P}{\partial y}+\rho g_y\right)\right) - \frac{\kappa}{\varphi\eta}\frac{\partial}{\partial z}\left(\rho_m\left(\frac{\partial P}{\partial z}+\rho g_z\right)\right)=0$$

(5.6)

The thermal energy conservation equation is expressed as follows:

$$\frac{\partial(\rho C_\mathrm{p})_\mathrm{e}T}{\partial t} + \varphi\vec{V}\bullet\nabla\left((\rho C_\mathrm{p})_\mathrm{fl}T\right) = k_\mathrm{e}\nabla^2 T$$

(5.7)

where $\left(\rho C_p\right)_e$ is the effective volumetric heat capacity of the system and k_e is the effective thermal conductivity of the system. These effective physical parameters are related to the fluid properties and the solid matrix properties as follows:

$$\left(\rho C_p\right)_e = \varphi\left(\rho C_p\right)_\mathrm{fl} + (1-\varphi)\left(\rho C_p\right)_s$$

(5.8)

$$k_e = \varphi k_\mathrm{fl} + (1-\varphi)k_s$$

(5.9)

The boundary conditions in this model are: (1) zero mass flux through all walls; (2) no-slip walls; and (3) lateral heating condition on two side walls and other walls are adiabatic. Figure 5.1 depicts the boundary conditions.

5.4 Molecular Diffusion and Thermodiffusion Model

The thermodiffusion can be described through the theory of non-equilibrium thermodynamics, (de Groot and Mazur, 1984). In an n-component fluid, by neglecting the

viscous pressure tensor and reaction, and assuming a mechanical equilibrium in the system, linear relations can be established between the mass and heat fluxes and their driving forces, respectively. These relations, as explained in Chapter 2, are called Onsager Equations and can be expressed by:

$$J_q' = -L_{qq}\frac{1}{T^2}\nabla T - \frac{1}{T}\sum_{k=1}^{n-1}L_{qk}\left\{\frac{\nabla_T\mu_k}{M_k} - \frac{\nabla_T\mu_n}{M_n}\right\}$$

(5.10)

$$J_i = -L_{iq}\frac{1}{T^2}\nabla T - \frac{1}{T}\sum_{k=1}^{n-1}L_{ik}\left\{\frac{\nabla_T\mu_k}{M_k} - \frac{\nabla_T\mu_n}{M_n}\right\}$$

(5.11)

where J_q' is the heat flux, L_{qq}, L_{qk}, L_{iq} and L_{ik} are the phenomenological coefficients called Onsager coefficients, μ_k is the chemical potential of component k. Through Eqs. 5.3 and 5.11, one can get the following formulation, (Firoozabadi *et al.*, 2000):

$$\left.\begin{array}{l}D_{ij} = \dfrac{R}{\rho_m x_n M_n}\displaystyle\sum_{k=1}^{n-1}L_{ik}\sum_{l=1}^{n-1}\dfrac{x_l M_l + x_n M_n\delta_{lk}}{M_j}\left.\dfrac{\partial\ln f_l}{\partial x_j}\right|_{x_j,T} \\[3mm] \\ D_{T,i} = \dfrac{L_{iq}}{\rho_m T^2}\end{array}\right\}$$

(5.12)

where x_j is the mole fraction of component j, M_j is the molecular weight of component j, $M = \sum_{j=1}^{n}M_j x_j$ is the molecular weight of the mixture, f_j is the fugacity of component j, R is the gas constant, L_{ik} and L_{iq} are Onsager coefficients, and δ_{jk} is the Kronecker delta ($\delta_{jk}=1$, if j=k and $\delta_{jk}=0$, if j≠ k).

All diffusion coefficients are defined as functions of thermodynamic properties of the mixture and Onsager coefficients. As shown from Eq. 5.12, both thermodiffusion and molecular diffusion coefficients can be given in terms of phenomenological coefficients.

83

According to the theory of non-equilibrium thermodynamics, a relationship between L_{iq} and L_{ik} is found by introducing the net heat of transport Q_k^*. This relation is given by:

$$L_{iq} = \sum_{k=1}^{n-1} L_{ik} \left(\frac{Q_k^*}{M_k} - \frac{Q_n^*}{M_n} \right)$$ (5.13)

In the Firoozabadi model the net heat of transport is given by:

$$Q_i^* = -\frac{\Delta \bar{U}_i}{\tau_i} + \left(\sum_{j=1}^{n} \frac{x_j \Delta \bar{U}_j}{\tau_j} \right) \frac{\bar{V}_i}{\sum_{j=1}^{n} x_j \bar{V}_j}$$ (5.14)

where $\Delta \bar{U}_i$ is the residual partial molar internal energy of the component i; $\bar{V}_i$ is the partial molar volume of component i; τ_i is the ratio of vaporization energy (also called cohesive energy) to energy of viscous flow of component i $\left(\tau_i = \Delta U_i^{vap} / \Delta U_i^{visc} \right)$. By following Eyring's viscosity theory (Glasstone *et al.*, 1941), the value of τ_i for each component can be obtained from plots of $\ln \eta_m$ against $1/T$ for pure components. In this work, the same value of 4.0 for τ_i of all components in hydrocarbon mixtures (non-associating mixtures) is assigned, as suggested by Shukla and Firoozabadi (1998).

Besides the net heat of transport (Eq. 5.14), molecular or Fick's diffusion coefficients are also needed to calculate thermodiffusion coefficients. The diffusion coefficients in a dilute binary mixture have to be evaluated before calculating Fick's diffusion coefficients. In this work, the expression given by Hayduk and Minhas (1982) is used for hydrocarbon binary mixture, (Taylor and Krishna, 1993):

$$D_{ij}^0 = 13.3 \times 10^{-8} V_i^{-0.71} \eta_j^{(10.2/V_i - 0.791)} T^{1.47}$$ (5.15)

where D_{ij}^0 is the binary infinite dilution diffusion coefficient of solute i in solvent j, [cm^2/s]; V_i is the molar volume of component i at its normal boiling point, [cm^3/mol]; η_j is the viscosity of pure component j, [MPa.s], and T is the mixture temperature, [K].

For a multicomponent mixture, the Maxwell-Stephan diffusion coefficient, $\bar{D}_{ij}$, is calculated based on the binary coefficients, D_{ij}^0. Taylor and Krishna (1993) have suggested the following formula:

$$\bar{D}_{ij} = (D_{ij}^o)^{x_j} (D_{ji}^o)^{x_i} \prod_{\substack{k=1 \\ k \neq i,j}}^{n} \left(D_{ik}^o D_{jk}^0 \right)^{x_k/2} \tag{5.16}$$

From the multicomponent mass transfer theory, the mass flux is given by:

$$\vec{J}_m = -\rho_m B^{-1} \Gamma \nabla X \tag{5.17}$$

Here the matrix B is defined by:

$$\left. \begin{aligned} B_{ij} &= -x_i \left(\frac{1}{\bar{D}_{ij}} - \frac{1}{\bar{D}_{in}} \right) \quad i \neq j \\[2em] B_{ij} &= \frac{x_i}{\bar{D}_{in}} + \sum_{\substack{k=1 \\ k \neq i}}^{n} \frac{x_k}{\bar{D}_{ik}} \qquad i = j \end{aligned} \right\} \tag{5.18}$$

and the elements of matrix Γ are:

$$\Gamma_{ij} = x_i \frac{1}{f_i} \frac{\partial f_i}{\partial x_j} \tag{5.19}$$

From Fick's law, the mass flux can be written as:

$$\vec{J}_m = -\rho_m D \nabla X \tag{5.20}$$

Comparing Eq. 5.20 with Eq. 5.17, one can have:

$$D = B^{-1}\Gamma \tag{5.21}$$

Therefore, the diffusion coefficient, D_{ij}, can be determined based on the elements in B and Γ matrices with the an equation of state and other physical properties.

With the Firoozabadi model for multicomponent mixtures and an equation of state, after specifying the mixture components and knowing the parameters of each pure component, the molecular diffusion coefficient and the thermodiffusion coefficient can be calculated by following these steps:

1. calculate thermodynamic properties of the mixture (partial molar volume, fugacity, internal energy, etc) using the equation of state. In this work, PR-EoS and vt-PR-EoS are used;
2. calculate the B (B_{ij}) and Γ (Γ_{ij}) matrices and then molecular diffusion coefficients;
3. calculate the Onsager coefficients (L_{ik}) from molecular diffusion coefficients following Eq. 5.12;
4. calculate the Onsager coefficients (L_{iq}) using Eq. 5.13;
5. finally, calculate the thermodiffusion coefficient and all mass flux terms.

In this work, the viscosity of the fluid mixture (η) is obtained with a method proposed by Lohrenz *et al*. (1964), as explained in detail in section 4.3, and given by

$$\eta = \eta^* + (\xi^4 - 10^{-4})/\zeta \tag{5.22}$$

5.5 Numerical Solution Procedure

Equations 5.1, 5.2, 5.5, 5.6 and 5.7 are solved numerically by using the control volume method, subject to the boundary conditions of zero flux at the rigid wall. All the walls are assumed to be solid walls, so three zero components of the velocity are maintained.

The second-order centred scheme is used in the space discretization, and a semi-implicit first-order scheme is used for the temporal integration. With respect to the non-linear convection terms, the power-law scheme is applied in order to achieve higher accuracy for the combined convection and diffusion cases. The obtained linear system of algebraic equations is solved at each time step using a bi-conjugated gradient iteration method with a given convergence criterion, which has been confirmed over many tests for the required accuracy. At the initial time step, the velocities were set to zero in the computational domain where initial pressure and concentration are specified. The convergence criterion is set for three parameters, the pressure, temperature and composition. The relative errors between internal iteration and any two successive time steps are calculated as follows:
For internal iteration at each time step,

$$\gamma_\theta = \frac{1}{nx \times ny \times nz} \sum_{i=1}^{nx} \sum_{j=1}^{ny} \sum_{l=1}^{nz} \left| \frac{\theta_{ijl}^{k,s+1} - \theta_{ijl}^{k,s}}{\theta_{ijl}^{k,s+1}} \right| \tag{5.23}$$

For convergence checking between two successive time steps after the convergence of the internal iteration,

$$\gamma_\theta = \frac{1}{nx \times ny \times nz} \sum_{i=1}^{nx} \sum_{j=1}^{ny} \sum_{l=1}^{nz} \left| \frac{\theta_{ijl}^{k,s+1} - \theta_{ijl}^{k-1,s0}}{\theta_{ijl}^{k-1,s0}} \right| \tag{5.24}$$

where θ represents the pressure, temperature, and composition, respectively, i, j, and l represent mesh indices along x, y, and z directions of the porous cavity; k denotes the time step; s is the indicator of inner iterations; s0 is the indicator of the converged inner iteration at the last time step and nx, ny, and nz represent the mesh number in x, y, and z

directions, respectively. The values of pressure, temperature and composition are defined in the centre of each control volume, but the velocities are defined on the surface of each control volume, or grid cell.

The solution procedure begins by assuming initial pressure, temperature and concentration values in the mixture. The fluid is considered to be weakly compressible, and the Peng-Robinson EoS is used to calculate the fluid thermodynamic properties. In fact, the density, and molecular diffusion and thermodiffusion coefficients are functions of the temperature and species compositions. They are evaluated for each control volume. The thermal conductivity is assumed constant in the analysis.

To get an optimum number of grids, mesh sensitivity analysis was examined for this work model. Performing a mesh sensitivity analysis is an integral part of producing accurate, time-efficient and cost-effective results. The mesh sensitivity is characterized by the average Nusselt number (Nu), as shown in Figure 5.2 and Table 5.2, which is defined at both lateral walls (hot and cold walls) of the porous medium as follows:

$$Nu = \frac{1}{WH}\int \left(\frac{L}{\Delta T}\frac{\partial T}{\partial x} \right)_{wall} dydz \qquad (5.25)$$

The average Nusselt number is equivalent to the non-dimensional heat flux averaged over the wall surface of the cavity. Figure 5.2 shows the relation between the average Nusselt number and different types of mesh. From this Figure, the best mesh can be chosen and adopted in the simulations. As can be seen, there is no significant difference in the average Nusselt number values between mesh type 4 and mesh type 8, so any mesh between them can be selected. The mesh type 6 (50x50x50 control volume) is selected.
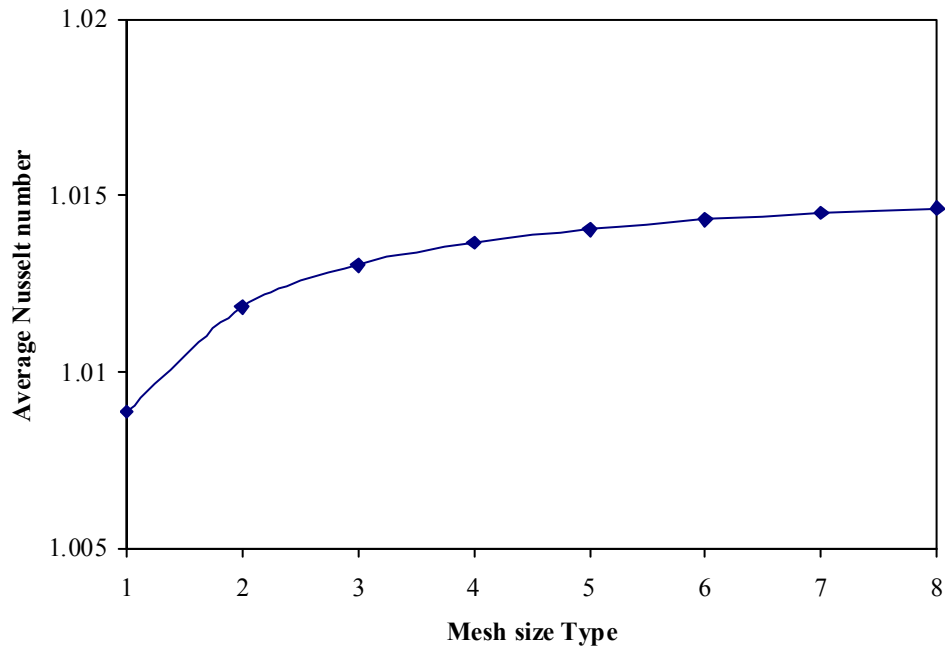
Figure 5.2: Nusselt number with mesh size.

Table 5.2: Mesh size sensitivity.

Type	3D Mesh number	Nu
1	10x10x10	1.008881
2	16x16x16	1.011856
3	20x20x20	1.013047
4	30x30x30	1.013677
5	40x40x40	1.014065
6	**50x50x50**	**1.014326**
7	60x60x60	1.014515
8	70x70x70	1.014656

5.6 Results and Discussion

5.6.1 Comparison between experimental data and numerical calculation

The only experimental data for a ternary mixture available in the literature is given by Leahy-Dios *et al*. (2005). Table 5.3 shows the comparison between our numerical result and the experimental data for a ternary mixture of nC12-THN-IBB. It is noticed that by using vt-PR-EoS for evaluating the thermodynamic properties, which are used in the Firoozabadi model, one obtains better agreement with the experimental data. It is found that the percentage errors for D_{T1}, D_{T2} and D_{T3}, when the vt-PR-EoS is used, are 12.63%, 23.11% and 49.65%, respectively. Furthermore, the mixture component's behaviour also is identical, for both experimental data and numerical values have the same sign for thermodiffusion coefficients. It can be concluded that the two components (nC12 and THN) migrate, one to the hot side and the other to the cold side, while the IBB was distributed randomly within the cavity, as its thermodiffusion coefficient value is small, and this confirmed that its separation remains small.

Table 5.3: The thermodiffusion coefficients (experimental and theoretical) of nC12-THN-IBB ternary mixture (33.3-33.3-33.4 wt%) at 25 $^{\circ}$C and 1 atm.

Method	$D_{T,nC12}$ ($10^{-12}\,\mathrm{m^2.s^{-1}K}$)	$D_{T,THN}$ ($10^{-12}\,\mathrm{m^2.s^{-1}K}$)	$D_{T,IBB}$ ($10^{-12}\,\mathrm{m^2.s^{-1}K}$)
Experimental	-1.021 ± 0.33	0.874 ± 0.43	0.147
Theo. PR-EoS	-1.523	1.262	0.261
Error	49.16%	44.39%	77.55%
Theo.vt-PR-EoS	-1.150	1.076	0.074
Error	12.63%	23.11%	49.65%

The density meter (DMA 5000-Anton Paar with an accuracy of $\pm 1\mathrm{x}10^{-6}\mathrm{g/cm^3}$ and temperature fluctuation $\pm 0.001\,^{\circ}\mathrm{C}$) has been used to measure the density of the nC12-THN-IBB mixture at different temperatures and compared with the numerical results in order to validate the equation of state (vt-PR-Eos). Figure 5.3 shows the variation of the density against the temperature for both the numerical model and the experimental data.

An excellent agreement was found between our numerical model and the experimental data, and the percentage error was less than 3.0%.
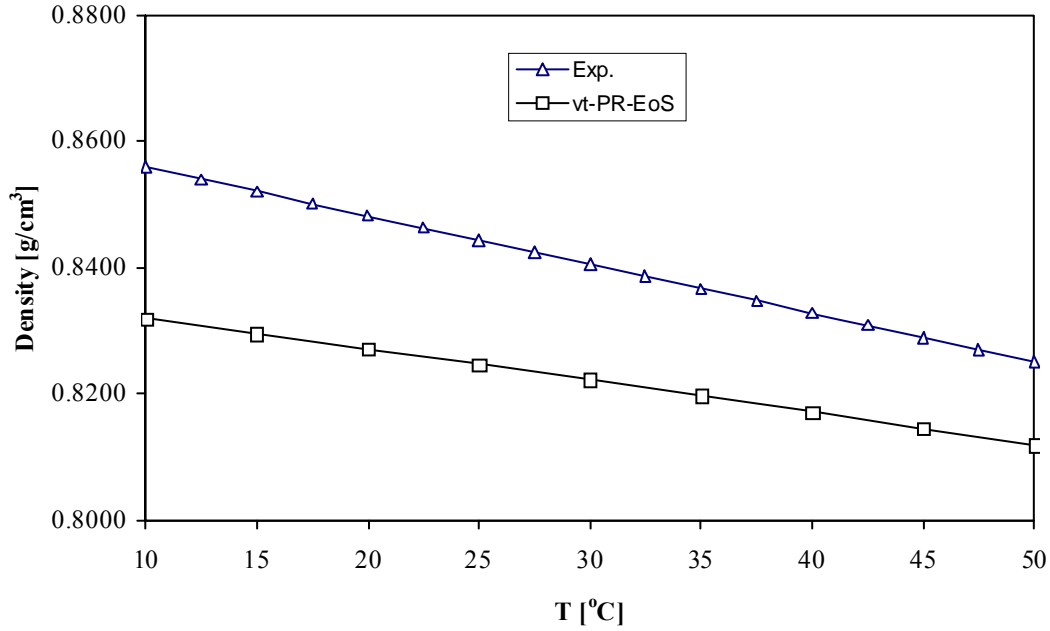
Figure 5.3: Density of nC12-IBB-THN mixture vs. temperature.

5.6.2 Permeability effect on composition distribution

As is known, the ternary mixture in this simulation consists of 50% methane (C1, component 1), 20% n-butane (nC4, component 2) and 30% n-dodecane (nC12, component 3). The compositional separation in the mixture is investigated for permeability ranging from 10^2 mD to 10^6 mD. It is found that the effect of permeability on separation is very strong, (see Figures 5.4 and 5.5), where the distribution of methane (C1) and n-butane (nC4) are illustrated along the vertical (z=0~H, x=L/2, y=W/2) and horizontal (x=0~L, z=H/2, y=W/2) directions. It is clear that the separation of mixture components in the horizontal direction decreases continuously as the permeability increases from 10^2 mD to 10^6 mD. When the permeability is 10^2 mD, the separation happens mainly along the horizontal direction, (see Figures 5.4a and 5.5a); while in the vertical direction it is very weak, (see Figures 5.4b and 5.5b).
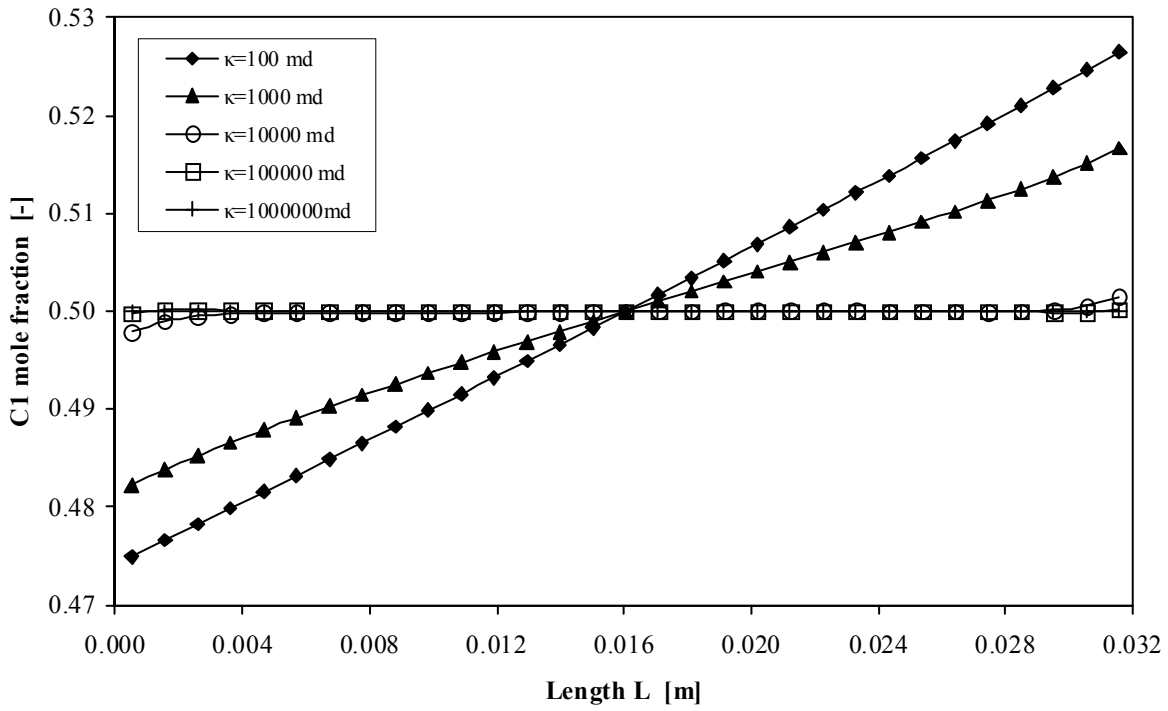
(a) Horizontal distribution
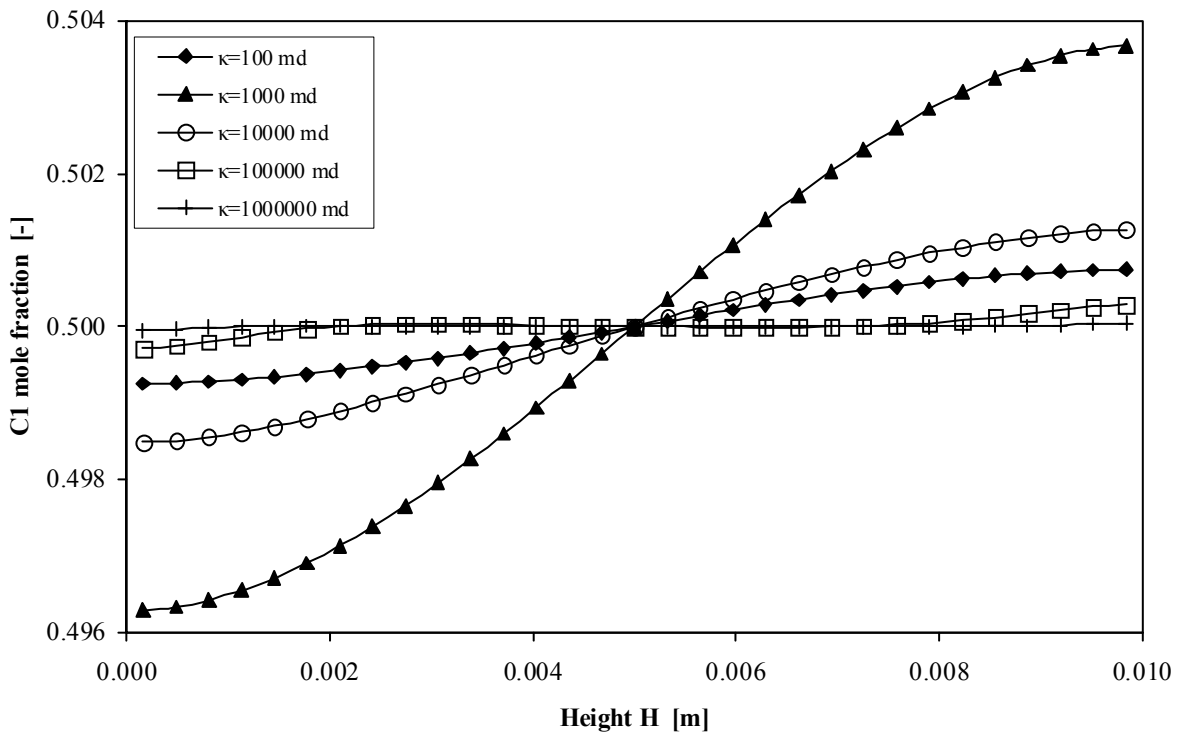
(b) Vertical distribution

Figure 5.4: Methane (C1) mole fraction distributions along the centre of the cavity.
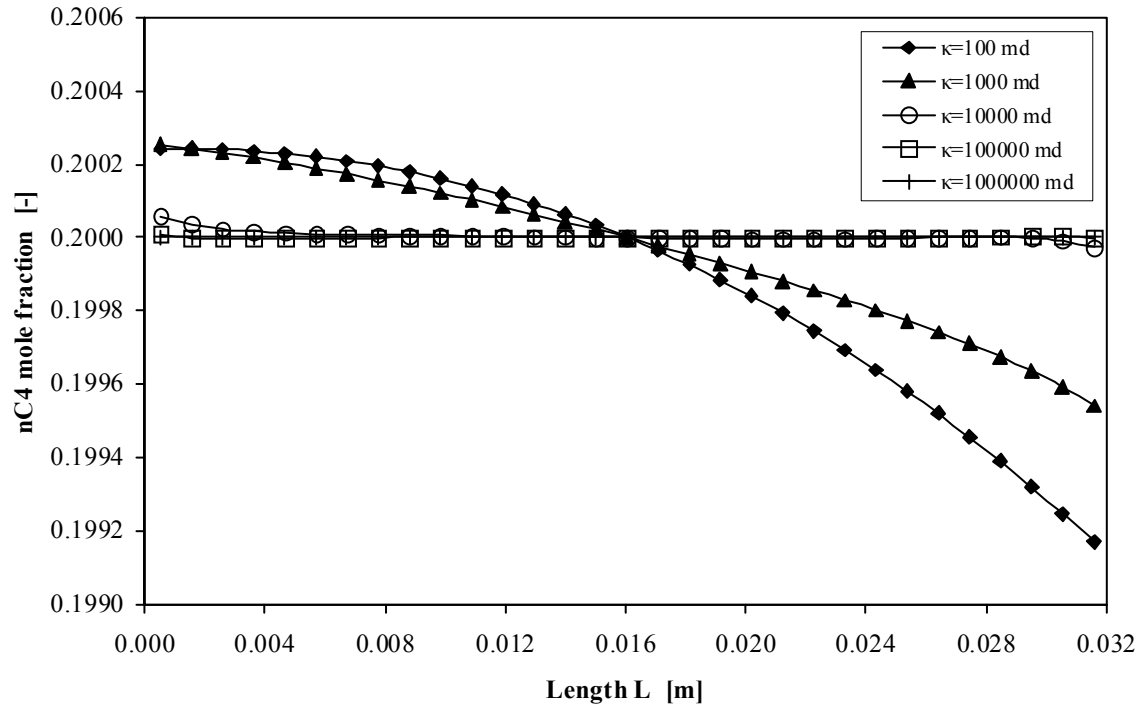
(a) Horizontal distribution
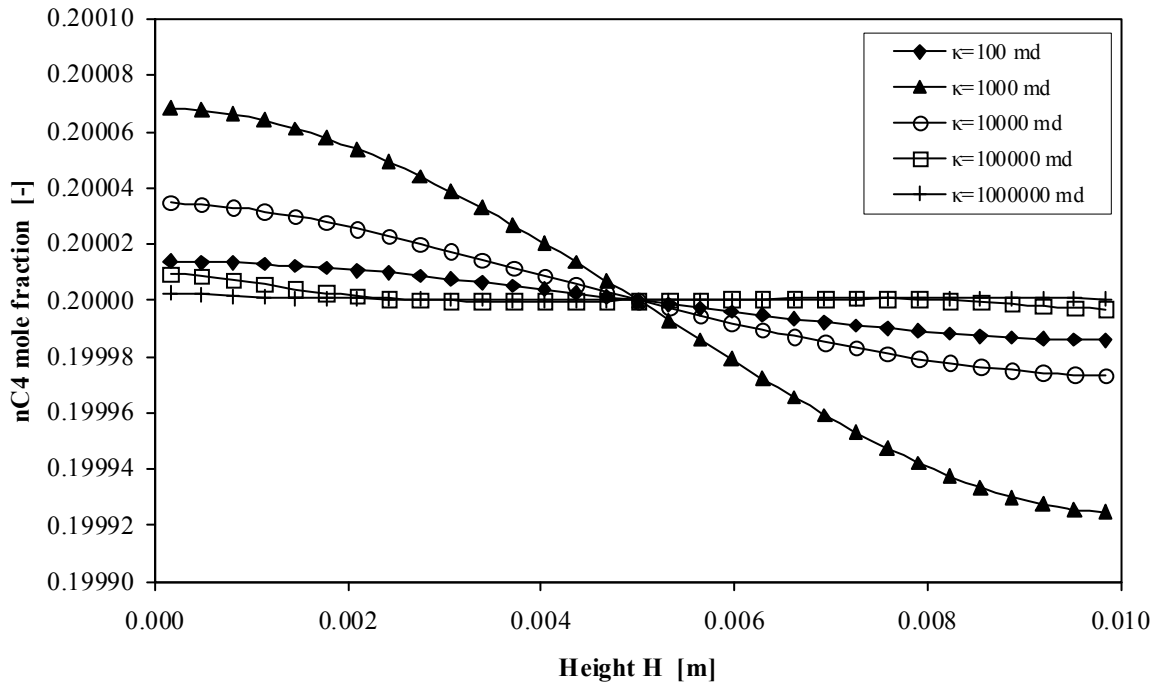
(b) Vertical distribution

Figure 5.5: n-butane (nC4) mole fraction distributions along the centre of the cavity.

Figure 5.6 displays the C1 and nC4 composition distribution in the centre x-z plane for different permeabilities (κ = 10, 10^2, 10^4, and 10^6 mD). An almost linear contour of methane and n-butane along the horizontal direction at 10, and 10^2 mD, is found. At those low permeabilities, the convection effect is greatly suppressed and the thermodiffusion effect is dominant, (see Figures 5.6a and 5.6b). As the permeability increases to 10^4 mD, the buoyancy convection begins to play a role causing a mixing in the cavity; therefore, the separations of methane and n-butane show a weakening in the horizontal direction, and curved lines are found in the vertical direction, (see Figure 5.6c). As the permeability continues to increase beyond 10^5 mD, the Soret effect is greatly weakened and the dominant effect of convection makes the separation almost impossible, (see Figure 5.6d). Figures 5.6a and 5.6b also illustrate the direction of the component separation due to thermodiffusion at low permeabilities. Methane, being the light component, moves towards the hot wall; and n-butane, being heavier than methane, moves towards the cold wall. Figure 5.7 shows the nC12 and THN composition distribution in the centre x-z plane for different permeabilities (κ = 10^2, 10^4, 10^5 and 10^7 mD). In this Figure, the trend of nC12 and THN is similar to those in Figure 5.6. As can be seen, the nC12 component migrates toward a hot side, being a lighter component and has a negative thermodiffusion coefficient, and the THN migrates to the cold side which is the heavier component and has a positive thermodiffusion coefficient, (see Figure 5.7a and 5.7b).

As already noticed, the permeability has a significant effect on the separation of mixture components. At low permeability the Soret effect is significant; while at high permeability convection becomes dominant. To further examine this phenomenon, a variable known as the separation ratio, q, is introduced:

$$q = \frac{x_{max}/(1-x_{max})}{x_{min}/(1-x_{min})} \qquad (5.26)$$

where x_{max} and x_{min} are the maximum and minimum concentrations of a solute component in the porous cavity, respectively.

The permeability impact on separation in the porous cavity can be shown with the separation ratio versus the permeability relation, given in Figures 5.8 and 5.9 for mixtures C1-nC4-nC12 and nC12-THN-IBB, respectively. From Figure 5.8, three distinct zones can be identified: (I) the permeability is below 10^2 mD. In this zone, the Soret effect is completely dominant. The separation ratio remains constant, and is about 1.248 for methane and 1.007 for n-butane; (II) the permeability is between 10^2 mD to 10^5 mD. In this zone both Soret and convection play important roles and as a result of this combined effect the separation ratio gradually reduces as the permeability increases; (III) the permeability is higher than 10^5 mD. In this zone the convection is the dominant mechanism, therefore, the separation ratio decreases rapidly towards 1.0, which indicates that the components are largely mixed in the cavity and no noticeable separation can be achieved.

Three zones are noticed in Figure 3.9 (similar behaviour to the one in Figure 3.8). In the first zone (I), the thermodiffusion is dominant and the separation ratio is constant (q=1.31 for THN component and q=1.45 for nC12 component), where the permeability value is between 0.01 to 30 mD. The permeability value for the second zone (II) is between 30 and 10^5 mD; both thermodiffusion and convection effect are found. In the third zone (III), the convection   plays a significant roll, and the permeability in this zone is between 10^5 to 10^7 mD.

 This theoretical analysis can be very useful in many ways. For example, in the case of measuring diffusion coefficients in a porous cavity, an optimal design of the porous cavity will be the key to determine if the experiments can be feasibly performed. A too low permeability cavity will require a long time for experiments to establish the steady state; therefore, it is ineffective or even infeasible. A too high permeability cavity, on the other hand, will fail to suppress the negative effect of convection. If the mixture of methane (50%), n-butane (20%) and n-dodecane (30%) is to be measured, the optimal permeability would be around 10^2 mD.

Benano-Melly *et al.* (2001) found that the maximum value for the separation ratio, q=q$_{max}$, existed for the permeability value, $\kappa = \kappa_m$ given by:

$$\kappa_m = \frac{\eta_m D^M \phi \sqrt{120}}{g \beta_T \Delta T H \rho} \qquad (5.27)$$

This analytical expression predicts that the maximum separation of methane will occur at κ_m=320 mD whereas our numerical calculation showed that the maximum separation ratio occurred at κ_m=350 mD (q$_{max}$=1.2509). This discrepancy between the analytical and the numerical modeling is justified by the fact that in our case the solutal buoyancy is included and both the thermodiffusion and molecular diffusion coefficients are functions of temperature and fluid mixture.
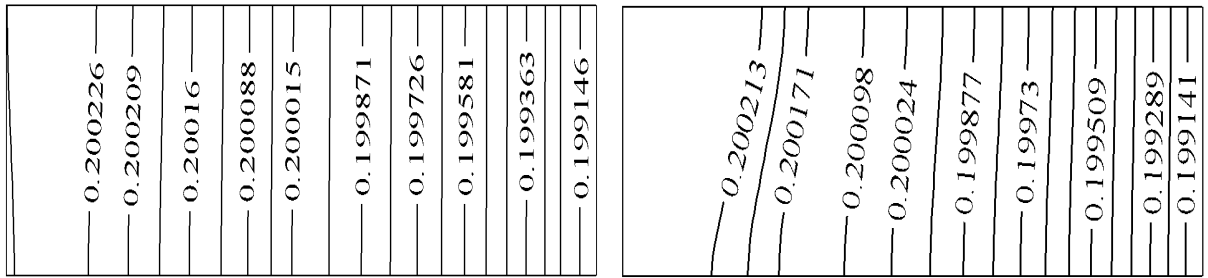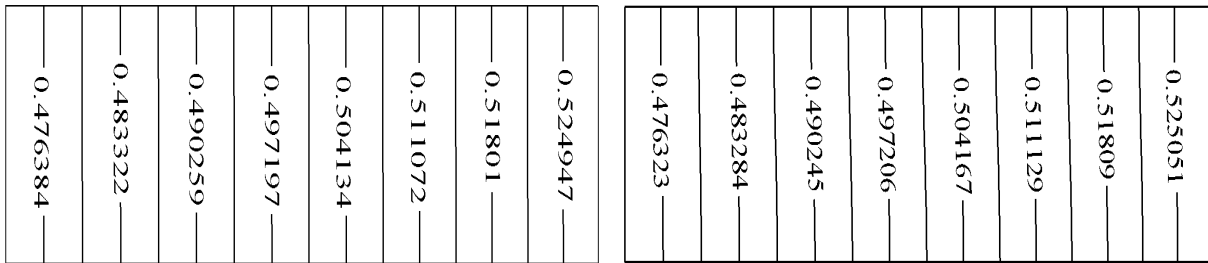
(a) $\kappa = 10$ mD   (b) $\kappa = 10^2$ mD
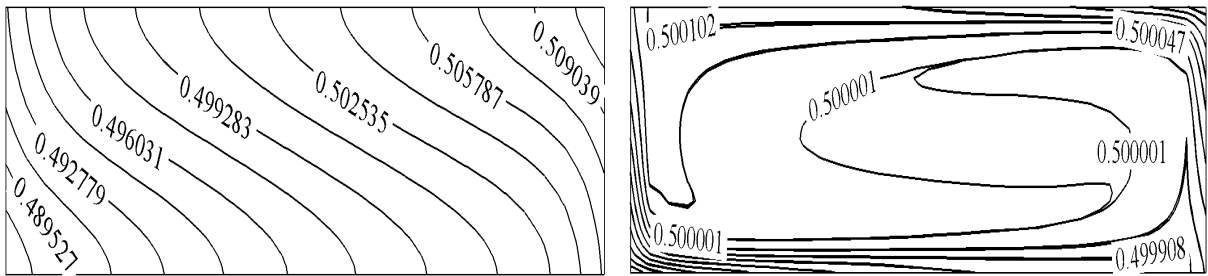
(c) $\kappa = 10^4$ mD   (d) $\kappa = 10^6$ mD

Figure 5.6: C1/nC4 compositional distributions in the centre x-z plane of the C1-nC4-nC12 ternary mixture.
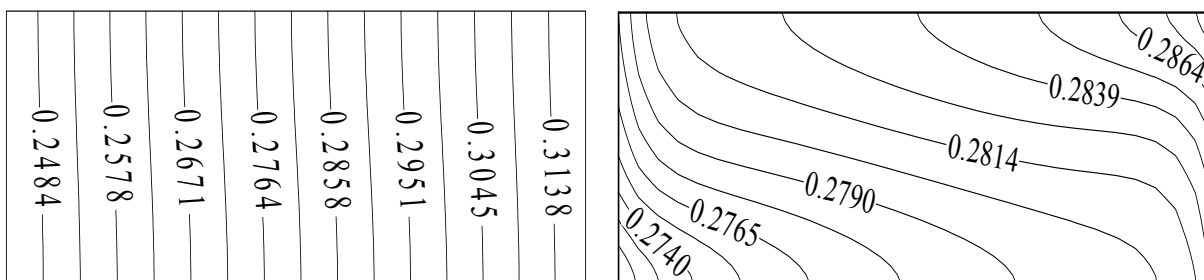
(a) $\kappa = 10^2$ mD
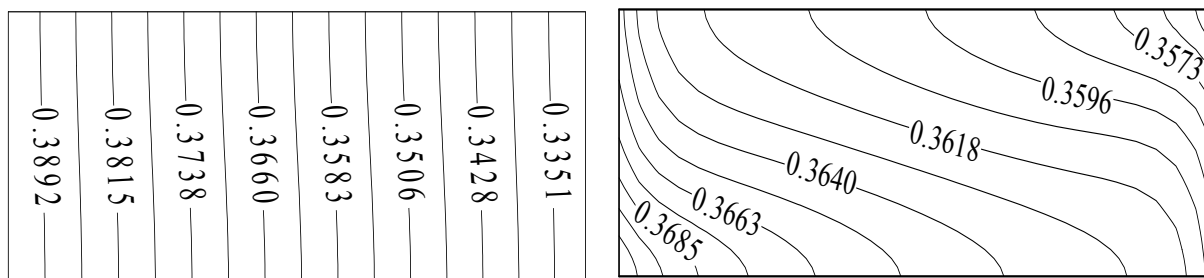
(b) $\kappa = 10^4$ mD
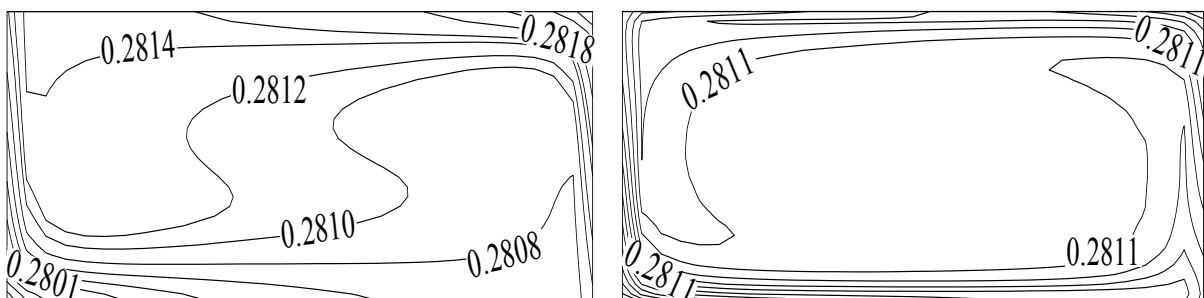
(c) $\kappa = 10^5$ mD
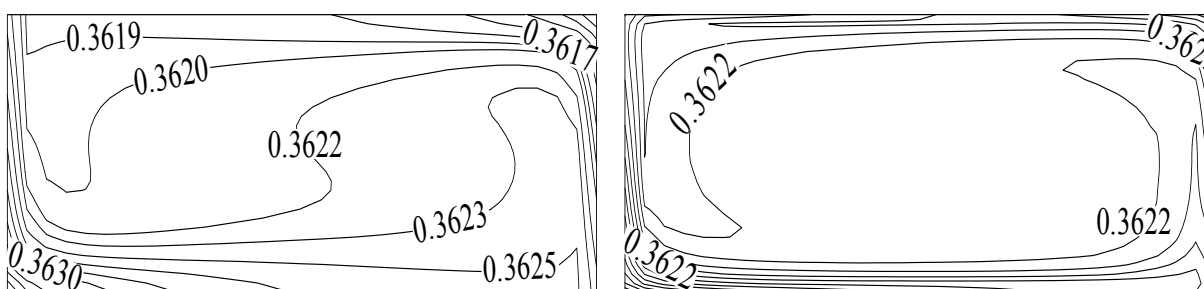
(d) $\kappa = 10^7$ mD

Figure 5.7: nC12/THN compositional distribution in the centre x-z plane of the nC12-THN-IBB ternary mixture.
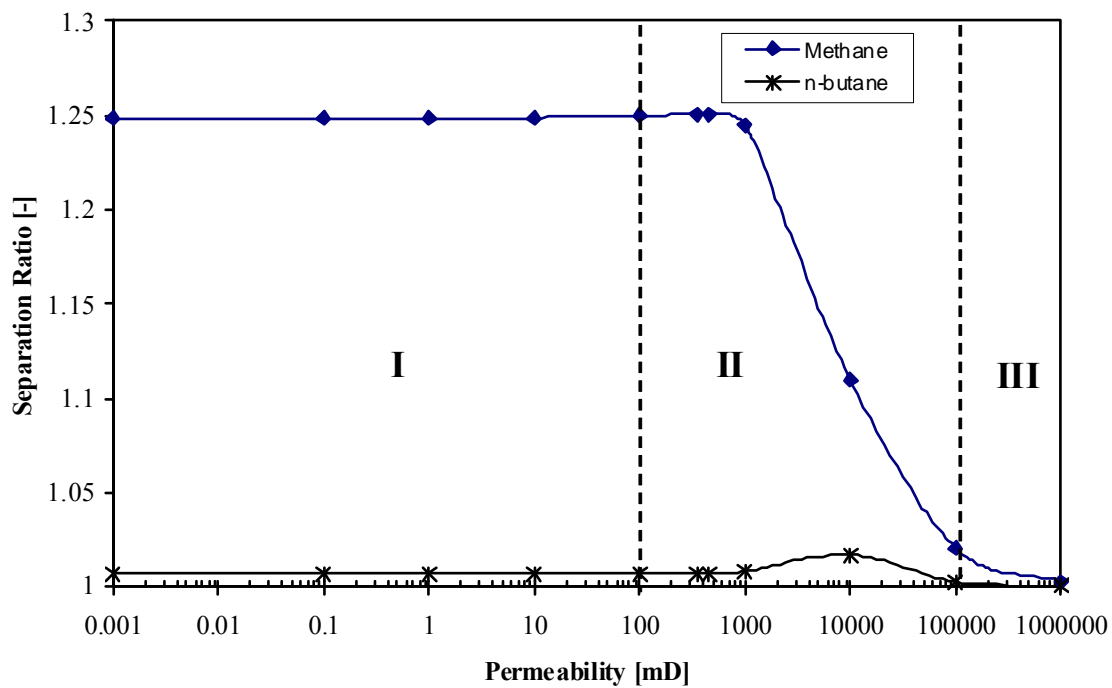
Figure 5.8: Permeability vs. separation ratio of C1-nC4-nC12.
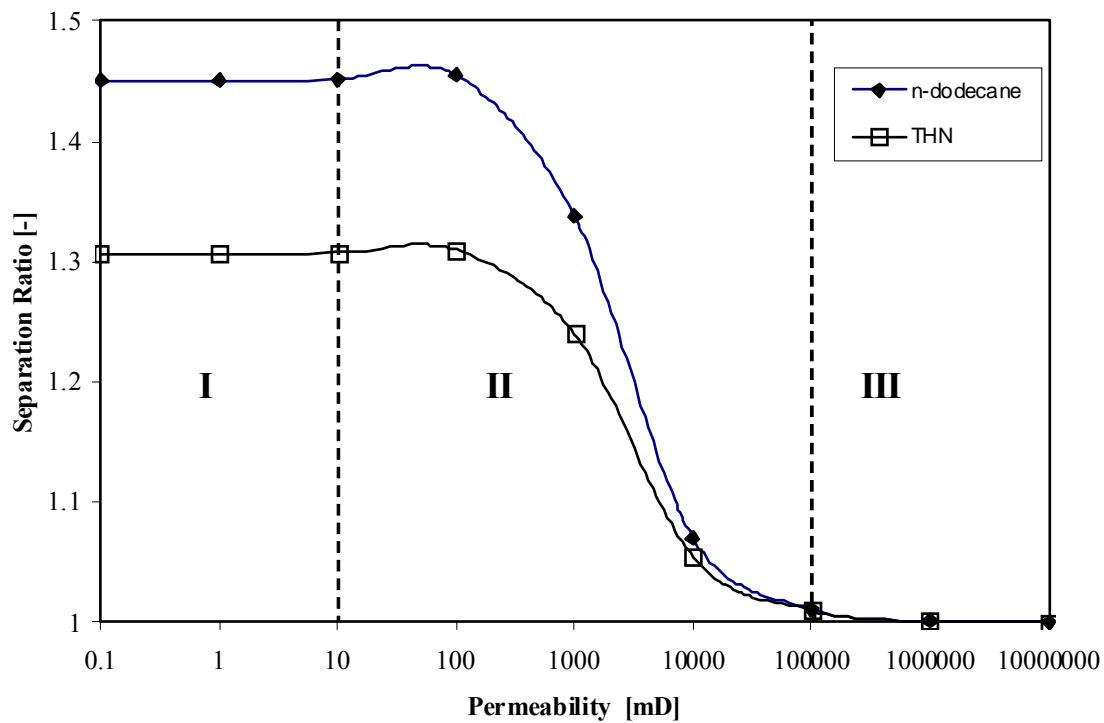
Figure 5.9: Permeability vs. separation ratio of the nC12-THN-IBB ternary mixture.

5.6.3 Viscosity effect on diffusion coefficients

All the calculations in previous sections assume that the viscosities of the mixture components are constants and are evaluated at the average temperature (T_{av}=303 K). In this section the viscosity variation due to the temperature will be considered for each component in order to investigate the viscosity effect on D, D_T and the compositional calculation. Figure 5.10 shows the variation of the n-dodecane and n-butane viscosity as a function of the temperature. It can be seen that the viscosity of n-dodecane (nC12, carrier fluid) changes significantly with the temperature. When the temperature varies between T_c=283 K and T_h=323 K, the viscosity of n-dodecane varies between 1.85×10^{-3} Pa.s and 9.45×10^{-4} Pa.s, while for n-butane no major variation is observed. As for the methane, it was found that the viscosity does not vary with temperature, which is similar to the n-butane behaviour.

The viscosity of each component at three different temperatures, which are the cold temperature T_c, the hot temperature T_h and the average temperature T_{av}, was estimated. For each temperature condition the calculation was repeated taking into consideration the new estimated viscosity. The variation of molecular diffusion and thermodiffusion coefficients versus the horizontal direction are shown in Figures 5.11 and 5.12, when the permeability is set equal to 10^2 mD. It is found that the thermodiffusion is affected by the change in viscosity. The deviation of the methane thermodiffusion coefficient is about $\pm 10\%$ (see Figure5.11a), while the deviation of the n-butane thermodiffusion coefficient is about $\pm 4.5\%$, (see Figure 5.11b).

Figure 5.12 illustrates the variation of the molecular diffusion coefficient along the horizontal centre line direction for methane when the permeability is set equal to 10^2 mD. Results reveal that again the molecular diffusion coefficient based on the viscosity at T_c and T_h deviates about $\pm 9\%$ from the one at T_{av}. A Similar variation is observed for the n-butane component.
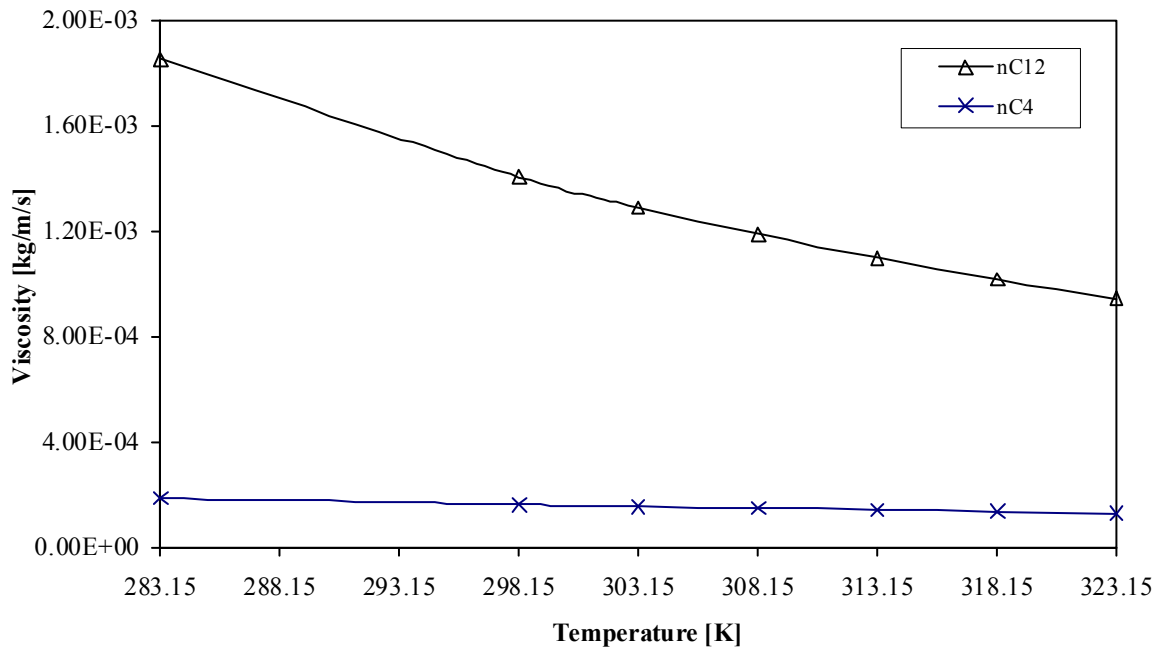
Figure 5.10: Viscosity variation with temperature of n-dodecane and n-butane.
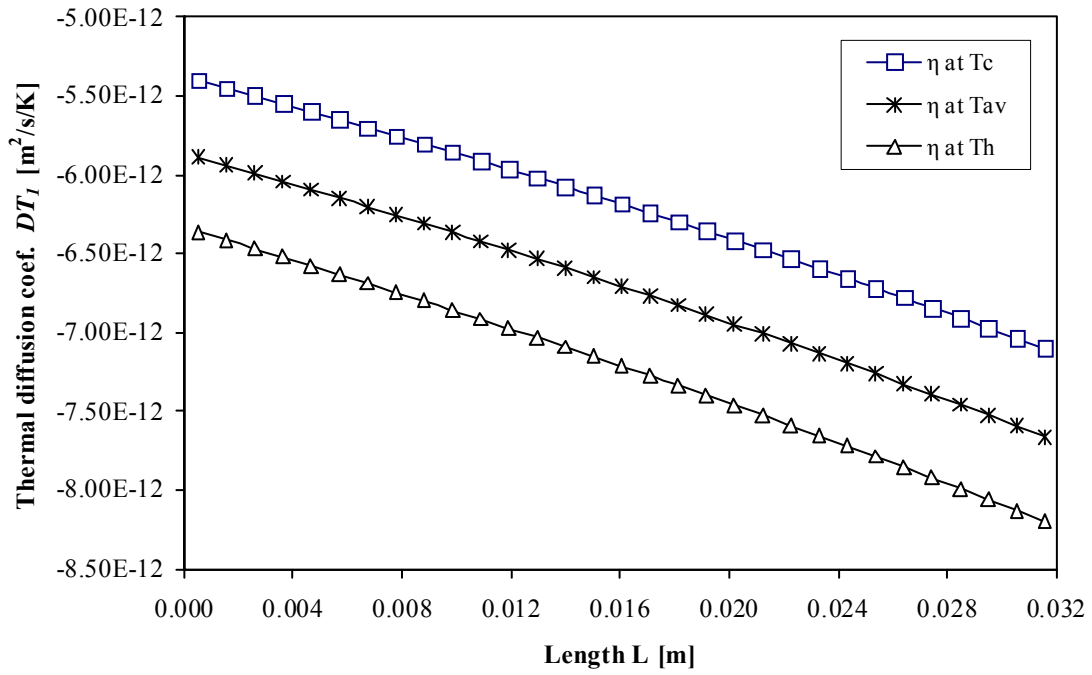
(a) Methane
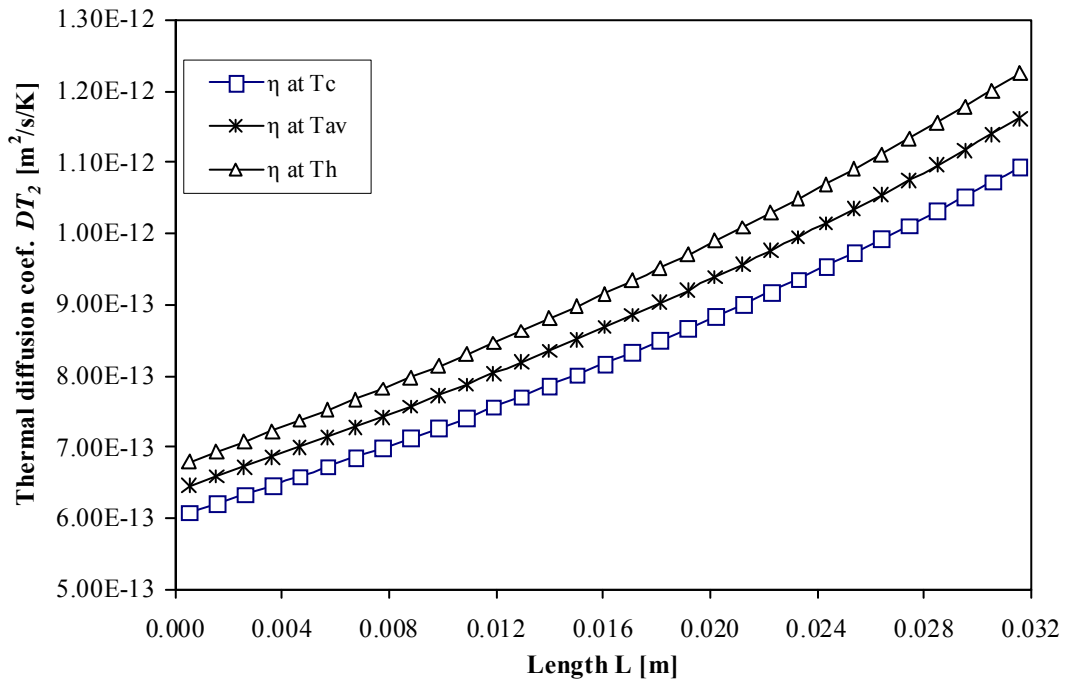
(b) n-Butane

Figure 5.11: Thermodiffusion coefficient distributions for methane and n-butane along the horizontal direction ($\kappa = 10^2$ mD).
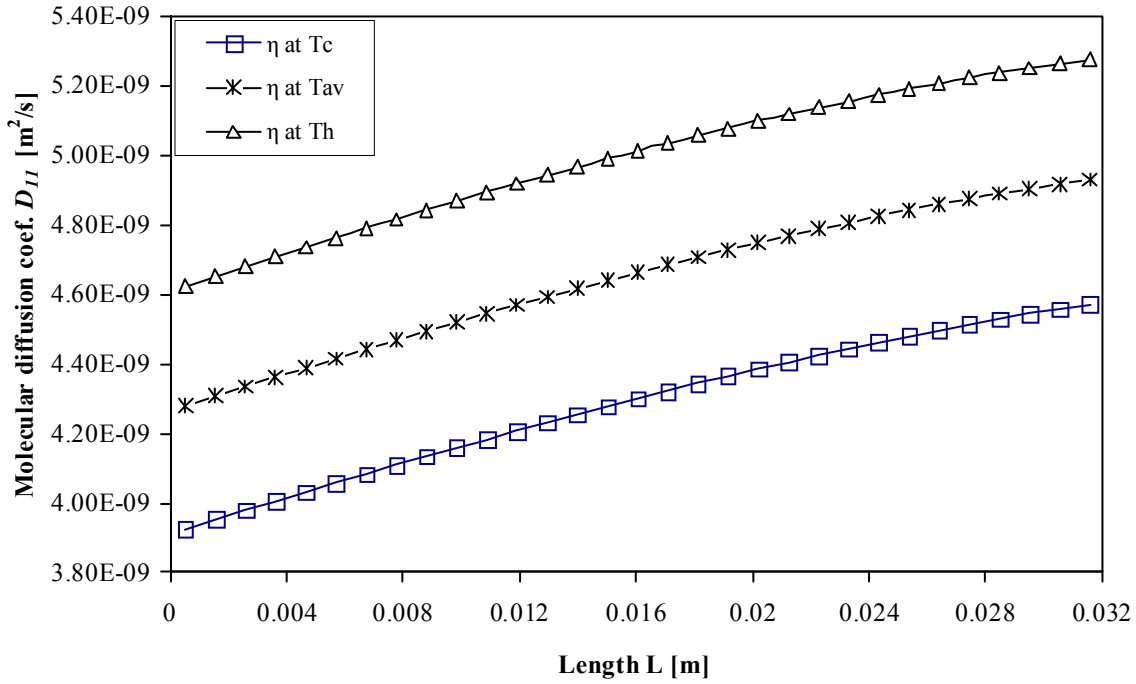
Figure 5.12: Variation of the molecular diffusion coefficient of methane along the horizontal cavity (κ =10^2 mD).

5.8 Summary

The thermosolutal convections of two ternary mixtures, C1-nC4-nC12 and nC12-THN-IBB in a porous cavity subjected to, respectively, 35.0 MPa and 1 atm pressure, and a horizontal temperature gradient are investigated over a wide range of permeability. The model was based on the non-equilibrium thermodynamics theory, and diffusion coefficients were calculated with time and space dependent fluid properties and compositions. The component concentration distribution and the separation ratio were used to examine the behaviour of the thermodiffusion and buoyancy-driven convection. The impact of permeability variation on the component separation results at steady state is numerically investigated. It was found that for permeability below 300 mD the thermodiffusion (or Soret coefficient) for both mixtures is dominant; and above this level,

buoyancy convection became the dominant mechanism. The viscosity is found to influence the evaluation of the molecular and thermodiffusion coefficients. Furthermore, the results showed that with variable viscosity the flow due to thermodiffusion is affected.

The comparison between numerical result and the experimental data for a ternary mixture of THN-IBB-nC12 is carried out. It is noticed that by using vt-PR-EoS for evaluating the thermodynamic properties, which are used in the Firoozabadi model, one obtains better agreement with the experimental data.   It is found that the percentage errors for D_{T1}, D_{T2} and D_{T3}, when the vt-PR-EoS is used, are 12.63%, 23.11% and 9.65%, respectively. Furthermore, the mixture component's behaviours also are identical, for both experimental data and numerical values have the same sign for thermodiffusion coefficients. The two components (nC12 and THN) migrate, one to the hot side and the other to the cold side, while the IBB was distributed randomly within the, as its thermodiffusion coefficient value is small, and this confirmed that its separation remains small.

Finally, the density of the nC12-THN-IBB mixture at different temperatures was compared with the numerical results in order to validate the equation of state (vt-PR-Eos). The results showed an excellent agreement between numerical model and the experimental data, and the percentage error was less than 3.%.

Chapter 6

Three-Dimensional Study of Permeability Effect on Convection in Heterogeneous Porous Medium Filled with a Ternary Hydrocarbon Mixture

In this chapter, the effect of permeability in the heterogeneous porous medium on fluid transport is studied with consideration of thermodiffusion (Soret effect) and molecular diffusion. A ternary mixture of nC12-THN-IBB in a porous medium subjected to lateral heating is numerically investigated at atmospheric pressure. Employing a single phase model and Darcy's law, the continuity and the energy equations are solved numerically, using the finite volume method (a combination of a commercial Computational Fluid Dynamics software, Fluent, and our FORTRAN Code). Various permeability ratios ($\kappa_f / \kappa_s = 10$, 100, 1000 and 10000) are examined in this study, and they cover a wide range of oil reservoirs. The temperature, fluid flow and solute fields are discussed in detail in order to show the sub-domain's effect on fluid transport, especially when thermodiffusion is taken into consideration.

6.1 Introduction

This work focuses on fluid transport in a heterogeneous porous medium, where molecular diffusion and thermodiffusion or Soret effect have been taken into consideration. This work is considered an extension to our previous work (Chapter 5), in which molecular and thermodiffusion in a homogeneou*s* porous medium are examined. It was shown that the permeability has a significant effect on the separation of the mixture components. At low permeability the thermodiffusion effect was significant; whereas at high permeability convection becomes dominant and the concentration of mixture components becomes uniform.

There are many applications related to fluid flow through a heterogeneous or fractured porous medium, such as in the areas of geosciences, oil reservoirs, ground-water hydrology and nuclear waste storage, (Tsang and Birkholzer *et al*. 1999, Jianchun *et al*. 2003, Wu *et al*. 2006). The research on fluid flow in fractured porous reservoirs dates back to the 1960's. Barenblatt *et al*. (1960) and Warren and Root (1963) presented the concept of dual-porosity within petroleum reservoirs to investigate the fractures of the porous media. They assumed interconnected set fractures which are supplied with fluid from numerous small matrix blocks between them, and they called this system an idealized model. Kazemi *et al*. (1976) were the first to incorporate the dual-porosity concept into a numerical model, with application to fluid flow on a large scale. One porosity is associated with the porous matrix and the other associated with the fracture. They also extended the dual-porosity model to a dual-porosity/dual-permeability model, where the simulation of fractured reservoirs involves discretization of the solution domain into two continua, one the domain representing the primary matrix, and a secondary domain representing fractured formulations.

Saghir and Islam (1999) numerically investigated the effect of convection in a dual-porosity/dual-permeability porous medium by using salty and fresh water. They applied the Brinkman momentum balance equation and simultaneously solved the mass and energy equations using a two-dimensional model. Ghorayeb and Firoozabadi (2000) studied the effect of the fracture parameters on the fluid compositional variation, including the fracture aperture (or fracture permeability), fracture intensity, and fracture connectivity. Numerical results revealed that for a high fracture aperture, a pronounced convective motion within the fracture takes place, whereas the composition is only affected beyond a certain fracture aperture. They also examined the effect of connected and discrete fractures on compositional variation: connected fractures influence the compositional variation much more than discrete fractures. Their results also indicated that the main effects on the compositional variation are due to the surrounding fractures. A model for flow interaction between a fracture and the rest of the porous medium has been presented by Alboin *et al*. (2002). In this model the fracture is an interface dividing

the domain of calculation into sub-domains. Fractures in a porous medium were considered individually with higher permeability than the surrounding rock.

The phenomenon of three-dimensional variable-density flow in fractured porous media was studied by Graf and Therrien (2005). Two cases were tested: in the first case, the fracture was discretized by inclined two-dimensional elements, while in the second case, the fracture consisted of horizontal and vertical elements. They found that the variable-density flow in a porous matrix with a 45° inclined fracture shows two different convention cells that form at different times. Both cells grew with time and migrated downwards into the aquifer. They also found that the high permeability fractures appear as a barrier to convection. Jiang $et\ al.$ (2006) carried out a mathematical simulation to illustrate the thermodiffusion phenomena of binary mixtures in the two-dimensional heterogeneous porous medium, which was laterally heated while filled with a binary mixture of methane and n-butane. The thermodiffusion process, the concentration distribution, and the separation ratio due to the temperature gradient and natural convection flow were investigated. The numerical model was based on a vertical porous medium, where the permeability in the lower region of the porous medium was kept constant, while varying the permeability in the upper region of the porous medium. They found that as the permeability increases in the upper domain, the convection flow dominates in the upper region, and the opposite results were obtained when the permeability was lower. Thus, they observed that the heterogeneity of the porous medium has a strong effect on the convective flow pattern. In addition, they argued that the Soret effect varied drastically in the upper region of the model in accordance with the variation of the permeability.

In this present work, an attempt is made to simulate the thermosolutal convection of a ternary mixture of nC12-THN-IBB in the presence of thermodiffusion in a non-homogeneous porous medium; also, in the present study, the geometry, which was used in the previous chapter, is scaled up by a factor of 1000.

6.2 Model Description

A rectangular prism of heterogeneous porous medium, with a horizontal length L of 32 m, thickness W of 10 m and height H of 10 m is used (see Figure 6.1). The permeability of the matrix (main domain) is lower than the permeability of the sub-domains, and these sub-domains are assumed to be in equilibrium with the rest of the porous medium (matrix). In order to examine the effect of the sub-domains on the fluid flow and mixture composition, two different configurations of a saturated heterogeneous porous medium are examined here, (see Figure 6.2). The width of the sub-domain is assumed to be 2 m. Physical properties of the ternary mixture and its components are given in Tables 6.1 and 6.2, respectively. The walls are assumed to be non-reacting, solid, impermeable, with lateral heating in the x direction, where the left wall of the heterogeneous porous medium is kept at a temperature $T_c = 10$ °C and the right wall at $T_h = 50$ °C ; and the remaining walls are assumed to be adiabatic; the pressure in the whole rectangular prism is maintained at 1 atm. The fluid is assumed to be compressible, with no chemical reaction, no interactive forces between the porous medium particles and the fluid mixture.
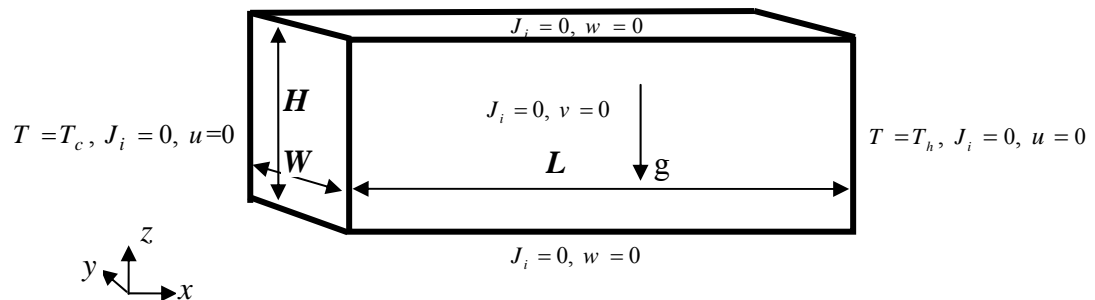
Figure 6.1: Schematic diagram of the rectangular porous medium and boundary conditions.
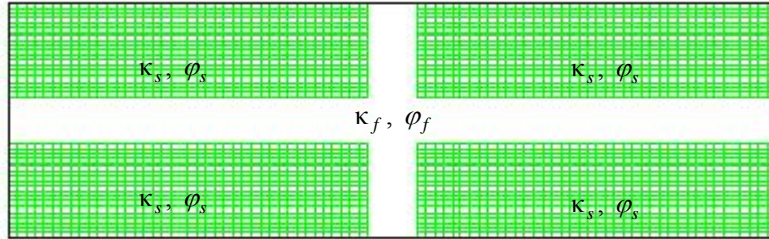
a) Configuration 1
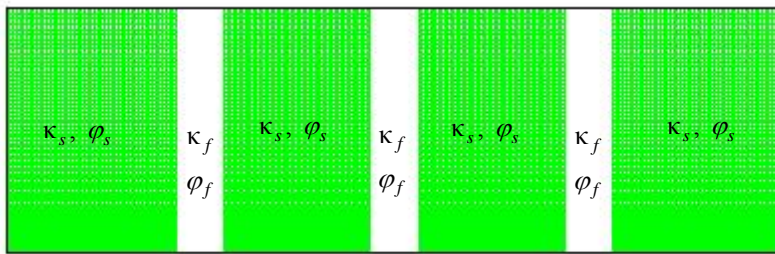
b) Configuration 2

Figure 6.2: Heterogeneous porous medium configurations, x-z plane.

Table 6.1: Physical properties of the fluid mixture and porous material at T_0=303.15 K and p_0=1 atm.

Name	Value	Unit
porous medium density	3983.6	$kg.m^{-3}$
porous medium heat capacity	786.2745	$J.kg^{-1}.K^{-1}$
porous medium thermal conductivity	43	$W.m^{-1}.K^{-1}$
nC12-THN-IBB mixture compositions	33.3-33.3-33.4 or 0.281-0.362-0.357	(% mass fr.) (% mole fr.)
Heat capacity of mixture	1885.9	$J.kg^{-1}.K^{-1}$
Molecular weight of nC12	170.33	$kg.kmol^{-1}$
Molecular weight of THN	132.20	$kg.kmol^{-1}$
Molecular weight of IBB	134.22	$kg.kmol^{-1}$
Thermal conductivity of mixture	0.123	$W.m^{-1}.K^{-1}$
$\begin{bmatrix} \bar{D}_{11} & \bar{D}_{12} \\ \bar{D}_{21} & \bar{D}_{22} \end{bmatrix}$	$\begin{bmatrix} 7.52 \times 10^{-10} & 9.06 \times 10^{-10} \\ 3.00 \times 10^{-10} & 1.11 \times 10^{-09} \end{bmatrix}$	$m^2.s^{-1}$
$\begin{bmatrix} D^*_{T,1} & D^*_{T,2} \end{bmatrix}$	$\begin{bmatrix} -4.41 \times 10^{-7} & 2.84 \times 10^{-7} \end{bmatrix}$	$kg.s^{-1}.m^{-1}$

Table 6.2: Physical properties of the mixture components at T_0=303.15 K.

Component	T_c (K)	P_c (Pa)	$\rho \left(kg.m^{-3} \right)$	$C_p \left(J.kg^{-1}.K^{-1} \right)$	$k \left(W.m^{-1}.K^{-1} \right)$
$nC_{12}H_{26}$	658.20	1.82×10^6	741.86	2220.97	0.1368
THN	720.15	3.62×10^6	963.48	1662.63	0.1293
IBB	650.15	3.04×10^6	844.95	1820.52	0.1205

6.3 Governing Equations

The following are the governing equations, which were introduced in Chapter 2.

6.3.1 Conservation of mass

The differential mass continuity equation for the entire mixture is given as follows:

$$\frac{\partial \rho}{\partial t} + \frac{\partial (\rho u)}{\partial x} + \frac{\partial (\rho v)}{\partial y} + \frac{\partial (\rho w)}{\partial z} = 0 \tag{6.1}$$

where ρ is the density of the mixture fluid, u, v, and w are the velocity components in x, y and z directions, respectively. The mass continuity equation for species i is:

$$\frac{\partial (\rho \omega_i)}{\partial t} + \nabla \cdot \left(\rho \omega_i \vec{\mathbf{V}} \right) = -\nabla \cdot \vec{j}_i \quad i = 1,2,.......n-1, \ \sum_{i=1}^{n} \vec{j}_i = 0 \tag{6.2}$$

where $\vec{j}_i$ is the diffusive mass flux of species i, ω_i is the mass fraction of the component i. The diffusive mass flux can be expressed as follows, (Taylor and Krishna 1993):

$$\vec{j}_i = -\sum_{j=1}^{n-1} \rho D_{ij}^* \nabla \omega_j - D_{T,i}^* \frac{\nabla T}{T} \tag{6.3}$$

where T is temperature, D_{ij}^* is the binary molecular diffusion coefficient of the fluid mixture in the porous medium, D_T^* is the thermodiffusion coefficient in the porous medium of component i. In this study, the thermodiffusion coefficients are assumed constant, and have been evaluated with time and space dependent fluid properties based on the non-equilibrium thermodynamics theory (as explained in the previous chapter). The molecular diffusion coefficients can be defined as follows, (Taylor and Krishna 1993):

$$D_{ij}^* = [D] = [A]^{-1}[B] \tag{6.4}$$

where

$$A_{ii} = -\left(\frac{x_i M}{\bar{D}_{in} M_n} + \sum_{\substack{j=1 \\ j\neq i}}^{n} \frac{x_j M}{\bar{D}_{ij} M_i} \right) \tag{6.5}$$

$$A_{ij} = x_i \left(\frac{1}{\bar{D}_{ij}} \frac{M}{M_j} - \frac{1}{\bar{D}_{in}} \frac{M}{M_n} \right) \tag{6.6}$$

$$B_{ii} = -\left(x_i \frac{M}{M_n} + (1 - x_i) \frac{M}{M_i} \right) \tag{6.7}$$

$$B_{ij} = x_i \left(\frac{M}{M_j} - \frac{M}{M_n} \right) \tag{6.8}$$

Where $\bar{D}_{ij}$ is the Maxwell-Stefan coefficient, M is the molecular weight of the mixture ($M = \sum_{i=1}^{n} M_i x_i$), and M_i is the molecular weight of the component i.

6.3.2 Conservation of momentum

In porous media, Darcy's equation can be used and is valid, when $\vec{v}$ is sufficiently small (i.e. the Reynolds number of the flow, based on a typical pore diameter, is of the order of unity or smaller), as explained by Nield and Bejan (2006). Darcy's equation can be expressed as follows:

$$\vec{V} = -\frac{\kappa}{\varphi\eta}(\nabla P - \rho\vec{g}) \tag{6.9}$$

The Boussinesq approximation is assumed to be valid for the range of temperature and composition in this study, so that the density of fluid the mixture is expressed as follows:

$$\rho = \rho_0 \left[1 - \beta_T \left(T - T_0 \right) - \sum_{i=1}^{n-1} \beta_{\omega i} \left(\omega_i - \omega_{0i} \right) \right] \qquad (6.10)$$

where

$$\beta_T = -\frac{1}{\rho_0} \left(\frac{\partial \rho}{\partial T} \right)_{\omega} \qquad (6.11)$$

$$\beta_{\omega i} = -\frac{1}{\rho_0} \left(\frac{\partial \rho}{\partial \omega_i} \right)_T \qquad (6.12)$$

β_T is the thermal expansion coefficient due to temperature change, and $\beta_{\omega i}$ is the compositional expansion coefficient of component i due to the concentration gradient. The volume-translated Peng-Robinson Equation of State (vt-PR-EoS), (Peneloux *et al.*, 1982 and Jhaverl and Youngren, 1988), is used to calculate the thermal expansion coefficient and the volumetric concentration expansion coefficient.

By substituting the Darcy relation (6.9) into the mass conservation Eq. 6.1, the pressure differential equation becomes the following:

$$\frac{\partial \rho}{\partial t} - \frac{\kappa}{\varphi \eta} \frac{\partial}{\partial x} \rho \left(\frac{\partial P}{\partial x} + \rho g_x \right) - \frac{\kappa}{\varphi \eta} \frac{\partial}{\partial y} \rho \left(\frac{\partial P}{\partial y} + \rho g_y \right) + \frac{\kappa}{\varphi \eta} \frac{\partial}{\partial z} \rho \left(\frac{\partial P}{\partial z} + \rho g_z \right) = 0 \qquad (6.13)$$

6.3.3 Conservation of energy

Since the velocity of the matrix is zero, and there is no heat generation in either porous medium or the fluid mixture, and since in addition, thermal equilibrium was assumed between the solid and the liquid phases and occurs very quickly, the temperature of the

matrix is assumed to be equal to the temperature of the fluid mixture. The energy conservation equation can be written as follows:

$$\left(\rho C_p\right)_e \frac{\partial T}{\partial t} + \varphi \vec{V} \bullet \nabla \left(\left(\rho C_p\right)_{fl} T\right) = k_e \nabla^2 T \tag{6.14}$$

where $\left(\rho C_p\right)_e$ is the effective volumetric heat capacity and k_e is the effective thermal conductivity of the system. These effective physical parameters are related to the fluid properties and the solid matrix properties, as shown in Chapter 2.

6.4 Boundary Conditions

The boundary conditions used in the model, also shown in Figure 6.1, are as follows:

1. The lateral walls have constant temperatures, and other walls are assumed to be adiabatic

$$x = 0, L \qquad T\big|_{x=0} = T_c, \quad T\big|_{x=L} = T_h \tag{6.15}$$

$$y = 0, W \qquad \frac{\partial T}{\partial y} = 0 \tag{6.16}$$

$$z = 0, H \qquad \frac{\partial T}{\partial z} = 0 \tag{6.17}$$

2. There is neither fluid flow nor diffusion flux through the boundaries

$$x = 0, L \qquad \vec{V}.N = 0, \quad J_x = 0 \tag{6.18}$$

$$y = 0, W \qquad \vec{V}.N = 0, \quad J_y = 0 \tag{6.19}$$

$$z = 0, H \qquad \vec{V}.N = 0, \quad J_z = 0 \tag{6.20}$$

where N is the unit normal vector. The initial conditions are $p_0 = 1$ atm, and $T_0 = 303.15$ K. The conditions at the matrix and sub-domain interface are assumed to be continuous for the normal component of the diffusion flux, pressure, and mole fraction. The Darcy's law is used to calculate the velocity ($\vec{V}$).

6.5 Numerical Solution Procedure

Equations 6.1, 6.2, 6.13 and 6.14 are solved numerically by using the control volume technique (*Fluent User's Guide 2006*), subject to the boundary conditions as depicted in Figure 6.1. The SIMPLE algorithm is implemented for solving the governing equations. It uses a relationship between velocity and pressure correction to obtain the pressure field. The second-order upwind scheme is used in the discretization of the governing equations. The resulting linear system of algebraic equations is solved at each time step using a bi-conjugate gradient iteration method with a given convergence criterion, which has been confirmed over many tests for the required accuracy. The numerical procedure derived from the SIMPLE algorithm is summarized by Anderson (1995) as:

1. Guess the pressure field P^*, and start the iterative solution with the guessed pressure.

2. Solve the momentum equations for the three velocity components (u, v, and w) using the P^* values. The velocities obtained may be symbolized u^*, v^* and w^* due to P^*.

3. Solve the pressure-correction equation; because the values of u^*, v^* and w^* were obtained from the guessed values, therefore, an equation for pressure correction is needed using the continuity equation, so that the corrected pressure is given by

$$P = P^* + P'$$
(6.21)

The same method can be applied to obtain the corrected velocity components

115

$$u = u^* + u'$$
$$v = v^* + v'$$
$$w = w^* + w'$$

(6.22)

where the velocity correction u', v' and w' may be obtained from P'.

4. Solve the other conservation equation using the corrected values of u, v and w and P.

5. Set u, v and w and P obtained from step 2 and step 3 as new values for u^*, v^*, w^* and P^* and return to step 2. Repeat this process until a convergence criterion is reached.

At the initial time step, the velocities were set to zero in the computational domain, where initial pressure, temperature, and concentration are specified. The criterion of convergence is set for the unknown parameters including pressure, temperature, velocities, and concentration. Convergence is reached when the iterations of the system continue until an error value of 10^{-6} is found between two successive iterations. More details of the numerical procedure may be found in Patankar (1980), and Versteeg and Malalasekera (2007).

After discretization, the conservation equation for a general variable (ϕ), at any control volume or cell (and a general nodal point is identified by P) can be written as

$$a_P \phi_P = \sum_{nb} a_{nb} \phi_{nb} + b$$

(6.23)

where a_P is the centre coefficient, a_{nb} represents the influence coefficients for neighboring cells, and b is the contribution of the constant part of the source term and of the boundary conditions. The residual, R^ϕ, or the error between iterations is defined as

$$R^{\phi} = \frac{\sum\limits_{cells\ P} \left| \sum\limits_{nb} a_{nb}\phi_{nb} + b - a_{P}\phi_{P} \right|}{\sum\limits_{cells\ P} \left| a_{P}\phi_{P} \right|}$$

(6.24)

The values of pressure, temperature and composition are defined in the centre, whereas the velocities are defined on the surface of each control volume, or grid cell. Different mesh sizes are tested in order to adopt the proper mesh size in a three-dimensional porous medium. A mesh size of $80 \times 40 \times 40$ control volume has been adopted.

6.6 Results and Discussion

In this work, lateral heating in a heterogeneous porous medium filled with a hydrocarbon ternary mixture has been simulated. Porosity is an important parameter when simulating the transport phenomena in porous media. Bulk volume and porosity are typically larger in the matrix than in the sub-domains, while permeability of sub-domains is typically much larger than that of the matrix. The permeability (κ_s) and porosity (φ_s) in the primary domain are assumed 10 mD, and 0.4, respectively, whereas the permeability of sub-domains (κ_f) ranges from 10 to 10000 mD with a porosity (φ_f) of 0.2. Different configurations were adopted, but for simplicity, the results of only two configurations are presented in this chapter, (see Figure 6.2). The width of the sub-domain in all the configurations is assumed to be 2 m.

6.6.1 Variation of concentration with permeability

In this section, the composition of a hydrocarbon ternary mixture of nC12-THN-IBB is investigated for different ranges of κ_f / κ_s and for two configurations, which are shown in Figure 6.2. Sub-domains have been created by putting a layer in the porous medium with a different porosity and corresponding permeability to mimic the heterogeneity. The concentration of the first component (nC12) and second component (THN) against the

permeabilities ratio are examined. Figures 6.3 to 6.10 illustrate the mole fraction at the centre of the geometry (x-z plane).

Figure 6.3 shows the mole fraction of nC12 along the horizontal direction (*x*-direction) for configuration1 (Conf.1) at three different locations along the vertical direction (z = 2.5 m, z = 5 m, and z = 7.5 m). There is no noticeable effect from the sub-domains on the concentration, because the permeability of the sub-domains is equal to that of the matrix ($\kappa_f = \kappa_s = 10$ mD). It is observed that the lighter component (nC12) concentration migrates to the hot side (has a negative thermodiffusion coefficient); this is consistent with our previous work in a homogeneous porous medium (Jaber *et al*. 2008). A higher concentration of nC12 is found near the bottom edge of the porous medium. Furthermore, it is observed that the nC12 concentration is decreased at the top edge because of the role of thermodiffusion. The nC12 concentration is repeated in Figure 6.4 for configuration2 (Conf.2). The same findings as above have been noticed, but the minimum and maximum values of the concentration are not the same, due to orientation of the sub-domains. For instance, at location z = 7.5 m, the values of the nC12 (Conf.1) are between 0.25 and 0.294, (see Figure 6.3), while for Conf.2, the values are between 0.245 and 0.293, (see Figure 6.4).

Figures 6.5 and 6.6 show the THN concentration at three different elevations (z = 2.5 m, z = 5 m, and z = 7.5 m) along the horizontal direction for Conf.1 and 2, respectively. The results shown in these Figures are for $\kappa_f = \kappa_s = 10$ mD. It is noticeable that THN (the heavier component) migrates to the cold side (has a positive thermodiffusion coefficient); also, it is observed that the THN accumulates near the top edge of the porous medium. For instance, the THN concentration at z = 7.5 m (near the top edge) varies from 0.342 at the hot side to 0.386 at the cold side, while for z = 2.5 m (near the bottom edge) it varies from 0.33 to 0.375 (Figure 6.5). It can be concluded from Figures 6.3 to 6.6 that the nC12 and THN concentrations vary nearly linearly along horizontal direction, when $\kappa_f = \kappa_s = 10$ mD.
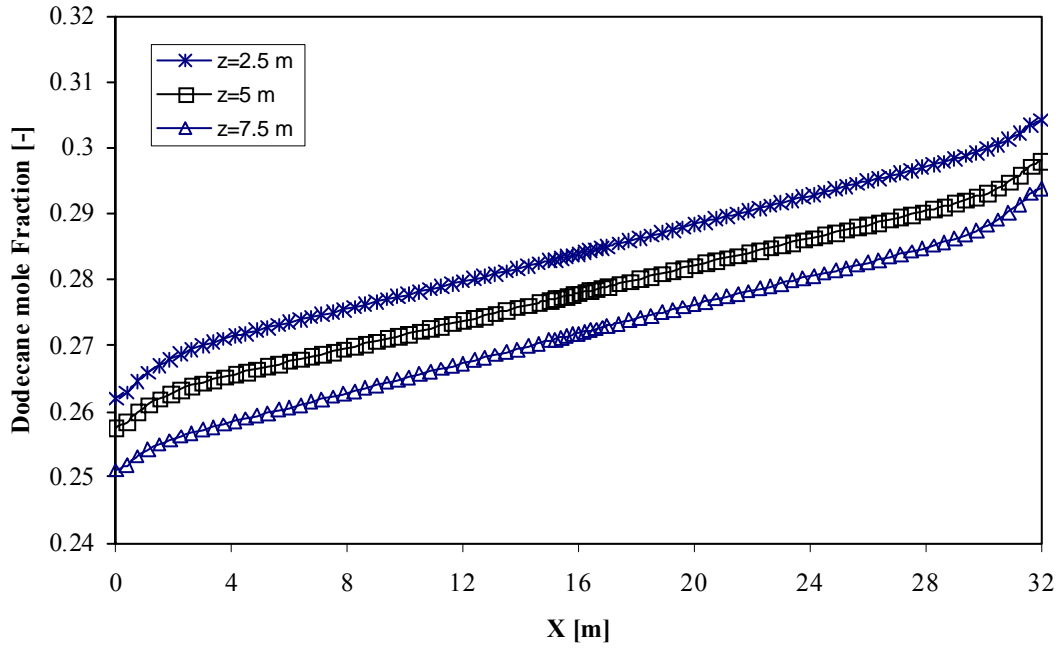
Figure 6.3: n-dodecane (nC12) mole fraction along the horizontal direction ($\kappa_f / \kappa_s = 10/10$), Conf.1.
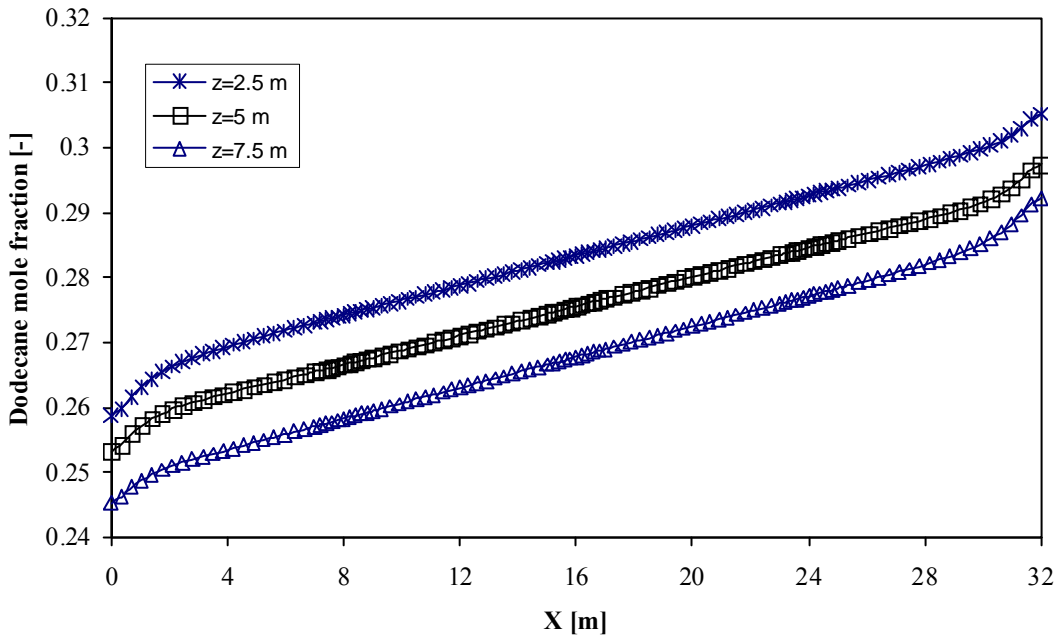
Figure 6.4: n-dodecane (nC12) mole fraction along the horizontal direction ($\kappa_f / \kappa_s = 10/10$), Conf.2.
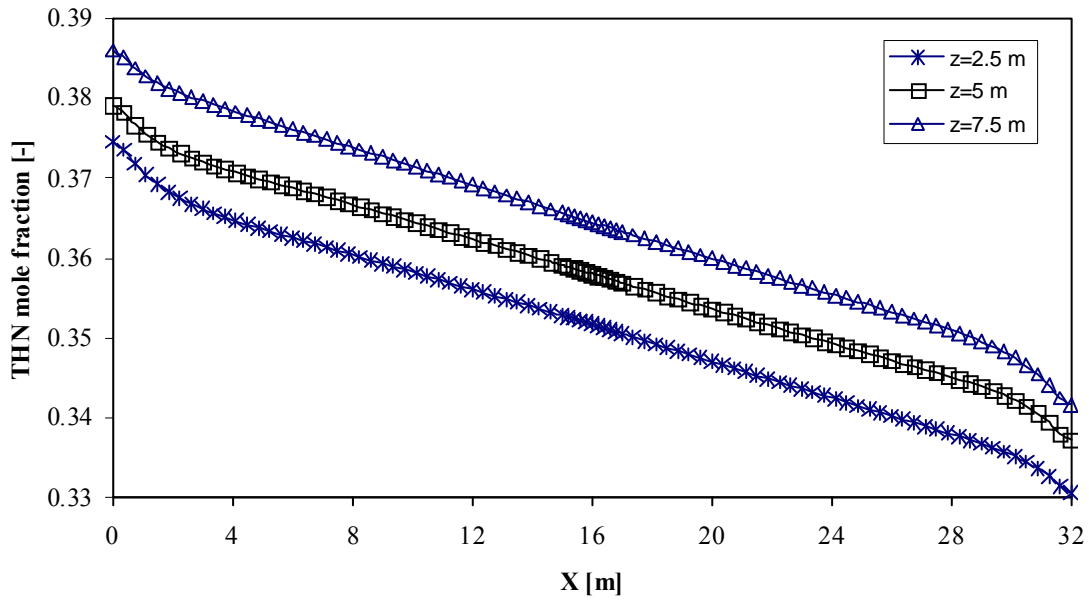
Figure 6.5: THN mole fraction along the horizontal direction ($\kappa_f / \kappa_s = 10/10$), Conf.1.
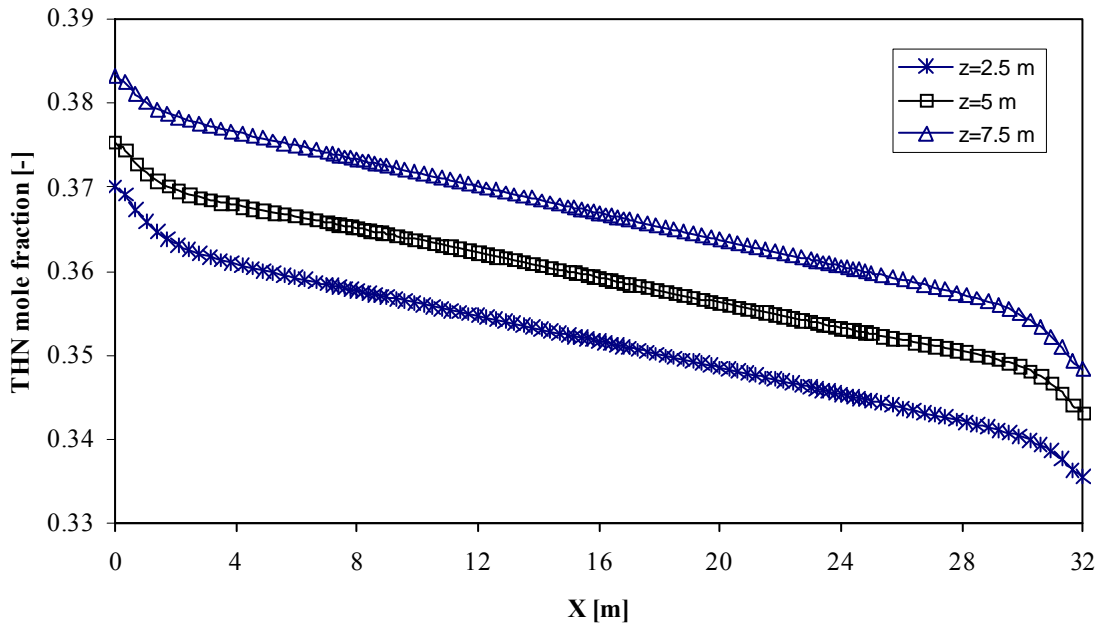
Figure 6.6: THN mole fraction along the horizontal direction ($\kappa_f / \kappa_s = 10/10$), Conf.2.

Figures 6.7 and 6.8 show the concentration distribution of nC12 for $\kappa_f / \kappa_s = 10000/10$. It can be seen that the sub-domains have a significant influence on the compositional variation of the mixture components. By comparing Figure 6.3 with Figure 6.7 (both Figures for Conf.1), the concentration at $z = 5$ m becomes larger near the cold side than at other elevations ($z = 2.5$ m and 7.5 m), which is due to the convection inside the sub-domain. In addition, in the sub-domain zones, the mixing is enhanced, because of the enhanced flow rate, (Figure 6.7). For Conf.2, in Figure 6.8, the concentration in the sub-domain regions (three vertical sub-domains) is not linear when compared to the concentration in Figure 6.4. The same scenario has been noticed for the second component (THN), as shown in Figures 6.9 and 6.10.

In general, the lighter and the heavier components' behaviour within the ternary mixture is similar to the one in a binary mixture (Ghorayeb *et al.*, 2003), where the lighter component migrates to hot side and increase with depth.
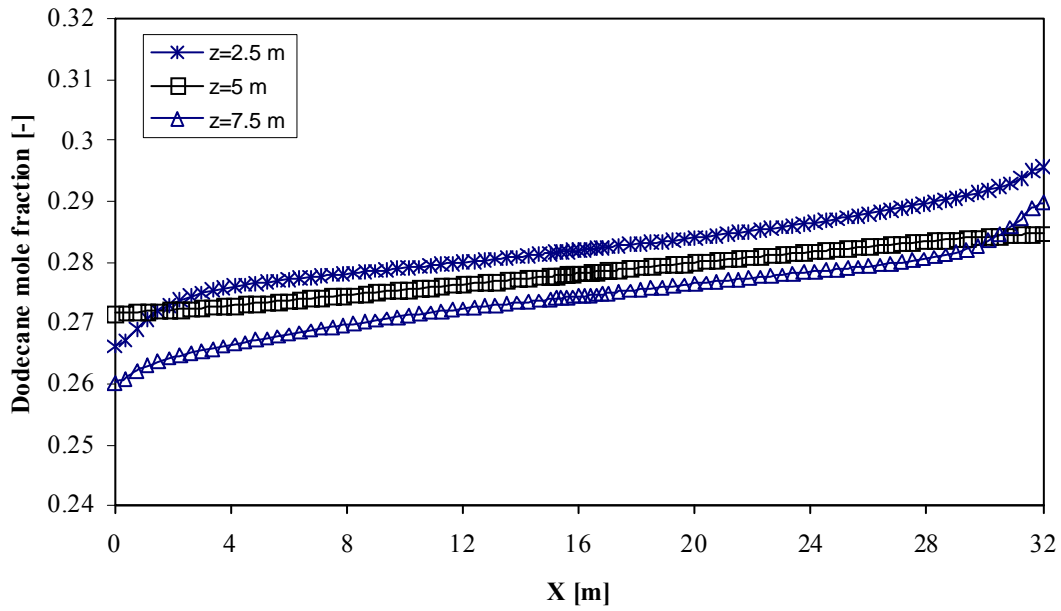
Figure 6.7: n-dodecane (nC12) mole fraction along the horizontal direction
($\kappa_f / \kappa_s = 10000 / 10$), Conf.1.
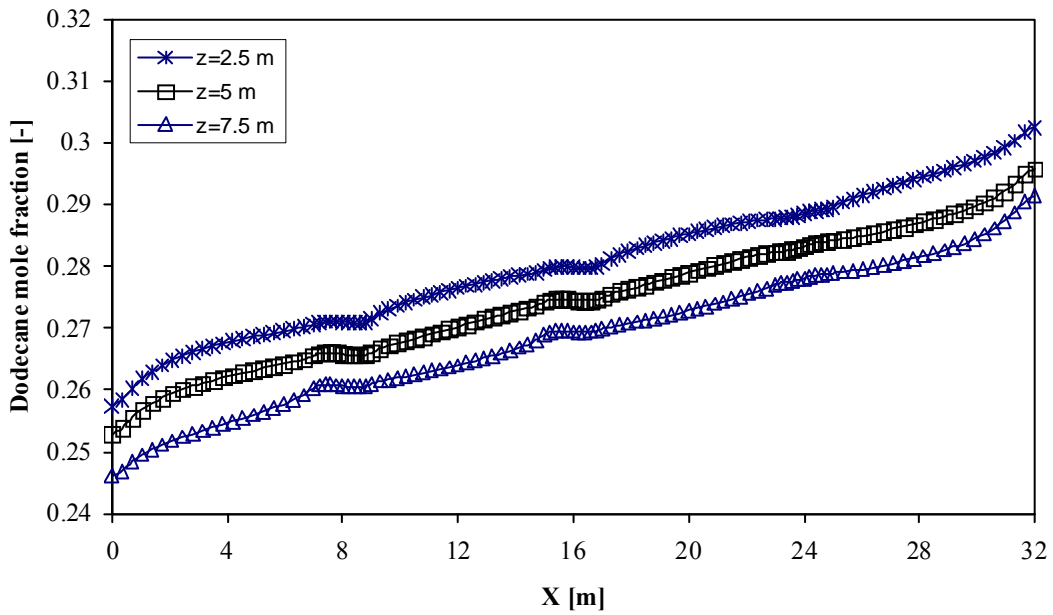
Figure 6.8: n-dodecane (nC12) mole fraction along the horizontal direction
($\kappa_f / \kappa_s = 10000 / 10$), Conf.2.
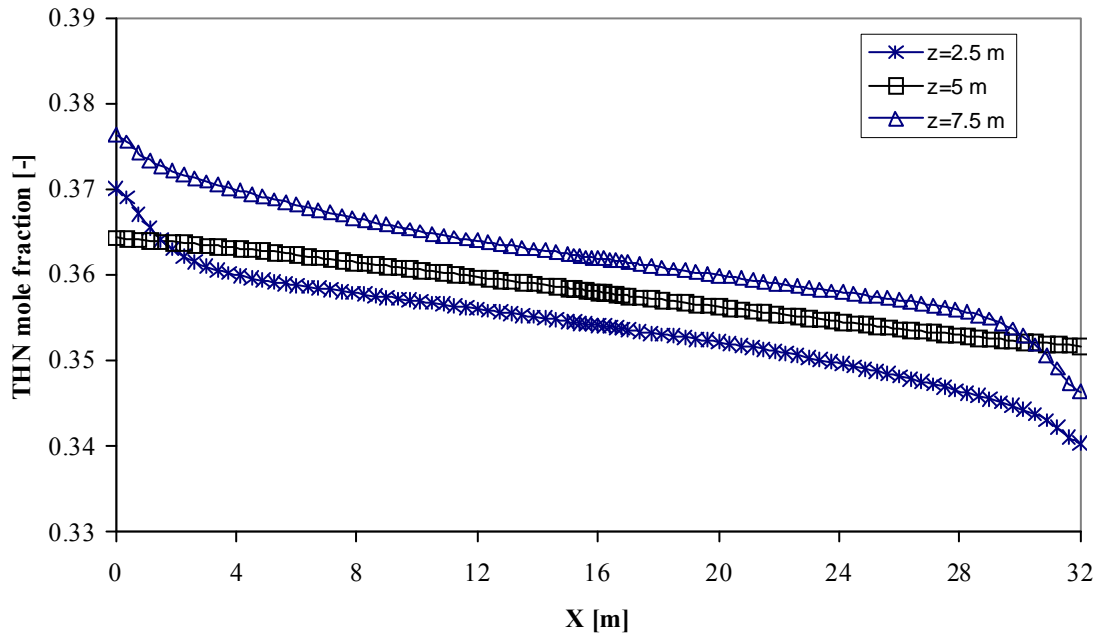
Figure 6.9: THN mole fraction along the horizontal direction ($\kappa_f / \kappa_s = 10000 / 10$), Conf.1.
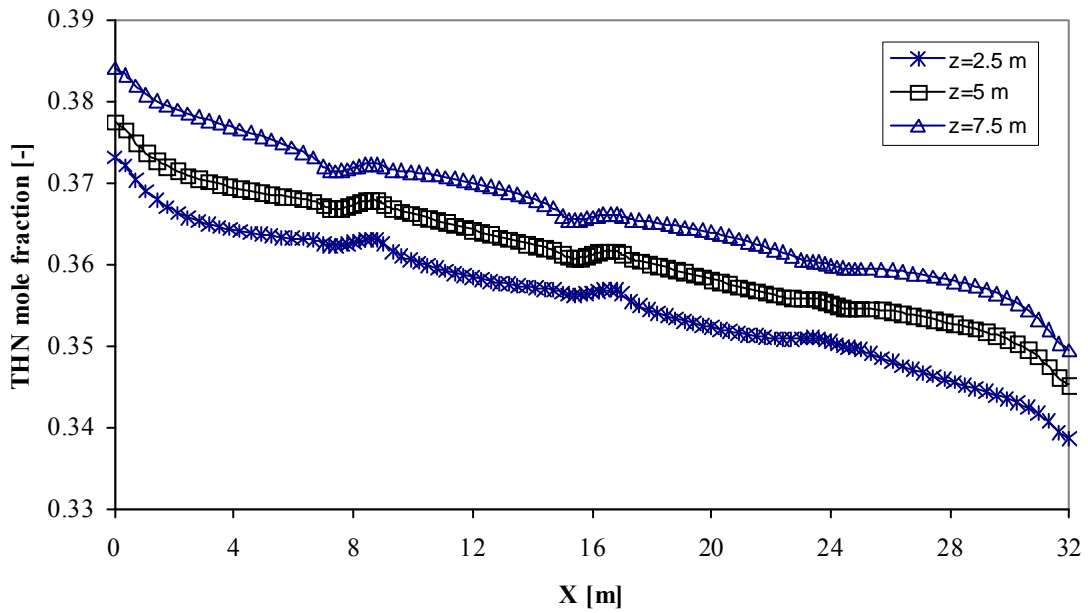
Figure 6.10: THN mole fraction along the horizontal direction ($\kappa_f / \kappa_s = 10000 / 10$), Conf.2.

6.6.2 Comparison of flow patterns

The flow patterns in the centre of the porous medium for the x-z plane at different elevations (z = 2.5 m, z = 5 m, and z = 7.5 m) are plotted in Figures 6.11-6.14. This may help to illustrate the sub-domains' effect on the fluid behaviour inside the heterogeneous porous media. Figure 6.11 shows the magnitude of velocity for the $\kappa_f = \kappa_s = 10 \, \mathrm{mD}$ case. It is found that the value of velocity is minimum at z = 5 m, while it is identical for z = 2.5 m and 7.5 m. This case is identical to the case without sub-domain because the permeability of the matrix and sub-domain are the same. As a result, the presence of the sub-domains cannot be seen to be influential in this Figure. The same behaviour has been observed for Conf.2, (see Figure 6.12).

Figures 6.13 and 6.14 present the magnitude of velocity for $\kappa_f / \kappa_s = 10000 / 10$. In Figure 6.13, the fluid velocity for z = 5 m (Conf.1), which is located at the centre of the sub-domain zone along the horizontal direction, is higher than that at z = 2.5 m and 7.5 m. The fluid velocity at z = 2.5 m and 7.5 m are almost similar. Also it can be seen that there are two peaks in the middle, which are inside the vertical sub-domain. In the first one, the flow enters the sub-domain zone and in the second one, the flow leaves the sub-domain zone. Figure 6.14 shows the flow pattern for Conf.2. It is observed that in the sub-domain zones, the flow becomes stronger and much higher than the one in the matrix; this is attributed to the high permeability in the sub-domain zones.

In summary, the buoyancy-driven convection is stronger in the sub-domains because the permeability is higher, and the fluid can move easily. It is evident that the acceleration of the fluid in the sub-domain zones is much higher.
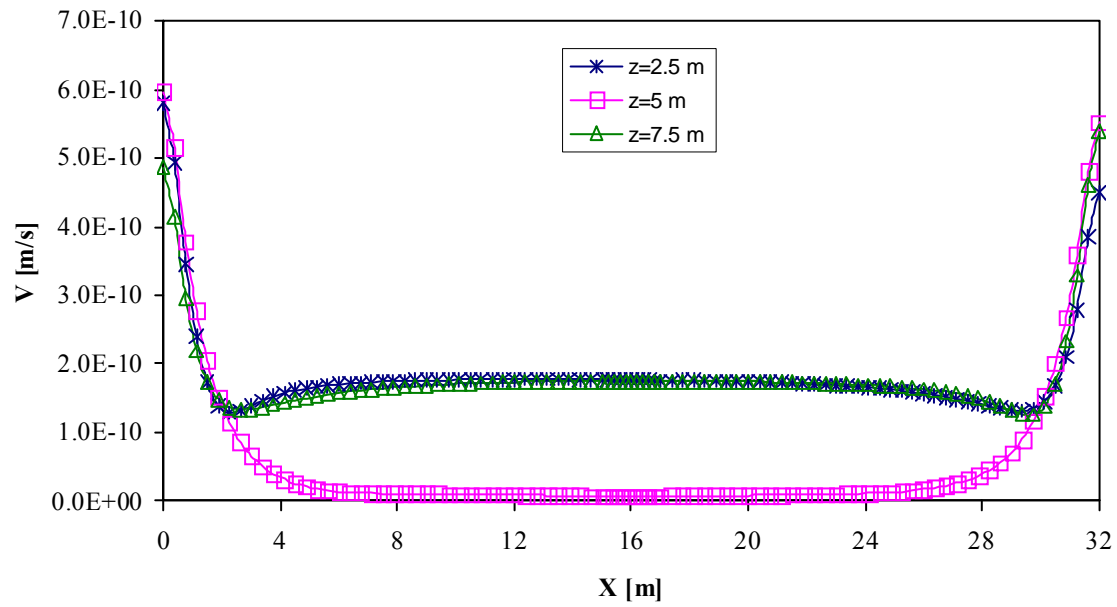
Figure 6.11: The magnitude of velocity along the horizontal direction ($\kappa_f / \kappa_s = 10/10$), Conf.1.
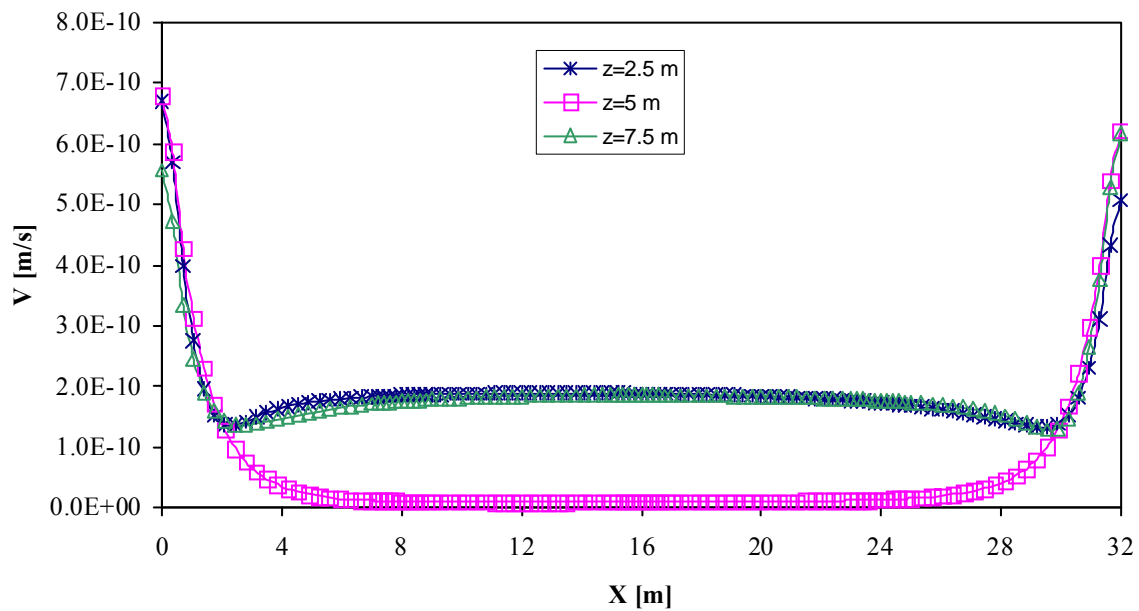
Figure 6.12: The magnitude of velocity along the horizontal direction ($\kappa_f / \kappa_s = 10/10$), Conf.2.
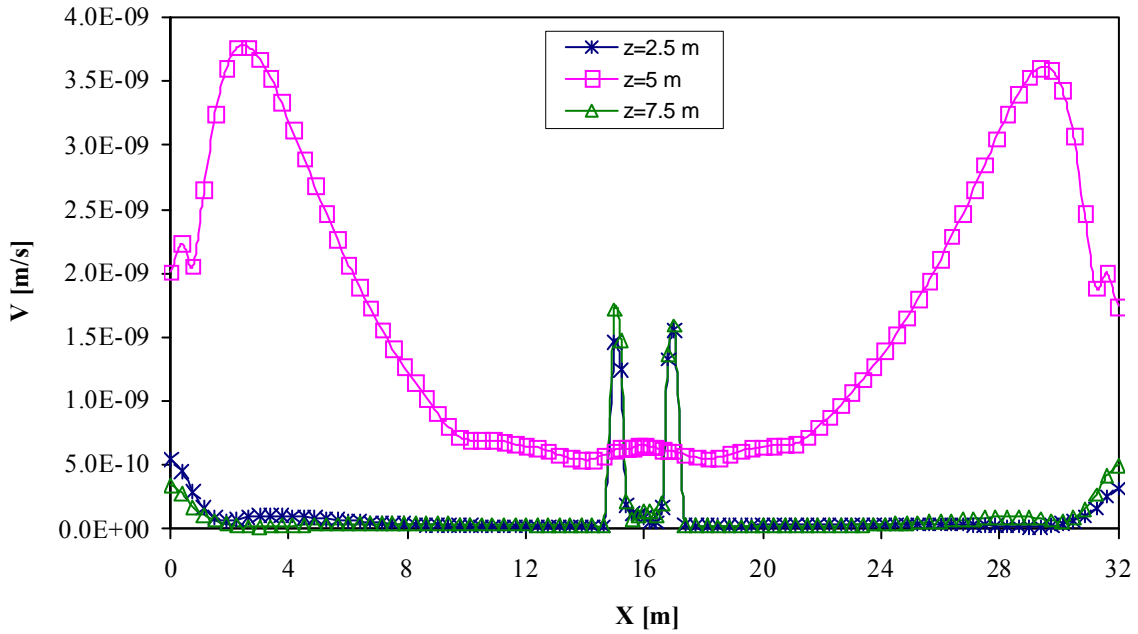
Figure 6.13: The magnitude of velocity along the horizontal direction ($\kappa_f / \kappa_s = 10000 / 10$), Conf.1.
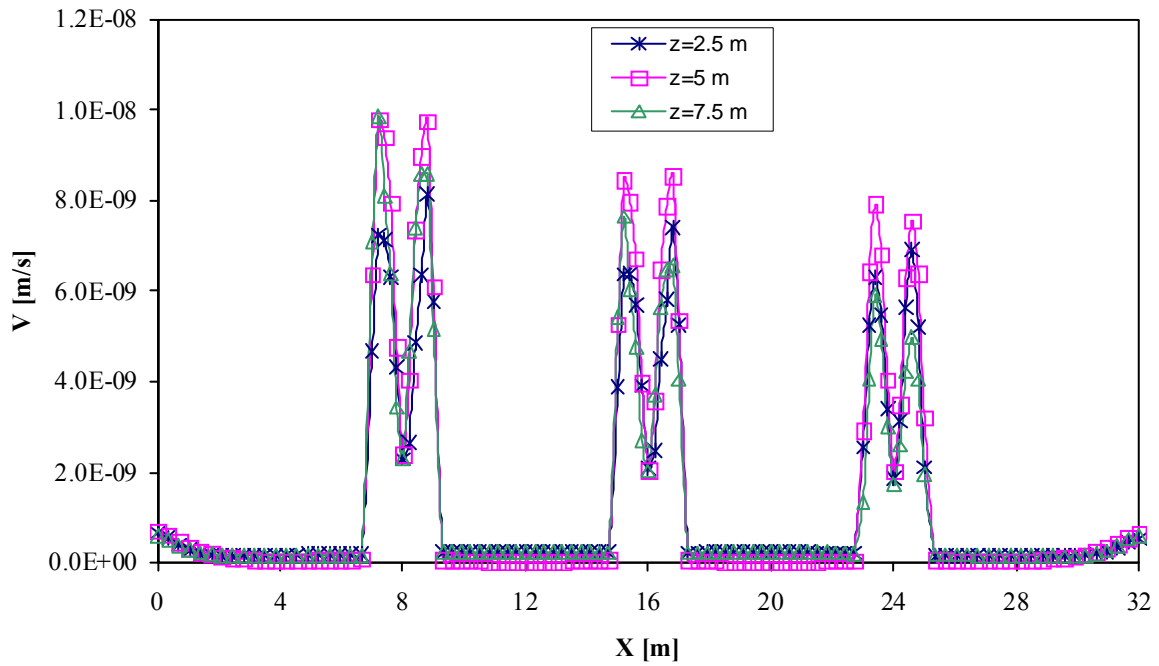
Figure 6.14: The magnitude of velocity along the horizontal direction ($\kappa_f / \kappa_s = 10000 / 10$), Conf.2.

6.6.3 Separation ratio

The separation ratio parameter may play a role in understanding the mass transfer process, so that the convection effect on the thermodiffusion process is investigated for different permeability ratios in terms of the separation ratio. The permeability has a significant effect on the separation of mixture components. At low permeability the Soret effect is significant; while at high permeability convection becomes dominant. To further examine this phenomenon, and to understand how the thermodiffusion convection coupling works, a variable known as the separation ratio, q, is introduced. The separation ratio of each component can be defined as follows, as introduced in section 5.6.2:

$$q = \frac{x_{max}/(1-x_{max})}{x_{min}/(1-x_{min})} \qquad (6.25)$$

where x_{max} and x_{min} are the maximum and minimum mole fractions of component i. In this study, the trend of the separation ratio is identical to the one presented in Chapter 5[2]. The separation ratio, q, can be plotted against the permeability ratio as shown in Figures 6.15 and 6.16 for Conf. 1 and 2, respectively. In each Figure, the separation ratio for component 1 (nC12) and component 2 (THN) is shown.

In these Figures, the permeability values of the primary domain and sub-domains vary between 10 mD and 10000 mD, which represent the values in the oil reservoir rocks (Bear 1972). Three different regions can be identified in these two Figures. From Figure 6.15 for Conf.1, Region (I) is for the permeability ratio of 10 ($\kappa_f / \kappa_s = 100/10$). In this region, the separation ratio is almost constant; the separation ratio of nC12 (the lighter component) is 1.2 and higher than that of the THN (the heavier component), which is 1.055. In this region the Soret effect or thermodiffusion is dominant. Region (II) is for a permeability ratio in a range from 10 to 100. In this region both the Soret effect and convection play a role. In Region (III), the Soret effect gradually decreases, as the convection increases.

---

[2] This result has already been presented in Jaber *et al.* (2008a).

In general, it is found that the separation ratio value for Conf.2 is higher than that for Conf.1 due to the orientation of sub-domains. For instance, the separation ratio of the lighter component (nC12) is between 1.48 and 1.43 for Conf.2, and is between 1.22 and 1.19 for Conf.1.
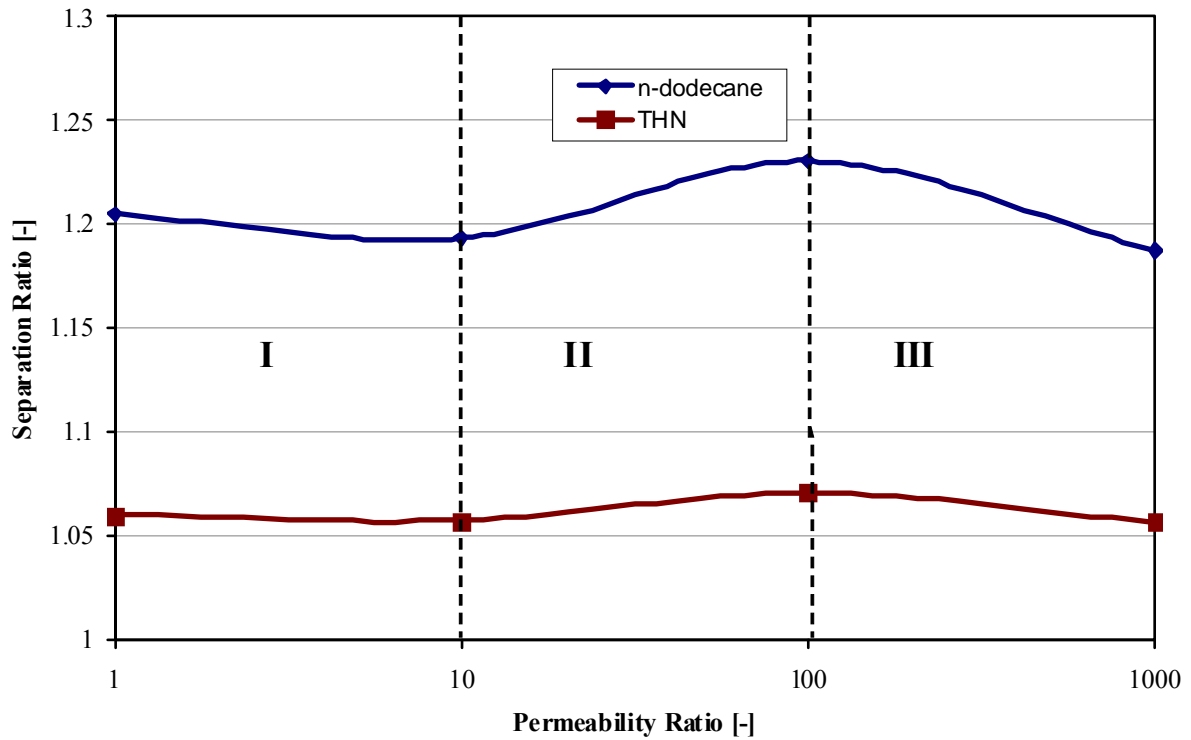
Figure 6.15: Separation ratio as a function of the permeability ratio, Conf.1.
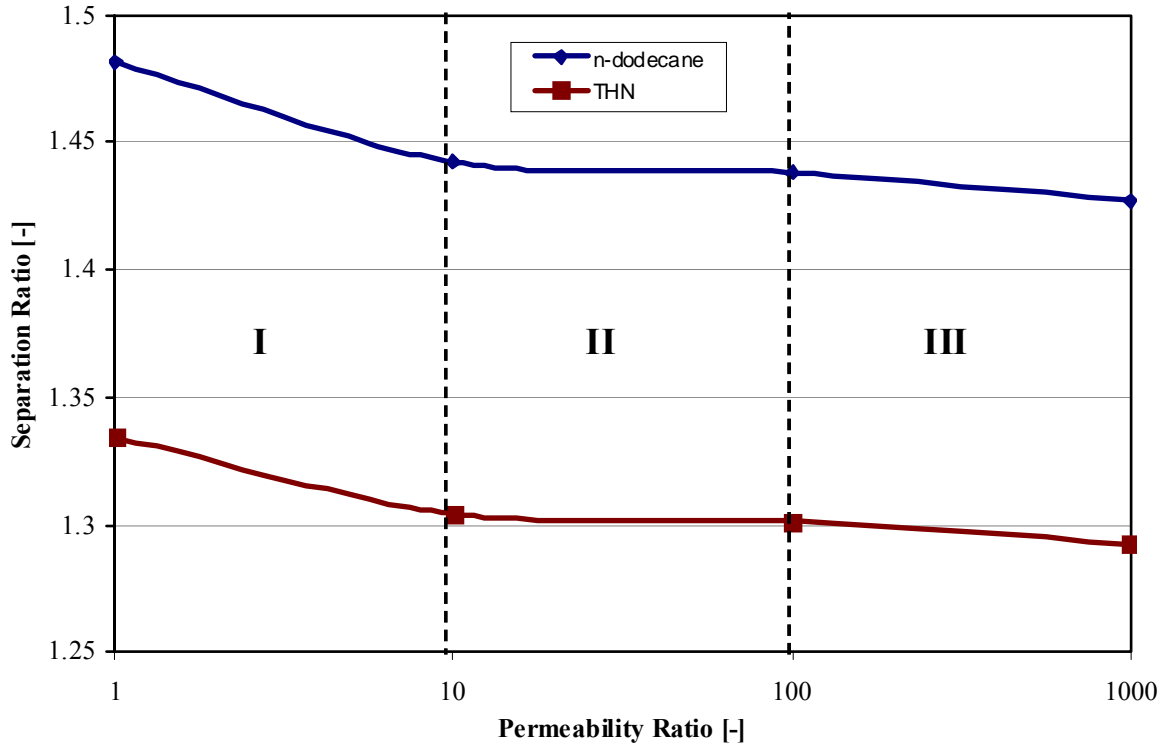
Figure 6.16: Separation ratio as a function of the permeability ratio, Conf.2.

6.7 Summary

In this work, a three-dimensional model has been numerically simulated to illustrate the interaction between thermodiffusion and buoyancy-driven convection in a single phase hydrocarbon ternary mixture (nC12-THN-IBB) inside a heterogeneous porous medium. A horizontal temperature gradient was applied in a porous medium under atmospheric pressure. In the analysis, the impact of the permeability ratio on the composition of the mixture components, velocity in the porous medium, and the separation ratio was investigated. It was found that the heterogeneous porous medium has a significant influence on the composition of the mixture components. It was also found that the sub-domains have a strong effect on the convective patterns, and the fluid flow in the sub-domain zones is much higher than that in the matrix domain. Furthermore, the separation ratio of Conf.2 is higher than that for Conf.1 due to the orientation of the sub-domains.

Chapter 7

Conclusions and Recommendations

7.1 Conclusions

The Thermodiffusion phenomenon (or Soret effect) is a coupling between a temperature gradient and its resulting mass flux in a multicomponent system. As an important non-equilibrium process, this phenomenon appears in a wide range of physical and chemical processes in nature, including studies of oil reservoir analysis, and fluid separation.

In this work, an extensive numerical modelling and estimation of the diffusion coefficient of hydrocarbon mixtures was complemented with an experimental approach. Based on the theoretical and experimental work carried out, the following conclusions can be drawn:

1. In thermodiffusion models, equilibrium thermodynamic quantities are widely used. Therefore, it is a prerequisite to know reliable thermodynamic properties for the theoretical research on thermodiffusion. An irreversible thermodynamics model, which combines Onsager's theory with the theory of rate and equation of state, yielding the Firoozabadi model, appear to be appropriate for thermodiffusion estimation for multicomponent hydrocarbon mixtures, and it is derived based on the four postulates in non-equilibrium thermodynamics. Two equations of state, the Peng-Robinson Equation of State (PR-EoS) and the volume translated Peng Robinson Equation of State (vt-PR-EoS), were adopted to estimate the thermodynamic properties of mixtures.

2. A new thermodiffusion cell designed for high pressure was validated at atmospheric pressure. The cell was installed in a Mach-Zehnder interferometer. Two mixtures of the Benchmark of Fontainebleau were tested in the vertical position (nC12-IBB and nC12-THN at 50% mass fraction and T_{mean} = 25 °C). From the analysis of the

second kinetic of the evolution of the phase difference between the laser beams that passed through the hot and the cold dead volumes, the diffusion coefficient in free liquid, D, and Soret coefficient, S_T, of the two mixtures and the tortuosity τ for the porous medium were determined. For both mixtures, an excellent agreement was found between the molecular diffusion coefficient of this work and the benchmark values, and the percentage error was less than 1%. Also, it was found that the difference between the Soret coefficients for this work and the benchmark data was acceptable for the experiments of duration up to seven days. To improve the determination of S_T with the cell in a vertical position, increasing the value of the imposed temperature gradient and increasing the time of the experiment (about two weeks in order to reach the steady state condition) were suggested. Furthermore, it was concluded that, when the cell was set in the horizontal position, convection in dead-volumes became possible. For a difference of the temperature applied between thermoregulator baths ($\Delta T' = 5\ ^\circ C$), a diffraction pattern came up at the beginning of the experiment, and the procedure of analysis of interferograms became difficult.

3. The measurements for the thermal expansion and concentration expansion coefficients and for the viscosity of the binaries of nC12, IBB and THN for pressures varying from 0.1 to 20 MPa at 25 °C and concentrations centred on 50% were measured. The densities of binaries under the same conditions were measured as well. In addition, viscosities were directly measured using a high pressure high temperature viscometer (HPHTV-100). The comparisons with measured densities show that vt-PR-EoS has a better agreement with experiments than the PR-EoS. The combination of the model of Lohrenz-Bray-Clark for the viscosity of liquid mixtures, and the densities calculated with the two equations of state, proved to be inefficient for the prediction of the viscosities of the binaries.

4. Thermodiffusion plays a significant role in the variation of the composition mixture components in a porous medium reservoir, such as in oil reservoirs. The interaction between the thermodiffusion phenomenon and buoyancy driven convection in a porous medium reservoir filled with a ternary hydrocarbon mixture was numerically

investigated. Two different ternary mixtures, a C1-nC4-nC12 at 35 MPa and nC12-THN-IBB at 1 atm pressure, were investigated for different permeabilites ranging from 10 to 10^7 mD. The model was based on the non-equilibrium thermodynamics theory, and diffusion coefficients were calculated with time- and space-dependent fluid properties and compositions. The component concentration distribution and the separation ratio were used to examine the behaviour of the thermodiffusion and buoyancy-driven convection inside the cavity. It was found that, for permeability below 300 mD, the thermodiffusion for both mixtures was dominant; and above this level, buoyancy convection became the dominant mechanism. The viscosity was found to influence the evaluation of the molecular and thermodiffusion coefficients. The result showed that, with variable viscosity, the flow due to thermodiffusion was affected.

Throughout, the comparison between the numerical results and the experimental data for a ternary mixture of THN-IBB-nC12, using vt-PR-EoS for evaluating the thermodynamic properties, yields better agreement with the experimental data. It was found that the percentage errors for D_{T1}, D_{T2} and D_{T3}, when the vt-PR-EoS was used, were 12.63%, 23.11% and 49.65%, respectively. Furthermore, the mixture component's behaviour also was found to be identical, for both experimental data and numerical values, and was found to have the same sign for thermodiffusion coefficients. The two components (nC12 and THN) migrated, one to the hot side and the other to the cold side, while the IBB was distributed randomly within the cavity, as its thermodiffusion coefficient value is small, and this confirmed that its separation remains small. Finally, the density of the nC12-THN-IBB mixture at different temperatures was compared with the numerical results in order to validate the equation of state (vt-PR-Eos). The results showed an excellent agreement between the numerical model and the experimental data, with the percentage error being less than 3%.

5. A three-dimensional model was numerically simulated to illustrate the interaction between thermodiffusion and buoyancy-driven convection in a hydrocarbon ternary

mixture (nC12-THN-IBB) inside a heterogeneous porous medium. A horizontal temperature gradient was applied in a porous medium under atmospheric pressure. Employing a single phase model and Darcy's law, the continuity and the energy equations were solved numerically, using the finite volume method. The permeability of the matrix (main domain, $\kappa_s = 10$ mD) was kept constant, while the permeability of the sub-domain, κ_f, was varied. Different permeability ratios (κ_f / κ_s = 10, 100, 1000 and 10000) were examined in this study, which covered a wide range of oil reservoirs. The impact of the permeability ratio on the composition of the mixture components, velocity in the porous medium, and the separation ratio was investigated. It was found that the heterogeneous porous medium had a significant influence on the composition of the mixture components. Moreover, it was found that the sub-domains had a strong effect on the convective patterns, and the fluid flow in the sub-domain zones was much higher than that in the matrix domain. Furthermore, the separation ratio of Conf.2 was higher than that for Conf.1 due to the orientation of the sub-domains.

7.2 Contributions

The main goal of this work was to investigate experimentally and numerically the fluid transport of hydrocarbon mixtures inside porous media with consideration of thermodiffusion and molecular diffusion. The following are the contributions of this work:

- A FORTRAN program was developed to solve numerically the thermo-solutal convection for multicomponent mixtures inside porous media by applying the Firoozabadi model.

- A new experimental technique based on optical digital interferometry for measuring Soret and molecular coefficients in porous media was carried out. A publication related to this contribution is Jaber *et al.* (2009).

- The measurements for the thermal expansion and concentration expansion coefficients and for the viscosity of the binaries of the benchmark of

Fontainebleau for pressures varying from 0.1 to 20 MPa at 25 °C were presented. The predicted coefficients from the Peng-Robinson, and volume translated Peng-Robinson Equations of State were compared with the measured values. A publication related to this contribution is Batalle, *et al.* (2009).

- The Soret effect of two ternary mixtures in a homogenous porous medium cavity was studied for different permeabilities. A publication related to this contribution is Jaber and Saghir (2006), Jaber *et al.* (2008a), and Jaber *et al.* (2008b).

- An attempt was made to simulate the thermo-solutal convection of a hydrocarbon ternary mixture in the presence of thermodiffusion in a non-homogenous porous medium. A publication related to this contribution is Jaber and Saghir (2008) and Jaber and Saghir (2010).

7.3 Recommendations

There are still some related open issues that need to be studied, so future work may be carried out to address the following:

- The measurements of thermodiffusion and molecular diffusion coefficients for multicomponent hydrocarbon fluid mixtures;

- Further development of a theoretical model for multicomponent systems;

- The measurements of the Soret coefficients at high pressure for the three binary mixtures. The values of the contrast factor, $(\partial n / \partial c)_{P,T}$, at high pressure, which are needed to evaluate the Soret coefficient, must be measured because they are not present in the literature.

References

Alboin, C., Jaffre, J., Robert, J. E. and Serres, C. (2002): "Modeling Fractures as Interfaces for Flow and Transport in Porous Media" in Fluid Flow and Transport in Porous Media: Mathematical and Numerical Treatment, Z. Chen and R.E. Ewing eds., Contemporary Mathematics 295, *American Mathematical Society*, pp. 13-24.

Anderson, J. D. (1995): "Computational Fluid Dynamics: The Basics with Applications" McGraw-Hill, New York.

Barenblatt, G. I., Zheltov, I. P. and Kochina, I. N. (1960): "Basic Concepts in the Theory of Seepage of Homogeneous Liquids in Fissured Rocks" PMM, *Applied Mathematic and Mechanic*, vol. 24, pp. 1286-1303.

Bataller, H., Miqueu, C., Plantier, F., Daridon, J., Jaber, T. J., Abbasi, A. and Saghir, M. Z., (2009): "Comparison between Experimental and Theoretical Estimations of the Thermal Expansion, Concentration Expansion Coefficients and Viscosity for Binary mixtures under pressure up to 20 MPa" *Journal of Chemicals engineering data*, vol. 54, no.6, pp. 1710-1715.

Bear, J. (1972): "Dynamic of Fluid in Porous Media" Elsevier, New York.

Benano-Melly, L.B., Caltagirone, J.-P, Faissat, B., Montel, F. and Costeseque, P. (2001): "Modeling Soret Coefficient Measurement Experiments in Porous Media Considering Thermal and Solutal Convection" *International Journal of Heat and Mass Transfer*, vol. 44, pp. 1285-1297.

Bird, R. B., Stewart, W.E and Lightfoot, E. N. (2002): "Transport Phenomena" 2nd Ed, John Wiley and sons, p. 765.

Blanco, P., Bou-Ali, M. M., PLatten, J. L., Madariaga, J. A., Urteaga, P., and Santamaria, C. (2006): "The Thermodiffusion Coefficient for Organic Mixtures of n-alkanes n-Ci-nC18 (i=5,…,13): Influence of the Chain Length" Thermodiffusion: Basic & Applications, Bou-Ali, M. M. and Platten, J. K., Eds. Mondragon Unibertsitateko Zerbitzu Editorial, Mondragon, Spain, pp. 427-438.

Bou-Ali, M. M., Ecenarro, O., Madariaga, J. A., Santamaria, C. M. and Valencia, J. J. (1998): "Thermogravitational Measurement of the Soret Coefficient of Liquid Mixtures" *Journal* of *Physics*: *Condensed Matter*, vol. 10, pp. 3321-3331.

Bou-Ali, M.M., Valencia, J.J., Madariaga, J.A., Santamaria, C., Ecenarro, O., and Dutrieux, J.F., (2003): "Determination of the Thermodiffusion Coefficient in Three Binary Organic Liquid Mixtures by the Thermogravitational Method" *Philosophical Magazine*, vol. 83, no. 17-18, pp. 2011-2015.

Comunas, M.J.P., Bazile, J.P., Baylaucq, A., and Boned, C. (2008): "Density of Diethyl Adipate Using a New Vibrating Tube Densimeter from (293.15 to 403.15) K and up to 140 MPa Calibration and Measurements" *Journal of Chemical Engineering and Data*, vol. 53, no. 4. pp. 986-994.

Costeseque P., Pollak, T., Platten J. K., and Marcoux M. (2004): "Simultaneous Evaluation of Soret and Fick Coefficients in a Free and a Packed Vertical Gradient Soret Cell" *6th International Meeting on Thermodiffusion (IMT6)*, Varenna, Italy.

Costeseque, P., Pollak, T., Platten, J. K., and Marcoux, M. (2004): "Transient-state Method for Coupled Evaluation of Soret and Fick Coefficients, and Related Tortuosity Factors, Using Free and Porous Packed Thermodiffusion Cells: Application to $CuSO_4$ Aqueous Solution (0.25m)" *European Physical Journal*, vol. 15, no. 3, pp. 249–253.

Costeseque, P., El Maataoui, M., and Riviere, M. (1994): "Selective Enrichments Induced by Thermogravitational Diffusion in Porous Medium on Hydrocarbon Species of Crude Oil and Specific Case of Paraffin Isomers" Entropy, vol. 94, no. pp 94-100.

Costeseque, P. and Loubet, J-C. (2003): "Measuring the Soret Coefficient of Binary Hydrocarbon Mixture in Packed Thermogravitational Columns" *Philosophical Magazine*, vol. 83, pp. 2017-2022.

Darcy, H. (1856): Les fontaines publiques de la ville de Dijon, V. Dalmont, Paris, pp 305-401.

Daubert, T. E. and Danner, R. P. (1989): "Physical and Thermodynamic Properties of Pure Chemicals: Data Compilation" Hemisphere Publishing Corporation, New York.

de Groot, S. R. (1945): " L'Effect Soret" Amsterdam.

de Groot, S.R and Mazur, P. (1984): "Non-Equilibrium Thermodynamics" Dover Publication Inc., New York.

Delware, F., Chacha, M, Ghorayeb K, and Saghir, M.Z. (2004): "Compositional Variation Considering Diffusion and Convection for Binary Mixture in Porous Media" *Journal of Porous Media*, vol. **7,** no. 2, pp. 1-19.

de Marsily, G. (1986): "Quantitative Hydrogeology for Engineers" Academic Press, San Diego.

Denbigh, K. G. (1951): "The Thermodynamics of the Steady State" Wiley, New York.

Dougherty, E. L., and Drickamer H. G. (1955): "A Theory of Thermal Diffusion in Liquids" *Journal of Chemical Physics*, vol. 23, no. 2, pp. 295-309.

Dutrieux, J. F, Platten, J. K., Chavepeyer, G., and Bou-Ali, M. M. (2002): "On the Measurement of Positive Soret Coefficients" *Journal of Physical Chemistry B*, vol. 106, no. 23, pp. 6104–6114.

Et-Tahir, A. Boned, C., Lagourette, B., and Xans, P. (1995): "Determination of the Viscosity of Various Hydrocarbons and Mixtures of Hydrocarbons versus Temperature and Pressure" *International Journal of Thermophysics*, vol. 6, pp. 1309-1334.

Fick, A. (1855): "On Liquid Diffusion" *Philosophical Magazine*, vol. 10, no. 63, pp. 30-39.

Firoozabadi, A. (1999): "Thermodynamics of Hydrocarbon Reservoirs" McGraw-Hill, New York.

Firoozabadi, A., Ghoryeb, K., and Shukla, K. (2000): "Theoretical Model of Thermal Diffusion Factors in Multicomponent Mixtures" *American Institute of Chemical Engineers Journal*, vol. 46, no. 5, pp. 892-900.

FLUENT 6.3 User's Guide, 2006.

Ghoryeb, K, and Firoozabadi, A. (2000): "Molecular, Pressure, and Thermal Diffusion in Nonideal Multicomponent Mixtures" *American Institute of Chemical Engineers Journal*, vol. 46, no. 5, pp. 883-891.

Ghorayeb, K., and Firoozabadi, A. (2000): "Numerical Study of Natural Convection Diffusion in Fractured Porous Media" *Society of Petroleum Engineers Journal*, vol. 5, no.1, pp. 12-20.

Ghorayeb, K., Firoozabadi, A., and Toshiyuki, A. (2003): "Interpretation of the Unusual Fluid Distribution in the Yufutsu Gas-Condensate Field" *Society of Petroleum Engineers Journal*, vol. 8, no. 2, pp. 114-123.

Glasstone S, Laidler, K.J, and Eyring, H. (`1941): "The Theory of Rate Processes: the Kinetics of Chemical Reaction, Viscosity, Diffusion and Electrochemical Phenomena" New York, McGraw-Hill, McGraw-Hill, New York.

Graf, T., and Therrien, R. (2005): "Variable-density Groundwater Flow and Solute Transport in Porous Media Containing Non-uniform Discrete Fractures" *Advance in water Resources*, vol. 28, pp. 1351-1367.

Haase, R. (1950): *Z. Phys. Chem.*, vol. 196, p. 219

Haugen, K. B., and Firoozabadi, A. (2007): "Transient Separation of Multicomponent Liquid Mixtures in Thermogravitational Columns" *Journal of Chemical Physics*, vol. 127, pp. 154507(1-9).

Haugen, K. B., and Firoozabadi, A. (2005): "On Measurement of Thermal Diffusion Coefficients in Multicomponent Mixtures*" Journal of Chemical Physics*, vol. 122, pp. 14516 (1-7).

Hayduk, W. and Minhas, B. S. (1982): "Correlation for Predictions of Molecular Diffusivities in Liquids" *Canadian Journal of Chemical Engineering*, vol. 60, pp. 295-299.

Hildebrand, J. H., and Scott, R. L. (1950): "The Solubility of Nonelectrolytes" 3rd Ed, Reinhold Publishing Co., New York.

Israfilov, H., Jannataliyev, R., Safarov, J., Shahverdiyev, A., and Hassel, E. (2009): "The (p, ρ, T) Properties and Apparent Molar Volumes V_φ of LiNO$_3$ + C$_2$H$_5$OH" *Acta Chimica Slovenica*, vol. 56, no. 1, pp. 95-108.

Jaber, T. J. and Saghir, M. Z. (2006): "Numerical Analysis of Ludwig-Soret Effect of one Binary Mixture and Two Ternary Mixtures in an Al$_2$O$_3$ Porous Cavity" ASME *International Mechanical Engineering Congress and Exposition*, Nov. 5-10, Chicago, Illinois, USA.

Jaber, T. J., Yan, Yu and Saghir, M. Z. (2008a): "Soret Effect for a Ternary Mixture in Porous Cavity: Modeling with Variable Diffusion Coefficients and Viscosity" *Journal of Fluids Engineering*, vol. 30, pp. 081703-1.

Jaber, T. J., Yan, Yu and Saghir M. Z. (2008b): "Comparison between Theoretical Model and Experimental data of Thermodiffusion Coefficients for Ternary Hydrocarbon Mixtures of Methane, n-Butane and n-Dodecane" *International Meeting on Thermal Diffusion (IMT8)*, June 9-13, Bonn-Bad Godesberg, Germany.

Jaber, T. J. and Saghir, M. Z. (2008): "Numerical Study of Permeability Effect on Convection in Fractured Porous Media Filled with Hydrocarbon Ternary Mixture"

ICHMT International Symposium on Advances in Computational Heat Transfer, May 11-16, Marrakech, Morocco.

Jaber, T. J., Bataller, H. and Saghir, M. Z. (2009): "Measurement of Thermodiffusion Coefficient for Binary Hydrocarbon Fluid Mixtures in Porous Medium: Experimental and Numerical Results" *ASME International Mechanical Engineering Congress and Exposition*, Nov. 13-19, Lake Buena Vista, Florida, USA.

Jaber, T. J. and Saghir, M. Z. (2010): "Three-dimensional Study of Permeability Effect on Convection in Heterogeneous Porous Medium Filled with a Ternary Hydrocarbon Mixture" *Journal of porous medium*, accepted, No. 1511-JPM, in press.

Jhaver, B. S. and Youngren, G. K. (1988): "Three-Parameter Modification of the Peng-Robinson Equation of State to Improve Volumetric Prediction" *Journal of SPE Reservoir Engineering*, vol. 3, pp. 1033-1040.

Jiang, C. G., Saghir, M. Z., and Kawaji M. (2006): "Numerical Analysis of Thermal-Solutal Convection in Heterogeneous Porous Media" *Journal of Applied Mechanics*, vol. 73, pp. 21-25.

Jiang, C.G., Jaber, T. J., Batalle, H., and Saghir, M. Z. (2007): "Simulation of Ludwig-Soret effect of a Water-ethanol Mixture in a Cavity Filled with Aluminum Oxide Powder under High Pressure" *International Journal of Thermal Sciences*, vol. 47, no. 2, pp. 126-135.

Jossi, J. A., Stiel, L. I., and Thodos, G. (1962): "The Viscosity of Pure Substances in the Dense Gaseous and Liquid Phases" *American Institute of Chemical Engineers Journal*, vol. 8, no. 1, pp. 59-63.

Kanti, M., Zhou, H., Ye, S., Boned, C., Lagourette, B., Saint-Guirons, H., Xans, P., and Montel, F. (1989): "Viscosity of Liquid Hydrocarbons, Mixtures and Petroleum cuts, as a Function of Pressure and Temperature" *Journal of Chemical Physics*, vol. 93, pp. 3860-3864.

Kazemi, H. L., Merrill, S., Porterfild, K. L., and Zeman, P. R. (1976): "Numerical Simulation of Water-Oil Flow in Naturally Fractured Reservoirs" *Society of Petroleum Engineers Journal*, vol. 16, no. 6, pp. 317-326.

Kempers, L.J.T.M. (1989): "A Thermodynamic Theory of the Soret Effect in a Multicomponent liquid" *Journal of Chemical Physics.* vol. 90, pp. 6541-6548.

Kempers, L.J.T.M. (2001): "A Comprehensive Thermodynamic Theory of the Soret Effect in a Multicomponent Gas, Liquid, or Solid" *Journal of Chemical Physics*, vol. 115, no. 14, pp.6330–6341.

Kohler, W., and Muller, B. (1995): "Soret and Mass diffusion Coefficients of Toluene/n-hexane Mixtures" *Journal of Chemical Physics*, vol. 103**,** pp. 4367-4370.

Kolodner, P., Williams, H., and Moe, C., (1988): "Optical Measurement of the Soret Coefficient of Ethanol/water Solution" *Journal of Chemical Physics*, vol. 88, no. 10, pp. 6512-6524.

Lagourette, B., Boned, C., Saint-Guirons, H., Xans, P., and Zhou, H. (1992): "Densimeter Calibration Method Versus Temperature and Pressure" *Journal of Measurement Science and Technology*, vol. 3, pp. 699-703.

Leahy-Dios, A., Bou-Ali, M. M., Platten, J. K., and Firoozabadi A. (2005): "Measurements of Molecular and Thermal Diffusion Coefficients in Ternary Mixture" *Journal of Chemical Physics*, vol. 122, no. 23, pp. 1-12.

Leahy-Dios, A., and Firoozabadi, A. (2007): "Molecular and Thermal Diffusion Coefficients of Alkane-Alkane and Alkane-Aromatic Binary Mixtures: Effect of Shape and Size of Molecules" *Journal of Physical Chemistry B*, vol.111, no. 1, pp. 191-198.

Liu, Jianchun, Bodvarsson, G.S., and Wu, Yu-Shu (2003): "Analysis of Flow Behaviour in Fractured Lithophysal Reservoirs" *Journal of Contaminant Hydrology*, vol. 62-63, pp. 189–211.

Lohrenz, J., Bray, B. G., and Clark, C. R. (1964): "Calculating Viscosities of Reservoir Fluids from Their Compositions" *Journal of Petroleum Technology*, vol. 16, no. 10, pp. 1171–1176.

Ludwig, C. (1856): "Diffusion zwischen ungleich erwärmten Otern gleich zusammengesetzter Lösunger Sitzber" Akad. Wiss. Wien, Math. Naturw. Kl, vol. 20, p. 539.

Montel, F. (1998): "The Role of Thermodynamics in Modeling Species Distributions of Hydrocarbon in Petroleum Reservoirs" *Entropy*, vol. 34, no. 214, pp. 7-10.

Nield, D. A. and Bejan, A. (2006): **"**Convection in Porous Media" Springer, 3rd edition.

Miyake, Y., Baylaucq, A., Plantier, F., Bessieres, D., Ushiki, H., and Boned, C. (2008): "High-pressure (up to 140 MPa) Density and Derivative Properties of Some

(pentyl-, hexyl-, and heptyl-) Amines Between (293.15 and 353.15) K" *Journal of Chemical Thermodynamics*, vol. 40, pp. 836-845.

Melnikov D.E., Shevtsova V.M., Mialdum A., and Bataller H. (2009): "Role of Liquid-Porous Interface in Soret Separation" *Fourth International Conference on Thermal Engineering: Theory and Applications*, January 12-14, Abu Dhabi, UAE.

Mialdun, A., and Shevtsova, V.M. (2008): "Development of Optical Digital Interferometry Technique for Measurement of Thermodiffusion Coefficients" *International Journal Heat and Mass Transfer*, vol. 51, no. 11-12, pp.3164–3178.

Oliveira, C. M. B. P., and Wakeham W. A. (1992): "Vibrating-wire Viscometers for Liquids at High pressures" *International Journal of Thermophysics,* vol. 13, pp. 773-790.

Onsager, L. (1931): "Reciprocal Relations in Irreversible Processes" *Physical Review*, vol. 37, pp. 405-426.

Kashiwagi, H., and Makita, T. (1982): "Viscosity of Twelve Hydrocarbon Liquids in the Temperature Range 298–348 K at Pressures up to 110 MPa" *International Journal of Thermophysics*, vol. 3, pp. 289-305.

Pan, S., Yan, Y., Jaber, T. J., Kawaji, M., and Saghir, M. Z., (2007):"The Evaluation of Thermal Diffusion Models for Ternary Hydrocarbon Mixture" *Journal Non-Equilibrium Thermodynamics*, vol. 32, no**.** 3, pp. 1-9.

Patankar, S. V. (2006): "Numerical Heat Transfer and Fluid Flow" New York: McGraw-Hill.

Peneloux, A., Rauzy, E., and Freze, R. (1982): "A Consistent Correction for Redlich-Kwong-Soave Volumes" *Journal of Fluid Phase Equilibria*, vol. 8, no. 1, pp. 7–23.

Peng, D. Y. and Robinson, D. B. (1976): "A New Two-constant Equation of State" *Industrial Engineering Chemistry Fundamentals*, vol. 15, no. 1, pp. 59-64.

Platten, J. K. (2006): "The Soret Effect: a Review of Recent Experimental Results" *Journal of Applied Mechanics*, vol. 73, pp. 5-15.

Platten, J. K., Bou-Ali, M. M., and Dutrieux, J. F. (2004): "Thermal Diffusion in Ternary Systems: an Experimental Study" In Proceeding of the *6th International Meeting of Thermodiffuiosn* (IMT6), Varenna, Italy.

Platten, J. K., and Costeseque, P. (2004): "The Soret Coefficient in Porous Media" *Journal of Porous Media*, vol. 7, no. 4, pp. 317-329.

Platten, J. K., Bou-Ali, M. M., and Dutrieux, J. F. (2003): "Enhance Molecular Separation in Inclined Thermogravitational Columns" *Journal of Physical Chemistry B*, vol. 107, no. 42, pp. 11763-11767.

Platten, J. K., Bou-Ali M. M., Costeseque, P., Dutrieux J. F., Kohler W., Leppla C., Wiegand S., and Wittko G. (2003): "Benchmark Values for Soret, Thermal Diffusion and Diffusion Coefficients of Three Binary Organic Liquid Mixtures" *Philosophical Magazine*, vol. 83, pp.1965-1971.

Polyakov, P., Luettmer-Strathmann, J., and Wiegand, S. (2006): "Study of the Thermal Diffusion Behaviour of Alkane/Benzene Mixture by Thermal Diffusion Forced Rayleigh Scattering Experiments and Lattice Model Calculations" *Journal of Physical Chemistry B*, vol. 110, n. 51 pp. 26215-26224.

Riley, M. F. and Firoozabadi, A. (1998): "Compositional Variation in Hydrocarbon Reservoirs with Natural Convection and Diffusion" *American Institute of Chemical Engineers Journal*, vol. 44, no. 2, pp. 452-464.

Rutherford, W. M. and Drickamer, H. G. (1954): "Theory of Thermal Diffusion in Liquids and the Use of Pressure to Investigate the Theory" *Journal of Chemical Physics*, vol. 22, no. 7, pp.1157-1165.

Rutherford, W.M., and Roof, J.G. (1959): "Thermal Diffusion in Methane-n-Butane Mixtures in the Critical Region" *Journal of Physical Chemistry*, vol. 63, pp. 1506-1511.

Saghir, M. Z. and Islam, M. R. (1999): "Double Diffusive Convection in Dual-Permeability, Dual-Porosity Porous Media" *International Journal of Heat and Mass Transfer*, vol. 42, no. 3, pp. 437-454.

Scatchard, G. (1931): *Chemical Reviews*, vol. **8**, p. 321.

Shukla, K., and Firoozabadi, A. (1998): "A New Model of Thermal Diffusion Coefficients in Binary Hydrocarbon Mixtures" *Journal Industrial & Engineering Chemistry Research*, vol. 37, pp. 3331-3342.

Soave, G. (1972): "Equilibrium Constants from a Modified Redlich-Kwong Equation of State" *Journal of Chemical Engineering Science*, vol. 27, pp. 1197-1203.

Soret, C. (1879): "Sur l'état d'équilibre que prend au point de vue de sa concentration une solution saline primitivement homogène dont deux parties sont portées à des

températures différentes" *Archives des Sciences Physiques et Naturelles de Genève*, vol. 2, pp. 48-61.

Soret, C. (1880): "Influence de la temperature sur la distribution des sels dans leurs solutions" *Compte-Rendu de l'Academie des Sciences*, Paris, vol. 91, pp. 289-291.

Taylor, R., and Krishna, R. (1993): "Multicomponent Mass Transfer" New York, Wiley.

Tichacek, L. J., Kmak, W. L., and Drickamer, H. G. (1956): "Thermal Diffusion in Liquids; the Effect of Non-Ideality and Association" *Journal Physics Chemistry*, vol. 60, pp. 660-665.

Tsang, Y.W., and Birkholzer, J.T. (1999): "Predictions and Observations of the Thermal–hydrological Conditions in the Single Heater Test" *Journal of Contaminant Hydrology*, vol. 38, no. 1–3, pp. 385–425.

Urteaga, P., Plantier, F., Bou-Ali, M.M., and Bataller, H. (2008): "Thermodiffusion Coefficient (D_T) for Binary Hydrocarbon Mixtures at High Pressures, Thermal Nonequilibrium" Lecture Notes of *the 8th International Meeting on Thermodiffusion*, edited by S.Wiegand, W. Köhler, J.K.G. Dhont, Schriften des Forschungszentrums Jülich, Germany, pp. 77-82.

Urteaga, P., Bou-Ali, M.M, and Blanco, P. (2008): "Thermogravitational Technique at High Pressure for Liquid Mixtures, Thermal Nonequilibrium" Lecture Notes of *the 8th International Meeting* on Thermodiffusion, edited by S.Wiegand, W. Köhler, J.K.G. Dhont, Schriften des Forschungszentrums Jülich, Germany, pp. 71-76.

Urteaga, P., Bou-Ali, M.M., Platten, J.K., Madariaga, J.A., and Santamaria, C., in M.M. Bou-Ali and Platten, J.K. (Ed.) (2006): "Thermodiffusion: Basics and Applications" Mondragon Unibertsitateko Zerbitzu Editoriala: Mondragon, Spain.

Van Vaerenbergh, S., and Legros, J.C. (1998): "Soret Coefficients of Organic Solutions Measured in the Microgravity SCM Experiment and by the Flow and Benard Cells" *Journal of Physical Chemistry*, vol. 102, pp. 4426-4431.

Van Vaerenbergh S., Shapiro A., Galliero G., Montel F., Legros J., Caltagirone J., Daridon J., and Saghir M.Z. (2005): "Multicomponent Processes in Crudes" *European Space Agency Special Publication,* vol. 1290, pp. 202-213.

Van Vaerenbergh S., Srinivasan S., and Saghir M.Z. (2009): "Thermodiffusion in Multicomponent Hydrocarbon Mixtures: Experimental Investigations and Computational Analysis*" Journal of Chemical Physics*, vol. 131, pp. 114505-1-114505-8.

Vieira dos Santos, F.J. and Nieto de Castro, C. A. (1997): "Viscosity of Toluene and Benzene under High Pressure" *International Journal of Thermophysics*, vol. 18, no. 2, pp. 367-378.

Versteeg, H. K., and Malalasekera W. (2007): "An Introduction to Computational Fluid Dynamics, the Finite Volume Method" 2nd edition, Pearson.

Warren, J. E., and Root, P. J. (1963): "The Behaviour of Naturally Fractured Reservoirs" *Society of Petroleum Engineers Journal*, vol. 3, no. 3, pp. 245-255.

Wiegand, S. (2004): "Thermal Diffusion in Liquid Mixtures and Polymer Solutions" *Journal of Physics-condensed Matter*, vol. 16, no. 10:R357–R379.

Wiegand, S., and Köhler, W. (2002):"Thermal Nonequilibrium Phenomena in Fluid Mixtures" (Lecture Notes in Physics), Springer-Verlag, edited by W. Köhler and S. Wiegand, vol. 584, pp. 189-210.

Wittko, G., and Köhler, W. (2003):"Precise Determination of the Soret, Thermal diffusion and Mass Diffusion Coefficients of Binary Mixtures of n-Dodecane, Isobutylbenzene and 1,2,3,4-Tetrahydronaphthalene by Holographic Grating Technique" *Philosophical Magazine*, vol. 83, no. 17-18, pp. 1973-1987.

Wu, Y.S., Mukhopadhyay, S., Zhang, K., and Bodvarsson, G.S. (2006): "A Mountain-Scale Thermal-Hydrologic Model for Simulating Fluid Flow and Heat Transfer in Unsaturated Fractured Rock" *Journal of Contaminant Hydrology*, vol. 86, pp. 128-159.

Zhang, K.J., Briggs, M.E., Gammon, R.W., and Sengers, J.V. (1996): "Optical Measurement of the Soret Coefficient and the Diffusion Coefficient of Liquid Mixtures" *Journal of Chemical Physics*, vol. 104, no. 17, pp. 6881-6892.

Appendix A

Custom-Made Software Package

Custom-made software in the LabView environment allows the image acquisition and the extraction of useful quantities, see Figure A.1. The program simultaneously acquires the relevant parameters of the cell, namely, pressure and temperature of the hot and cold dead- volumes.

Schematically, the program Refr_In software performs the following operations:

1. Initialization of the link with the CCD camera; the COHU CCD Camera 7700 was used in this project (1004x1004 pixels with 10 bit depth at 30 FPS).

2. Acquisition of sequential images at constant, selectable time steps.

3. Showing of the acquired image (on/off) to allow visual check of the interferograms and choice of the Region of Interest (ROI).

4. Recording (on/off) of the pixel values of the entire image in tiff file.

5. Selection of the ROI in the form of a vertical (perpendicular to grating pattern) line over the image area.

6. Low-pass filtering (on/off) of the pixel values in the ROI to give better fit results.

7. Normalization (on/off) of the pixel values in the ROI to give better fit results.

8. Recording (on/off) of the pixel values of the ROI in txt file.

9. Initialization of the fitting parameters.

10. Fitting of the pixel values of the ROI to get the phase value of the sinusoidal pattern.

11. Plotting the data of the pixel values in the ROI, and the values given by fit process in a graph format to allow visual check of the fit process.

12. Acquisition of the values of the pressure, and temperatures of the hot and cold dead-volumes via NI-USB-9162 data acquisition card.

13. Plotting the data of the pressure in a graph format.

14. Plotting the data of the phase in a graph format.

15. Recording the data of phase, pressure, and temperatures of the hot and cold dead-volumes as a function of time.

Typical, interferograms consist of a vertical intensity grating, which is captured by the CCD camera and converted in a matrix of grey levels. The CCD camera utilized for these experiments is an 8-bit camera, so that images are digitized in grey levels ranging from 0 to 255. It has been chosen to investigate just one vertical line out of the entire image, because this is enough for a good characterization of the sinusoidal modulation. The intensity of the laser and the exposure time of the CCD camera are tuned in a preliminary set-up phase, so that the maximum grey level within an image is in the order of 240-250 not to saturate the image. Other parameters of the CCD camera are adjusted in order to exploit the CCD dynamic at its best. After selection of the Region of Interest (ROI) in the form of a vertical line on which all maths will be performed, a low-pass filter is applied to the pixel values of the ROI to eliminate most of the noise. Eventually ROI pixel values are normalized so that all peaks are at about unit height. This is sometimes necessary because of non-uniformities of the laser beam due to dust and other spurious in the beam path. The consequence of these non-uniformities is an increase in the convergence time and a decrease in the accuracy of the following fitting procedure through a sinusoidal function.

The fitting is operated on filtered and normalized ROI pixel values trough the equation:

$$I(x) = a\cos^2(bx + c')$$ (A.1)

At the beginning of the experiment the user must provide initial values for these parameters. Typical values are: $a = 1$, and $b = 0.01\text{-}0.05$. The half of the phase, c', is completely unknown in principle and is the output of the fitting procedure. The fitting then utilizes the output parameters of the preceding image as initial values for the fitting of the image under analysis. This has two important consequences; first, convergence is very fast since a and b should not vary during the entire experiment, and second, the value of c' (which here is not limited between 0 and π, like typically done) does not need unwrapping procedures and is directly displayed in the User Interface.
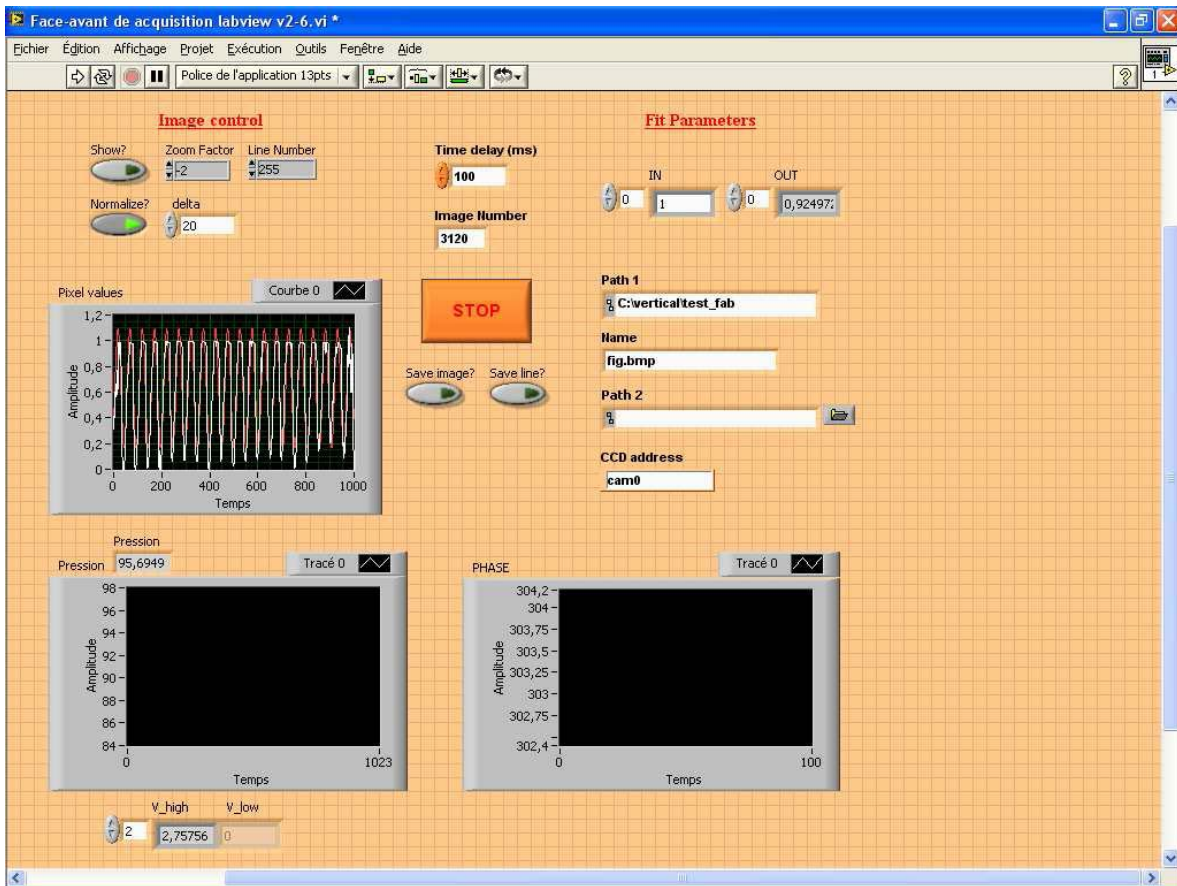
Figure A.1: Front-screen of the LabView-Refr_In software.

Appendix B

The measurement value of the Density of the three binary Mixtures
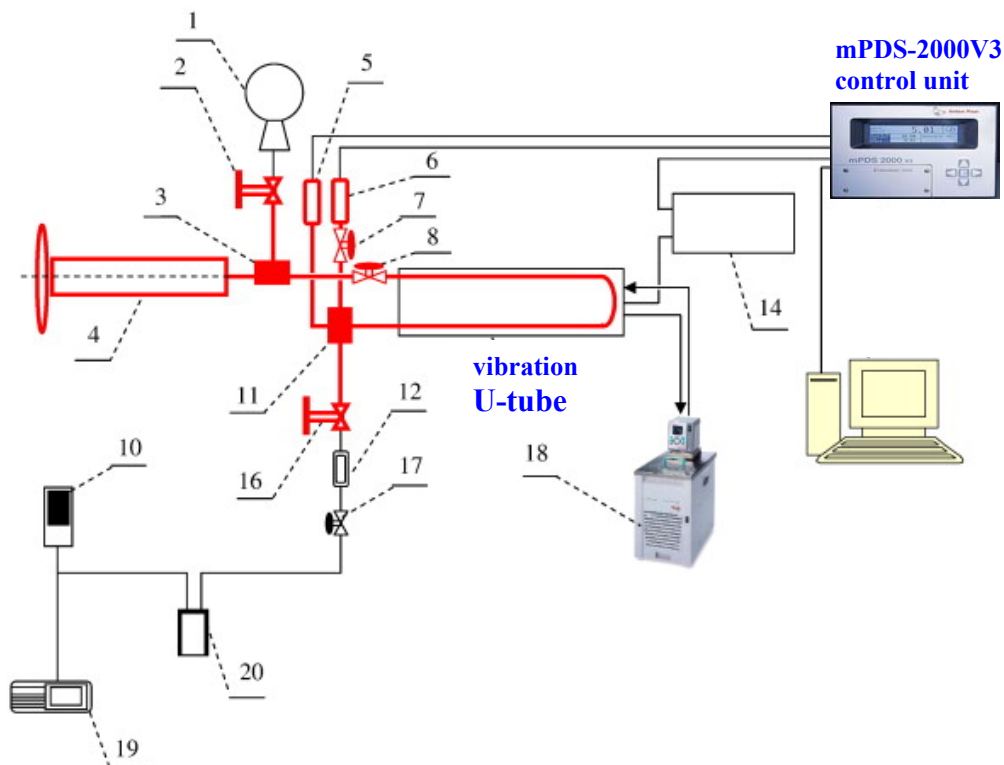
Figure B.1: Experimental setup of DMA HPM, Israfilov *et al.* (2009)**:** 1 flash for the probe; 2,7, 16, and 17 valves; 3 and 11 fitting; 4 pressure intensifier; 5 pressure sensor HP-1; 6 pressure sensor P-10; 8 valve for closing of system during experiment; 10 vacuum indicator; 12 visual window; 13 vibration tube; interface module; 18 thermostat F32-ME; 19 vacuum pump; 20 thermos for cooling.

Table B.1: Experimental densities of the binary IBB-nC12 (50 wt% mass fraction) as function of the temperature and the pressure.

P (MPa)	T (°C)	ρ (g.cm^{-3})
0.1	20.0	0.7954
0.1	22.5	0.7936
0.1	25.0	0.7917
0.1	27.5	0.7899
0.1	30.0	0.7881
2	20.0	0.7967
2	22.5	0.7949
2	25.0	0.7931
2	27.5	0.7912
2	30.0	0.7896
4	20.0	0.7981
4	22.5	0.7963
4	25.0	0.7945
4	27.5	0.7926
4	30.0	0.7911
6	20.0	0.7995
6	22.5	0.7977
6	25.0	0.7959
6	27.5	0.7940
6	30.0	0.7925
8	20.0	0.8011
8	22.5	0.7991
8	25.0	0.7973
8	27.5	0.7954
8	30.0	0.7940
10	20.0	0.8025
10	22.5	0.8005
10	25.0	0.7986
10	27.5	0.7968
10	30.0	0.7954
12	20.0	0.8037
12	22.5	0.8018
12	25.0	0.7999
12	27.5	0.7981
12	30.0	0.7967
14	20.0	0.8050
14	22.5	0.8031
14	25.0	0.8013
14	27.5	0.7994
14	30.0	0.7981
16	20.0	0.8063
16	22.5	0.8043
16	25.0	0.8026

16	27.5	0.8007
16	30.0	0.7994
18	20.0	0.8076
18	22.5	0.8056
18	25.0	0.8038
18	27.5	0.8020
18	30.0	0.8008
20	20.0	0.8089
20	22.5	0.8068
20	25.0	0.8051
20	27.5	0.8033
20	30.0	0.8020

Table B.2: Experimental densities of the binary THN-nC12 (50 wt% mass fraction) as function of the temperature and the pressure.

P (MPa)	T (°C)	ρ (g.cm^{-3})
0.1	20.0	0.8444
0.1	22.5	0.8424
0.1	25.0	0.8407
0.1	27.5	0.8388
0.1	30.0	0.8373
2	20.0	0.8457
2	22.5	0.8436
2	25.0	0.8420
2	27.5	0.8400
2	30.0	0.8385
4	20.0	0.8468
4	22.5	0.8449
4	25.0	0.8434
4	27.5	0.8413
4	30.0	0.8399
6	20.0	0.8480
6	22.5	0.8460
6	25.0	0.8447
6	27.5	0.8425
6	30.0	0.8411
8	20.0	0.8495
8	22.5	0.8474
8	25.0	0.8459
8	27.5	0.8438
8	30.0	0.8424
10	20.0	0.8508
10	22.5	0.8486
10	25.0	0.8471
10	22.5	0.8498
12	25.0	0.8484
12	27.5	0.8463
12	30.0	0.8449
14	20.0	0.8531
14	22.5	0.8510
14	25.0	0.8495
14	27.5	0.8475
14	30.0	0.8461
16	20.0	0.8542
16	22.5	0.8521
16	25.0	0.8507
16	27.5	0.8488
16	30.0	0.8475

18	20.0	0.8554
18	22.5	0.8533
18	25.0	0.8519
18	27.5	0.8499
18	30.0	0.8487
20	20.0	0.8566
20	22.5	0.8544
20	25.0	0.8530
20	27.5	0.8510
20	30.0	0.8498

Table B.3: Experimental densities of the binary THN-IBB (50 wt% mass fraction) as function of the temperature and the pressure.

P (MPa)	*T* (°C)	ρ (g.cm^{-3})
0.1	20.0	0.9079
0.1	22.5	0.9057
0.1	25.0	0.9036
0.1	27.5	0.9015
0.1	30.0	0.9000
2	20.0	0.9091
2	22.5	0.9068
2	25.0	0.9047
2	27.5	0.9029
2	30.0	0.9013
4	20.0	0.9103
4	22.5	0.9081
4	25.0	0.9061
4	27.5	0.9042
4	30.0	0.9026
6	20.0	0.9116
6	22.5	0.9093
6	25.0	0.9075
6	27.5	0.9054
6	30.0	0.9040
8	20.0	0.9130
8	22.5	0.9106
8	25.0	0.9088
8	27.5	0.9068
8	30.0	0.9053
10	20.0	0.9143
10	22.5	0.9119
10	25.0	0.9101
10	27.5	0.9080
10	30.0	0.9065
12	20.0	0.9154
12	22.5	0.9131
12	25.0	0.9113
12	27.5	0.9092
12	30.0	0.9078
14	20.0	0.9166
14	22.5	0.9143
14	25.0	0.9125
14	27.5	0.9104
14	30.0	0.9090
16	20.0	0.9177
16	22.5	0.9154
16	25.0	0.9137

16	27.5	0.9116
16	30.0	0.9103
18	20.0	0.9188
18	22.5	0.9166
18	25.0	0.9149
18	27.5	0.9128
18	30.0	0.9114
20	20.0	0.9201
20	22.5	0.9177
20	25.0	0.9161
20	27.5	0.9140
20	30.0	0.9126

Table B.4: Experimental densities of the binary IBB-nC12 (T_0=25 °C) as function of the mass fraction of the densest component and the pressure.

P (MPa)	ω_1	ρ (g.cm^{-3})
0.1	0.48	0.7895
0.1	0.49	0.7904
0.1	0.50	0.7917
0.1	0.51	0.7927
0.1	0.52	0.7936
2	0.48	0.7909
2	0.49	0.7920
2	0.50	0.7931
2	0.51	0.7941
2	0.52	0.7952
4	0.48	0.7924
4	0.49	0.7935
4	0.50	0.7945
4	0.51	0.7957
4	0.52	0.7966
6	0.48	0.7939
6	0.49	0.7949
6	0.50	0.7959
6	0.51	0.7970
6	0.52	0.7979
8	0.48	0.7953
8	0.49	0.7963
8	0.50	0.7973
8	0.51	0.7984
8	0.52	0.7993
10	0.48	0.7966
10	0.49	0.7974
10	0.50	0.7986
10	0.51	0.7997
10	0.52	0.8006
12	0.48	0.7979
12	0.49	0.7987
12	0.50	0.7999
12	0.51	0.8010
12	0.52	0.8019
14	0.48	0.7992
14	0.49	0.8001
14	0.50	0.8013
14	0.51	0.8023
14	0.52	0.8032
16	0.48	0.8005
16	0.49	0.80131
6	0.50	0.8026
16	0.51	0.8035
16	0.52	0.8045
18	0.48	0.8017

18	0.49	0.8026
18	0.50	0.8038
18	0.51	0.8047
18	0.52	0.8057
20	0.48	0.8031
20	0.49	0.8039
20	0.50	0.8051
20	0.51	0.8060
20	0.52	0.8070

Table B.5: Experimental densities of the binary THN-nC12 (T_0=25 °C) as function of the mass fraction of the densest component and the pressure.

P (MPa)	ω_1	ρ (g.cm^{-3})
0.1	0.48	0.8357
0.1	0.49	0.8384
0.1	0.50	0.8407
0.1	0.51	0.8427
0.1	0.52	0.8448
2	0.48	0.8369
2	0.49	0.8397
2	0.50	0.8420
2	0.51	0.8440
2	0.52	0.8461
4	0.48	0.8383
4	0.49	0.8410
4	0.50	0.8434
4	0.51	0.8453
4	0.52	0.8475
6	0.48	0.8396
6	0.49	0.8422
6	0.50	0.8447
6	0.51	0.8465
6	0.52	0.8487
8	0.48	0.8409
8	0.49	0.8435
8	0.50	0.8459
8	0.51	0.8478
8	0.52	0.8499
10	0.48	0.8421
10	0.49	0.8447
10	0.50	0.8471
10	0.51	0.8488
10	0.52	0.8511
12	0.48	0.8433
12	0.49	0.8459
12	0.50	0.8484
12	0.51	0.8503
12	0.52	0.8522
14	0.48	0.8446
14	0.49	0.8471
14	0.50	0.8495
14	0.51	0.8515
14	0.52	0.8535
16	0.48	0.8457
16	0.49	0.8483
16	0.50	0.8507
16	0.51	0.8527
16	0.52	0.8546
18	0.48	0.8469

18	0.49	0.8493
18	0.50	0.8519
18	0.51	0.8538
18	0.52	0.8557
20	0.48	0.8481
20	0.49	0.8506
20	0.50	0.8530
20	0.51	0.8550
20	0.52	0.8570

Table B.6: Experimental densities of the binary THN-IBB (T_0=25 $^\circ$C) as function of the mass fraction of the densest component and the pressure.

P (MPa)	ω_1	ρ (g.cm^{-3})
0.1	0.48	0.9013
0.1	0.49	0.9025
0.1	0.50	0.9036
0.1	0.51	0.9050
0.1	0.52	0.9060
2	0.48	0.9026
2	0.49	0.9038
2	0.50	0.9047
2	0.51	0.9062
2	0.52	0.9073
4	0.48	0.9040
4	0.49	0.9051
4	0.50	0.9061
4	0.51	0.9076
4	0.52	0.9088
6	0.48	0.9053
6	0.49	0.9064
6	0.50	0.9075
6	0.51	0.9088
6	0.52	0.9100
8	0.48	0.9066
8	0.49	0.9077
8	0.50	0.9088
8	0.51	0.9101
8	0.52	0.9112
10	0.48	0.9078
10	0.49	0.9090
10	0.50	0.9101
10	0.51	0.9112
10	0.52	0.9124
12	0.48	0.9090
12	0.49	0.9102
12	0.50	0.9113
12	0.51	0.9125
12	0.52	0.9136
14	0.48	0.9102
14	0.49	0.9115
14	0.50	0.9125
14	0.51	0.9137
14	0.52	0.9148
16	0.48	0.9114
16	0.49	0.9126
16	0.50	0.9137
16	0.51	0.9150
16	0.52	0.9160
18	0.48	0.9126

18	0.49	0.9137
18	0.50	0.9149
18	0.51	0.9161
18	0.52	0.9171
20	0.48	0.9138
20	0.49	0.9149
20	0.50	0.9161
20	0.51	0.9172
20	0.52	0.9182

Appendix C

Physical and Thermodynamic Properties of Pure Hydrocarbon

Components

Table C.1: Pure hydrocarbon components parameters which used in this work $T_{mean}=25\ ^{\circ}C$, (Daubert and Danner 1989).

Pure component	T_c (K)	P_c (Pa)	M (kg/kmol)	ω (-)	ρ (kg.m^{-3})	C_p (J.kg^{-1}.K^{-1})	k (W.m^{-1}.K^{-1})
CH_4 (C1)	190.58	4.60×10^6	16.043	0.0108	161.71	2913.29[3]	0.0790
nC_4H_{10} (nC4)	425.18	3.79×10^6	58.123	0.1993	572.92	2435.07	0.1048
THN ($C_{10}H_{12}$)	720.15	3.62×10^6	132.205	0.3811	967.48	1645.41	0.1300
IBB ($C_{10}H_{14}$)	650.15	3.04×10^6	134.221	0.3278	849.08	1801.57	0.1220
$nC_{12}H_{26}$ (nC12)	658.20	1.82×10^6	170.338	0.5734	745.34	2206.40	0.1368

---

[3] C_p value is obtained from National Institute of standards and Technology (NIST)